의학박사 학위논문

Functional proteomics study for neuro-immune system using in-depth proteome profiling and targeted proteomics techniques

고분해능 단백체 프로파일링 및 표적단백체 기술을 이용한 신경-면역 시스템에 대한 기능 단백체 연구

2018 년 2 월

서울대학교 대학원

의과학과 의과학전공

우 중 민

A thesis of the Degree of Doctor of Philosophy

고분해능 단백체 프로파일링 및 표적단백체 기술을 이용한 신경-면역 시스템에 대한 기능 단백체 연구

Functional proteomics study for neuro-immune system using in-depth proteome profiling and targeted proteomics techniques

February 2018

Major in Biomedical Sciences
Department of Biomedical Sciences
Seoul National University
Graduate School
Jongmin Woo

ABSTRACT

Functional proteomics study for neuro-immune system using in-depth proteome profiling and targeted proteomics techniques

Jongmin Woo

Major in Biomedical Sciences

Department of Biomedical Sciences

Seoul National University

Graduate School

Introduction: Although the average life expectancy of humans has been increasing steadily with advances in medicine, neurodegenerative disease such as Alzheimer disease (AD), Parkinson disease (PD), or Amyotrophic lateral sclerosis (ALS) has been decreasing the quality of life for humans. At the molecular level, it is essential to study the causes and mechanisms of these neurodegenerative diseases. In recent years, proteomics using high-resolution mass spectrometry has emerged as a useful technique for discovering marker proteins. In addition, a systematic network analysis of target proteins could be used to study mechanisms of neurodegenerative disease in the future.

Methods: In Chapter I, neuronal cell line (HT-22), astrocytic cell line (C8-D1A), and microglia cell line (BV-2) were used for the analysis of secretory protein analysis in central nervous system. 1x10e6 cells were cultured in a 100-mm dish for 24 hours, and the proteins obtained by concentration were treated with peptides using the FASP (Filter Aided Sample Preparation) technique and analyzed by Q-Exactive, a high-resolution mass spectrometer, for 4 hours. Data were processed with the MaxQuant program based on the Andromeda algorithm, and un-annotated MS/MS data were analyzed with the de-novo sequencing based PEAKS-7 program to identify additional proteins. The secretory proteins of each cell line were compared and analyzed by label-free quantitation technique, and the important functions of the secreted proteins were confirmed using the bioinformatics tool. In Chapter II, microglial cell lines were treated with lipopolysaccharide (LPS) and interferon gamma (IFN-γ) for 24 h, and proteins expressed in intracellular and extracellular were simultaneously quantified using dimethyl labeling analysis. In order to examine the changes in the candidate protein groups in the intra- and extracellular microglial cells activated with LPS, IFN-γ and LPS / IFN-γ for 6, 12, 24 and 48 hours, I conducted a systematic network analysis of the proteomes that change with time by performing relative quantification with label-free PRM (Parallel Reaction Monitoring).

Results: In Chapter I, 2795 secretory proteins were identified in three cell lines using a high-resolution mass spectrometer. In addition, 156 (BV-2), 44 (C8-D1A), and 93 (HT-22) cell-specific secretory proteins were identified. I also identified 302 additional proteins using de-novo sequencing analysis techniques. In order to

increase the reliability of excised secreted proteins, 2351 putative secretory proteins were classified using SignalP, SecretomeP, Exocarta and TMHMM database tools. The quantitative comparison analysis method with 2 fold-change between each cell secretory protein were confirmed 573 (BV-2 vs. C8-D1A), 694 (BV-2 vs. HT-22), and 475 (C8-D1A vs. HT, -22) putative secreted proteins. Pathway analysis of quantified proteins revealed important functions of secretory proteins such as lysosome and phagocytosis, and proteins associated with neurodegenerative diseases such as Parkinson disease and Huntington disease. In Chapter II, I investigated whole cell proteome (WCP) analysis of LPS and LPS / IFN-γ activated protein to identify 5492 proteins and quantify 4748 proteins. Analyze the same model of extracellular secretory proteome (SEC), 4938 proteins and 3558 proteins were identified and quantified, respectively. A total of 319 intracellular proteins and 170 secreted proteins were selected as final target candidates through analysis of bioinformatics such as KEGG pathway for statistically significant proteins. Using a label-free PRM technique that optimizes simultaneous quantitation of more than 450 peptides, I were able to draw a pathway network map that varies with activation time. In addition, I could suggest candidate protein markers that show intracellular and extracellular differences in activated microglial cell model.

Conclusions: Secretory protein differences of three cell lines were identified by label-free quantification through optimization and development of secretory proteome technique. These secretory proteomics techniques provide a basis for in-depth and accurate research of extracellular proteins that are present in small amounts. In addition, I aimed to investigate mechanism of degenerative brain disease by identifying marker proteins expressed during activation of microglial cells that

are immunocompetent in the CNS through a systematic quantitative proteomics approach on a single platform. Simultaneous quantification of dimethyl labeling and label-free PRM targeted proteomics were established for more precise and accurate quantitative analysis. In addition, quantitative analysis of the proteins involved in immune-inflammatory response and metabolism during microglial activation could be used to identify marker proteins that specifically expressed LPS and IFN-γ.

Keywords: CNS; Astrocyte; Microglia; Neuron; Activated microglia; Secretome; Dimethyl labeling; label-free PRM; Targeted proteomics

Student Number: 2013-21781

*This article has been published in *Proteomics* (2015, 15 (21), 3617-22.) and *Journal of proteome research.* (2017, 16 (9), 3419-3432.)

CONTENTS

Abstract…… i

Contents……v

List of Tables……. vii

List of Figures……viii

List of Abbreviations …… xi

Introduction ……..…….. 1

Chapter I: In-depth characterization of the secretome of mouse CNS cell lines by LC-MS/MS

Material and Methods ……..…… 6

Results ……..…… 16

Discussion …… 34

Chapter II: Quantitative proteomics reveals temporal proteomic changes in signaling pathways during BV2 mouse microglial cell activation

Material and Methods 37

Results 48

Discussion 90

Conclusion 93

References 94

Abstract in Korean 103

LIST OF TABLES

Table 1-1. Summary of GO terms and KEGG pathway analysis ……..… 33

Table 1-2. Summary of cytokines, hormones, and growth factors ….…….. 36

Table 2-1. List of target proteins and corresponding peptides ……..… 62

Table 2-2. Variation of label-free PRM analysis …… 69

Table 2-3. List of cell specific differentially expressed proteins on WCP group ……. 84

Table 2-4 List of cell specific differentially secreted proteins on SEC group ……. 87

LIST OF FIGURES

Figure 1-1. Detailed flowchart of the proteomic approach, label-free quantitation, and data analysis 9

Figure 1-2. Proteomic analysis of secreted proteins from three murine CNS cell lines in conditioned media 18

Figure 1-3. Distribution of putative secreted proteins predicted by bioinformatics tools 19

Figure 1-4. Proportion of putative secreted proteins 20

Figure 1-5. Characterization of proteomic data 21

Figure 1-6. Reproducibility between proteomics analysis 22

Figure 1-7. Precision of proteomic approaches 24

Figure 1-8. Principal component analysis (PCA) 26

Figure 1-9. Label-free quantitation of identified secretion proteins 27

Figure 1-10. Cluster analysis 29

Figure 1-11. Western blot for validation of label-free quantitation 30

Figure 1-12. Pathway analysis 32

Figure 1-13. Comparison our data with others reported in the literature 35

Figure 2-1. Confirmation of differential expression of iNOS and nitric oxide in activated microglia model …… 49

Figure 2-2. Systematic workflow of proteomic analysis for whole-cell and secreted proteomes in activated microglia cell line …… 50

Figure 2-3. Identification and quantification for dimethyl labeling …… 52

Figure 2-4. Assessment of global proteomics …….. 54

Figure 2-5. Heatmap of pairwise correlation values for discovery data ……. 55

Figure 2-6. Scheme for target protein selection ……..…… 57

Figure 2-7. Statistical analysis and bioinformatics …… 58

Figure 2-8. Filter criteria of targeted peptides for label-free PRM ……. 61

Figure 2-9. Characterization of label-free PRM analysis …….. 71

Figure 2-10. Distribution of XIC peak areas before and after normalization ……. 72

Figure 2-11. Proteomic changes in the WCP group …… 74

Figure 2-12. Significant proteomic changes and PPI network proteins in the WCP group …… 75

Figure 2-13. Proteomic changes in pathway networks …….. 77

Figure 2-14. Proteomic changes in the SEC group …… 80

Figure 2-15. Comparison proteomics data with transcriptome data to reveal microglia specific proteins …… 83

LIST OF ABBREVATIONS

LPS, lipopolysaccharide

IFN-γ, interferon-gamma

PRM, parallel reaction monitoring

MRM, multiple reaction monitoring

SRM, selected reaction monitoring

CNS, central nervous system

iNOS, nitric oxide synthase

NO, nitric oxide

SILAC, stable isotope labeling with amino acids in cell culture

DDA, data-dependent acquisition

LRPs, labeled reference peptides

DMEM, Dulbecco's modified Eagle's medium

DPBS, Dulbecco's phosphate-buffered saline

BCA, bicinchoninic acid assay

FASP, filter-aided sample preparation

AGC, automatic gain control

HCD, higher-energy collisional dissociation

FDR, false discovery rate

TMHMM, Transmembrane Helices−Hidden Markov Mode

WCP, whole-cell proteome

CMC, conditioned media collection

SEC, secretome

DEPs, differentially expressed proteins

RT, retention time

XIC, extracted-ion chromatogram

PCA, principal component analysis

PPIs, protein−protein interactions

MHC, major histocompatibility complex

TLR signaling, toll-like receptor signaling

ROS, reactive oxygen species

Mif, macrophage migration inhibitory factor

TLR4, toll like receptor 4

Pf4, platelet factor 4

Grns, Granulins

Cxcl4, chemokine C-X-C motif ligand 4

PGRN, progranulin

Spp1, secreted phosphoprotein 1

Gpi, glucose phosphate isomerase

Cxcl9, chemokine C-X-C motif ligand 9

Cxcl10, chemokine C-X-C motif ligand 10

Icam1, intercellular adhesion molecule 1

Lgmn, legumain

Ncf1, neutrophil cytosolic factor 1

INTRODUCTION

The central nervous system (CNS) comprises two major cell types, neurons and glia [1-2]. Neurons have been reflected to be the core components of the CNS, whereas glia were simply physical and metabolic support cells. However, recent studies [3-4] have showed that glia are significant mediators in the development, maintenance, and function of the nervous system and in disorders of the CNS. Further, impaired communication between neurons and glia alter normal brain function and effect neurodegenerative processes, including Parkinson disease (PD), Alzheimer disease (AD), and amyotrophic lateral sclerosis (ALS) [3, 5].

The recruitment and activation of glia cells, primarily astrocytes and microglia in the CNS, require constant shared communication between neurons and glia and among glial cells [3, 5]. Subsequently, reactive glial cells interpret extracellular cues to regulate neuronal function. Astrocyte and microglia communicate primarily with each other and neurons through secreted proteins, which mediate and modulate many normal and pathological processes in the CNS [5]. Thus, an in-depth proteomic analysis of secreted proteins is crucial to increase our understanding of the molecular interactions between neurons, astrocytes, and microglia under physiological and neuropathological conditions [5].

Mass spectrometry (MS)-based shotgun proteomic methods allow one to profile secreted proteins, and significant effort has been directed toward analyzing the proteomic profiles [6-9] of secreted proteins from astrocytes, microglia, and neurons. However, the integrated profile of the CNS secretome is limited, although research

on individual secretomes has made remarkable progress in recent years. Further, neuron-, astrocyte-, and microglia-secreted proteins have not been systematically identified or quantified largely under non-disease or inactive conditions, demanding improvements in the depth of coverage of the secretome.

First in Chapter I, I attempted to generate a large scale of secretome from microglia (BV-2), astrocyte (C8-D1A), and neuron (HT-22) mouse cell lines by combining filter aided sample preparation (FASP) method with high-resolution LC-MS/MS. The data were analyzed using MaxQuant and PEAKS 7 softwares for identification of proteins and quantification of differentially expressed proteins. Proteins identified in the conditioned media of three cell lines were processed using SignalP and SecretomeP softwares to predict the existence of signal peptide cleavage sites and to determine if a protein is non-classically secreted, respectively. This study contributed to the development of methods for analyzing proteins secreted from cell lines by proteomics using mass spectrometry. The technique of in-depth secretome analysis could be used to perform the following studies.

In Chapter 2, I focused on microglia to better understand the neuroimmune system. Microglia are cellular sentinels of innate immunity that are critical in the development of neurodegenerative diseases, the prevalence of which has risen worldwide as the average life expectancy has increased steadily. According to a recent study, microglia help maintain immune surveillance by responding quickly to pathogens that enter the parenchyma when the central nervous system (CNS) is compromised by foreign invaders [10]. Microglia have many functions, including

antigen presentation and processing [11], activation of T cells and B cells [12], and initiation of nonspecific immune responses following stimulation.

Microglia undergo a series of morphological changes in their active state. As part of this process, various surface receptors are upregulated to create a variety of biochemical repertoires that help in different subtypes of the immune reaction [13]. Moreover, microglial activation-mediated inflammatory responses normally cause neuronal damage and remove damaged cells through phagocytosis [14-15]. Activated microglia express various cytokines and growth factors in response to nerve injuries under pathological conditions [16]. To observe the active states of intracellular and intercellular microglia, two major inflammation-associated molecules lipopolysaccharide (LPS) and interferon-gamma (IFN-γ) have been used to stimulate BV2 mouse microglial cells. LPS induces dopaminergic neurodegeneration through NF-kB and Toll-like receptor signaling [17-18]. IFN-γ activates microbicidal effector functions through JAK-STAT signaling and the enhancement of innate immune responses [19]. LPS and IFN-γ synergize to amplify the expression of nitric oxide synthase (iNOS), which increases nitric oxide (NO) production [20-21]. The microglial active state has been examined simply with regard to a few factors to several hundred associated molecules [22-25] and has not been analyzed on a proteomic scale that takes into account the related pathway networks.

I have also attempted a systematic approach to combine global proteomics with targeted proteomics to further improve the technology. Many studies have attempted to identify specific proteins using a quantitative proteomics approach [26-28]. However, conventional targeted methods, such selected reaction monitoring (SRM)-based targeted proteomics, are labor-intensive and inconvenient, because separate

platforms are used for the discovery and targeted analysis [29]. Moreover, one is restricted to analyzing 100–200 target peptides, rendering this approach unsuitable for larger-scale applications [30]. To overcome these limitations, I designed a systematic proteomics approach that can track changes in more proteins on a single platform by mass spectrometry compared with current methods.

On a high-resolution quadrupole orbitrap, parallel reaction monitoring (PRM) can acquire full MS/MS spectra with high specificity and separate co-isolated interference ions from target peptides with a tolerance of approximately 10–20 ppm [31]. Technically, PRM can be performed with or without labels. A label-based method can be used to determine the absolute and relative levels of proteins in samples by spiking them with heavy isotope-labeled synthetic peptides, analogous to targeted endogenous peptides. In contrast, the label-free method is straightforward and suitable for hyper-multiplexed targeted proteomics for semi-quantitative measurements [32]. For label-free PRM approaches, single or multiple heavy isotope-labeled reference peptides (LRPs) can help normalize the peak areas of all endogenous target peptides, assess the performance of the system, and correct for variations in retention time shifts between LC runs [33-34].

In this study, dimethyl-labeled proteomics and label-free PRM were used to develop a systematic proteomics approach that allows simultaneous and targeted quantification on a high-resolution Q-Exactive orbitrap MS platform. Using this method, I examined the dynamic changes in proteins during microglial activation, induced by a single effector or a combination of factors. Our approach enabled the quantification of over 450 peptides in a single run by label- targeted analysis. Thus,

systematic proteomics identifies intracellular and intercellular proteins, the expression of which is regulated significantly during activation.

Based on these data, the construction and analysis of a pathway network model of proteins can reveal latent pathways that are associated with neurodegenerative diseases. Furthermore, this systematical quantification platform has great potential for large-scale targeted analysis.

Chapter I

Subtitle: In-depth characterization of the secretome of mouse CNS cell lines with LC-MS/MS

METERIALS AND METHODS

Cell culture and conditioned media collection

The 3 cell lines were cultured in 100-mm dishes with DMEM, supplemented with 10% inactivated FBS and 100 U/mL of penicillin-streptomycin, at 37°C with 5% CO_2. Then, the putatively secreted proteins were purified from the conditioned media (CM). Briefly, 1 x 10^6 cells were washed with PBS and incubated in serum- and phenol red-free media for 24 h. The CM was collected and centrifuged at 3000 rpm for 3 min to remove intact cells. After being passed through a 0.22-μm membrane, the CM was concentrated on an Amicon Ultra-centrifugal filter (EMD Millipore, Billerica, MA, USA). Protein concentration was measured using a BCA reducing agent compatibility assay kit (Thermo Scientific, Rockford, IL, USA). All procedures were performed in biological triplicates for each cell line.

Protein digestion and desalting

Proteins were digested by FASP as described with some modifications [6, 35].

Briefly, proteins (200 μg) were mixed with SDT buffer (4% SDS and 0.1 M DTT in 0.1 M Tris-HCl, pH 7.4) and loaded onto a 30 K spin filter (EMD Millipore, Billerica, MA, USA). Buffer was exchanged with UA solution (8 M urea in 0.1 M, pH 8.5) by centrifugation. Reduced cysteines were alkylated with IAA solution (0.05 M iodoacetamide in UA solution) for 30 min at room temperature (RT) in the dark. Additional buffer was exchanged with 40 mM ammonium bicarbonate. Protein digestion was performed at 37°C overnight with trypsin [enzyme-to-substrate ratio (w/w) of 1:100]. The resulting peptides were acidified with 1% TFA and desalted using homemade C18 Stage-Tips as described [6, 35]. Desalted samples were lyophilized in a speed-vacuum centrifuge and stored at -80°C.

Mass spectrometry analysis

The peptides were analyzed by LC-MS/MS on a Nanoflow Easy-nLC 1000 (Proxeon Biosystems, Odense, Denmark), coupled to a Q-Exactive mass spectrometer (Thermo Scientific, Bremen, Germany) through a nano-electrospray ion source, as described with some modifications [35]. Desalted peptides (1 μg) were separated on a 2-column system with a trap column (100 Å, 3-μm particle, 75 μm x 2 cm) and an analytical column (100 Å, 1.8-μm particle, 50 μm x 15 cm) with 180-min gradients from 5% to 30% acetonitrile and analyzed on the mass spectrometer. The samples were analyzed in data-dependent acquisition mode to acquire the mass spectra, and the MS1 spectra were measured at a resolution of 70,000 and an AGC target of $3e^6$. I selected the 20 most abundant ions with an isolation window of 2 m/z.

The selected ions were fragmented by HCD with a normalized collision energy of 27. The maximum ion injection time for the analysis scan and MS/MS scan were 20 ms and 60 ms, respectively. Each sample was analyzed in triplicate for technical replications.

Database search using MaxQuant

Raw files were processed in MaxQuant (version 1.3.0.5) [36] and using the Andromeda search engine [37], based on the IPI mouse database (version 3.87 and 59,534 entries), including forward and reverse proteins sequences and common contaminants. MS/MS searches were performed with the following parameters: a 6-ppm main search tolerance, a 20-ppm first search tolerance, carbamidomethylation as a fixed modification, and oxidation of methionine and protein N-terminal acetylation as variable modifications. The false discovery rate (FDR) for all peptides and protein identifications was set to 0.01. Label-free quantitation (LFQ) was performed in MaxQuant as described [38]. Briefly, the normalized spectral protein intensity (LFQ intensity) from MaxQuant was used as the protein intensity. Quantitation schemes are described in Figure 1-1.

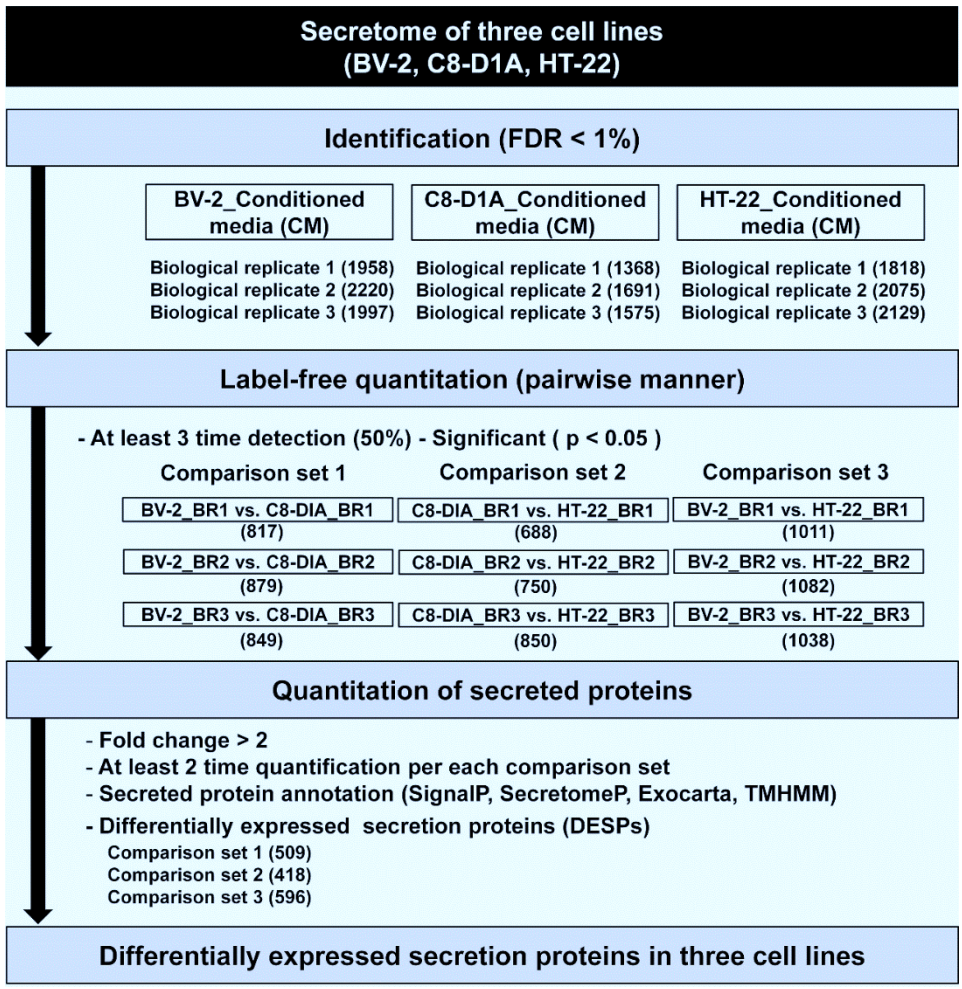

Figure 1-1. Detailed flowchart of the proteomic approach, label-free quantitation, and data analysis

Database search using PEAKS 7

To rescue unassigned MS/MS spectra resulted from MaxQuant search, I used the PEAKS 7 program that search MS/MS peaks by *de novo* sequencing, which generates amino acid sequences from the tandem mass spectrum of peptides without a database. After I extracted unassigned MS/MS spectra using MSconvert, spectrum files that were converted to mzXML were re-analyzed using PEAKS 7. The standard workflow PEAKS, comprising *de novo* sequencing, PEAKS DB, PEAKS PTM, and SPIDER, was performed to analyze data with high sensitivity and accuracy [39].

First, in the *de novo* step, the PEAKS algorithm [39] was used to perform *de novo* sequencing for 604,364 MS/MS spectra. To filter the *de novo* sequencing results, the threshold of average local confidence (ALC) score was set to 50%. I then performed a *de novo* sequencing-assisted database search with PEAKS DB against the IPI mouse database (ver. 3.87, 59,534 entries). The search parameters were as follows: trypsin as the enzyme, allowing semi-tryptic cleavage; 3 missed cleavages; precursor mass error tolerance of 15 ppm; fragment mass error tolerance of 0.02 Da; carbamidomethylation (C) as a fixed modification; oxidation (M), pyro-glu (Q and E), phosphorylation (S, T and Y), deamidation (N and Q), and acetylation of the peptide's N-terminus as variable modifications. The search results were filtered by a threshold score at a 0% FDR at the level of peptide-spectrum match (PSM), peptide, and protein to obtain only precise and confident data [40] (corresponding to a peptide score of -10logP $\geq$ 30.7 and protein score of -10logP $\geq$ 20).

An additional search for unexpected modifications was performed using the PEAKS PTM algorithm against the Unimod database [39]. Finally, a homology search,

based on de novo sequencing tags, was performed using the SPIDER algorithm to identify peptides that resulted from nonspecific cleavages or amino acid substitutions.

Label-free quantitation (pairwise analysis)

For relative quantitation in pairwise manner, I applied the label-free quantitation (LFQ) approach by comparing the normalized intensities of pairwise proteins. The identified proteins from 3 samples were paired to 3 groups (BV-2 vs. C8-D1A, C8-D1A vs. HT-22, and BV-2 vs. HT-22). The normalized intensity of each protein was calculated using MaxQuant (ver. 1.3.0.5), and the intensities were log-transformed (log_2) in Perseus (ver. 1.4.0.20).

A total of 9 comparison sets (3 biological replicates per cell line) were analyzed using LFQ. First, I required a minimum of 3 valid values in one comparison set, which comprised 6 technical replicates (50% detection). Missing values were replaced with expected values in Perseus using a normal distribution (width = 0.3; shift = 1.8) of the intensity of the proteins. To determine the quantified proteins, paired t-test was used with a Benjamini-Hochberg FDR value of 5%. Differentially expressed proteins (DEPs) with 2-fold intensity changes in at least 2 of 3 biological replicates were assumed to be part of the secretome by the prediction tools. Finally, the DEPs annotated as part of the secretome were ultimately considered differentially expressed secretion proteins (DESPs).

Statistical analysis

Statistical analysis was performed using Perseus as described [38]. After log_2

transformation of the protein intensities, paired *t*-test was applied to examine the differences in protein intensities between samples. The significance of outliers was calculated by multiple hypothesis testing (Benjamini Hochberg correction), with a threshold value of 0.05.

In comparing pairwise samples for label-free quantitation, I processed the 3 cell lines in cluster with ANOVA. Normalized LFQ intensities of the 3-cell-line secretome were categorized into 3 groups and filtered rows, based on proteins that had more than 5 valid values out of total 9 replicates (3 technical and 3 biological replicates). Following the replacement of missing values from the normal distribution parameterized with 0.3 width and 1.8 down shifts, the proteins were differentiated by ANOVA at a Benjamini-Hochberg FDR of less than 0.05. After normalization of the intensities value with z-score, hierarchical clustering was performed using Euclidean distance, complete linkage, and 1000 clusters as parameters in Perseus.

Principal component analysis (PCA) was performed to confirm the statistically correlated variables between cell lines. All lists of proteins and LFQ intensities were imported into Perseus, and the proteins categorized to pairwise groups. Proteins that contained at least 3 valid values of normalized intensities were filtered, and missing values were replaced with putative values from the normal distribution. Finally, a PCA graph was drawn in Perseus with non-category enrichment of components.

Secretome analysis

To confirm the putative secreted proteins, a bioinformatics analysis was performed with SignalP 4.1 (http://www.cbs.dtu.dk/services/SignalP/), SecretomeP 2.0 (http://www.cbs.dtu.dk/services/ SecretomeP/), and TMHMM server 2.0 (http://www.cbs.dtu.dk/services/TMHMM/) and by comparison with the Exocarta database (http://www.exocarta.org). The FASTA form of identified proteins was exported and used for this analysis. These protein lists were submitted to the SignalP 4.1 server. The prediction parameters were set up as follows: eukaryotes as the organism group and a cutoff value of more than 0.45. To determine whether the proteins were non-classically secreted, the SecretomeP 2.0 server was used, with mammal as organism and a threshold score of 0.5 as parameters. For the prediction of transmembrane helices in the proteins, TMHMM server 2.0 was used with the FASTA form. Further, I compared our dataset with exosomal proteins from Exocarta.

Bioinformatics

The gene ontology of analyzed proteins was explicated using the DAVID bioinformatics tool (http://david.abcc.ncifcrif.gov/) and UniprotKB database (http://www.uniprot.org/). Pathways were analyzed using the KEGG and Panther databases [41].

Western blot analysis

To confirm the contamination of CM, whole-cell lysates were prepared by lysis in RIPA buffer (8 M urea, 1 mM EDTA, 1% NP-40, Tris-Cl pH 7.4, and 150 mM NaCl), supplemented with a protease inhibitor cocktail (PMSF). The concentration of the whole-cell lysates and CM was determined by BCA assay. Equal amounts of proteins (30 μg) in the whole-cell lysates and CM were separated by 12% SDS-PAGE and transferred to PVDF (polyvinylidene fluoride) membranes (Hybond-P, GE Healthcare). After blocking the membranes with 5% BSA solution for 2 hours, they were incubated with the primary β-actin antibodies (1:1000 dilution, Sigma Aldrich, Louis, MO, USA) overnight at 4°C.

To validate results of label-free quantitation analysis, four proteins were analyzed in CMs of the 3 cell lines by western blot as described below. The primary antibodies were against peroxiredoxin (Prdx2, 1:1000, Santa Cruz Biotechnology, Santa Cruz, CA, USA), carboxypeptidase E (Cpe, 1:1000, Santa Cruz Biotechnology,

Santa Cruz, CA, USA), β-catenin (Ctnnb1, 1:1000, Santa Cruz Biotechnology, Santa Cruz, CA, USA), and *β*-filamin (Flnb, 1:1000, Santa Cruz Biotechnology, Santa Cruz, CA, USA).

The membranes were washed 5 times with TBS-T (Tris-buffered saline and Tween 20) for 1 hr and incubated with horseradish peroxidase-conjugated secondary antibodies for 2 hr at room temperature (goat anti-mouse IgG-HRP) (1:5000 dilution for each antibody, Santa Cruz Biotechnology, Santa Cruz, CA, USA). After being washed with TBS-T for 1 hr, the membranes were developed with a mixture of detection solution (West-Q Chemiluminescent Substrate Kit-*plus*, GenDEPOT, Barker, TX, USA) and quantified on an image reader (LAS-4000, Fujifilm, Japan). The resulting western blot images were scanned using LAS-4000 mini software (Fujifilm, Japan).

RESULTS

Confirmation of conditioned media samples

To evaluate interference by intracellular proteins within the secretome of the 3 cell lines, I compared the distribution of β-actin between total cell lysates and CMs. β-actin signal was only detected in the lysates, confirming high quality of secreted proteins (Figure 1-2A). To assess reproducibility of our secretome, 3 biological replicates of collected CMs were examined by high-resolution mass-spectrometry with technical triplicates.

Putative secreted proteome

After a total of 1,950,047 MS/MS scans were accumulated, 29,724 unique peptides that matched with 2795 protein groups were identified at an FDR of less than 1% by MaxQuant analysis (Figure 1-2B). Of these protein groups, 1975 (71%) were common to all 3 cell lines. Total identified proteins were subjected to sequential analysis with SignalP, SecretomeP, Exocarta, and TMHMM. Of 2795 proteins, 2125 proteins (76%) were predicted to be secretion or shedding proteins by the classical secretion pathway or a non-classical mechanism in all 3 cell lines (Figure 1-2B, and Figure 1-3 and 1-4). This subset of proteins was considered to be the putative secretome in the 3 cell lines.

Rescue of non-annotated MS/MS data

I searched for non-annotated peptide spectra derived from MaxQuant result using PEAKS 7.0, based on a de novo sequencing-assisted database search. From 604,364 unassigned MS/MS spectra, 95,145 peptide-spectrum matches (PSMs) that corresponded to 20,756 peptides and 1804 protein groups were identified at an FDR of 0% at the PSM, peptide, and protein levels, whereas 89,095 PSMs comprised 130 types of post-translational modification. Notably, I newly identified 302 proteins that were undetected at first search with MaxQuant, 231 of which were determined to be secreted proteins using the bioinformatics tools (Figure 1-2C).

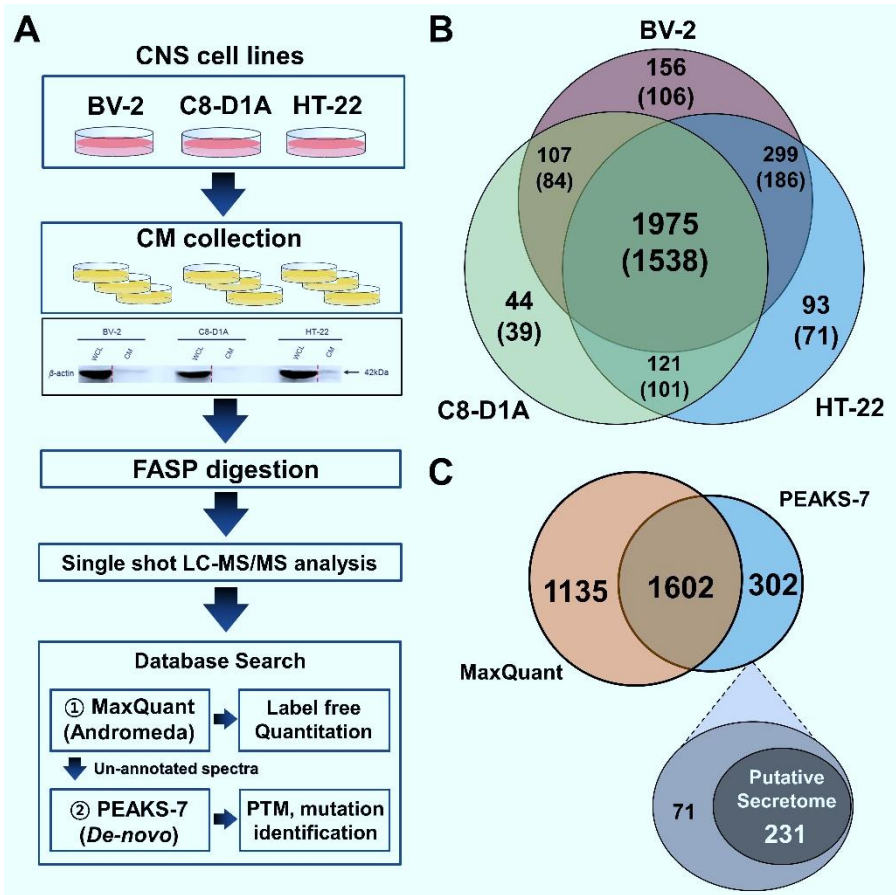

Figure 1-2. Proteomic analysis of secreted proteins from three murine CNS cell lines in conditioned media.

(A) Workflow of proteomic experiments. Illustration below CM collection is immune blot validation, describing that the CM does not contain contaminating intracellular proteins. (B) Venn diagram of all identified proteins in the 3 cell lines. The numbers in parentheses show the predicted secreted proteins. (C) Venn diagram of identified proteins from MaxQuant or PEAKS-7. To compare the two sets, the protein accession number was converted to the gene symbol. A total of 302 protein groups were identified with *de novo* sequencing.

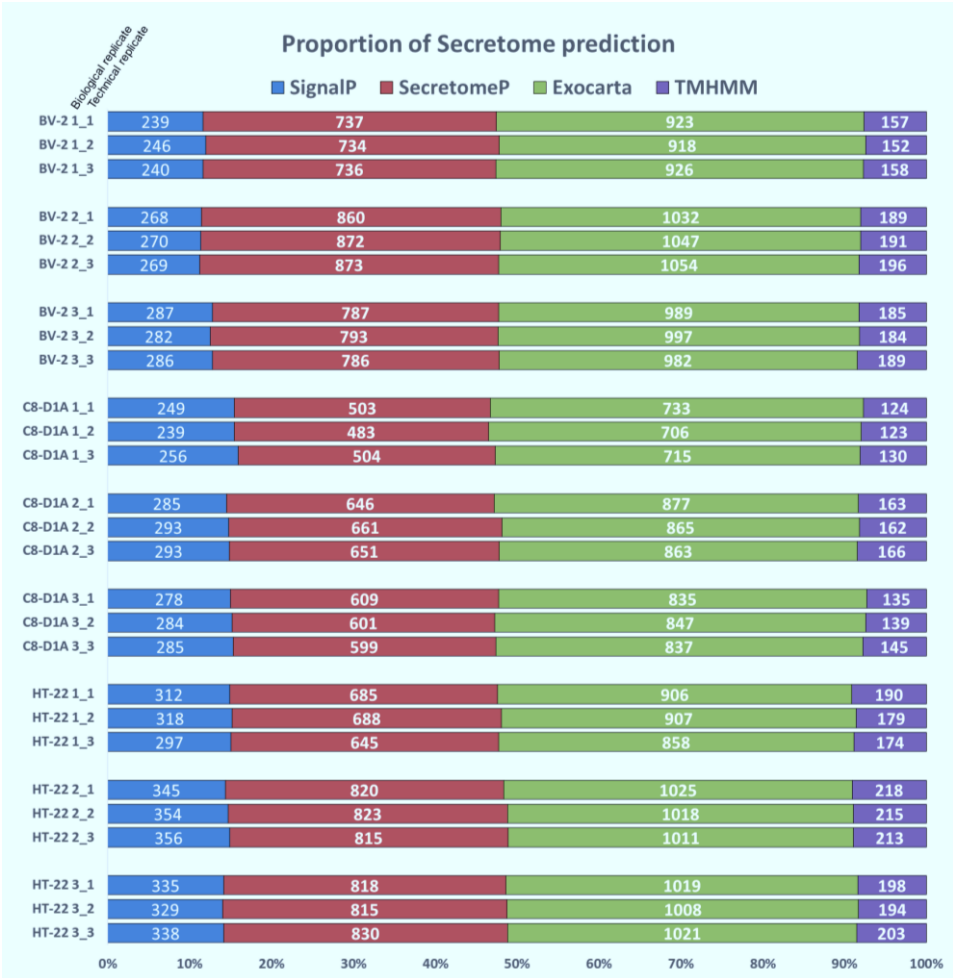

Figure 1-3. Distribution of putative secreted proteins predicted by bioinformatics tools

Identified proteins from each biological and technical replicate were subjected to bioinformatics analysis using the prediction tools SignalP, SecretomeP, Exocarta, and TMHMM. The number in each box indicates the resulting amount of putative secreted proteins from the tools.

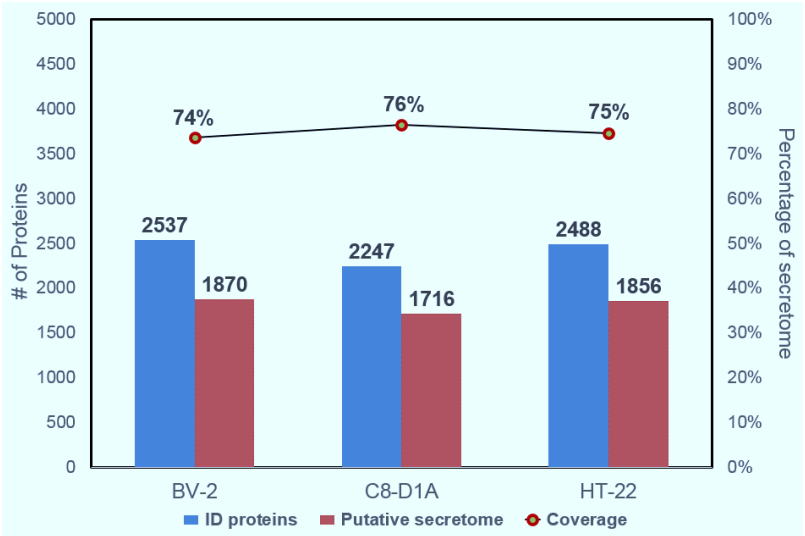

Figure 1-4. Proportion of putative secreted proteins

Number of identified proteins and putative secreted proteins are shown in the graph. The red dots indicate the percentage of predicted secretion proteins versus identified proteins in each cell line.

Characterization of secretome data

In this study, 87.69% of protein groups were classified by a minimum of 2 unique peptides. Most proteins were identified with at least 25% sequence coverage (Figure 1-5A). In addition, 60% of our 3-cell line secretome was identified with at least 5 distinct peptides (Figure 1-5B). The average Andromeda score of the peptides was 99.66 (Figure 1-5C). Moreover, the absolute mass deviation ranged from 0.65 ppm to 0.69 ppm for the analyzed peptides in the replicates. All identified proteins ranged in molecular weight from 5 kDa to 3906 kDa (Figure 1-5D).

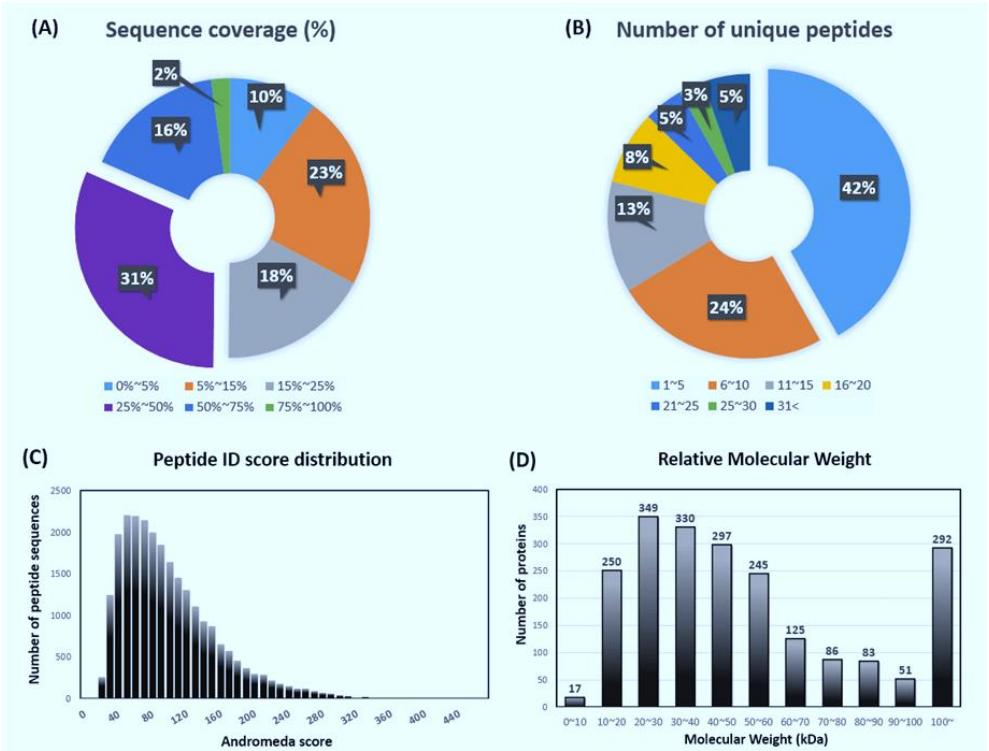

Figure 1-5. Characterization of proteomic data

(A) Sequence coverage of the identified proteins in the total proteome of the 3 cell lines. (B) Relative proportions of the number of unique peptides used for identification. (C) Histogram of distribution of Andromeda scores of identified peptides. (D) Relative molecular weights of the identified peptides.

The technical and biological variations were measured by cross-correlation analysis with protein intensities for the replications. I outlined the correlation of the intensities for all of replicates (Figure 1-6). The R^2 value of the technical replicates varied from 0.84 to 0.98. In addition, the average R^2 values of the biological replicates were 0.94, 0.86, and 0.92 in BV2, C8-D1A, and HT-22, respectively.

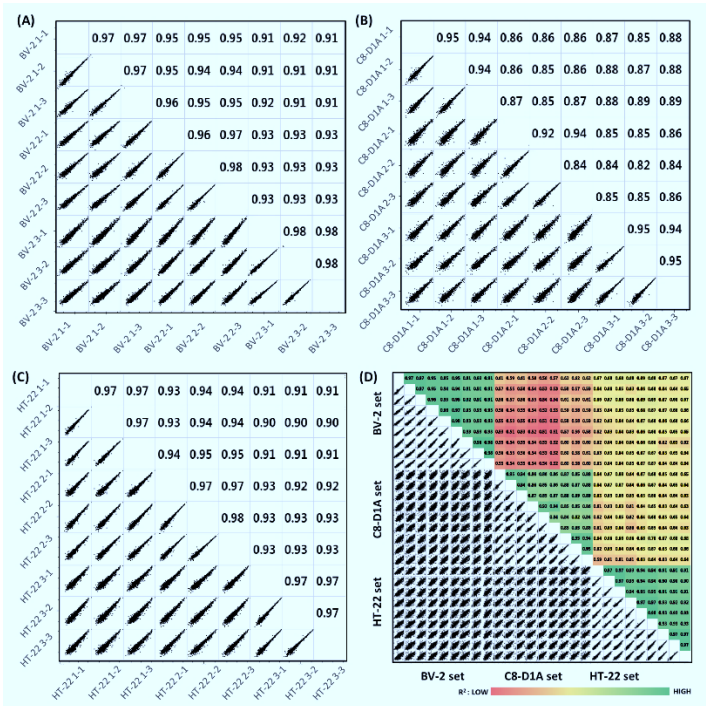

Figure 1-6. Reproducibility between proteomics analysis

Scatterplot of reproducibility between biological and technological triplicates, based on the coefficient of determination (R^2) in BV-2 (A), C8-D1A (B), and HT-22 (C) cells, respectively. (D) Total correlations between each cell line.

After log_2 tranformation, the median coefficient of variation (CV) values for the abundance of proteins in the BV2 cell line were 0.49%, 0.43%, and 0.41% within technical replicates and 1.05% between biological replications. In addition, the median CVs for the C8D1A cell line were 0.56%, 0.57%, and 0.51% within technical replications and 1.49% across biological replicates. The median CVs for the HT22 cell line were 0.48%, 0.42%, and 0.45% within technical replicates and 1.04% between biological replicates (Figure 1-7). By the results, I determined that the technical or biological variability was low, demonstrating that our experimental procedures accurately identified and quantified the proteins.

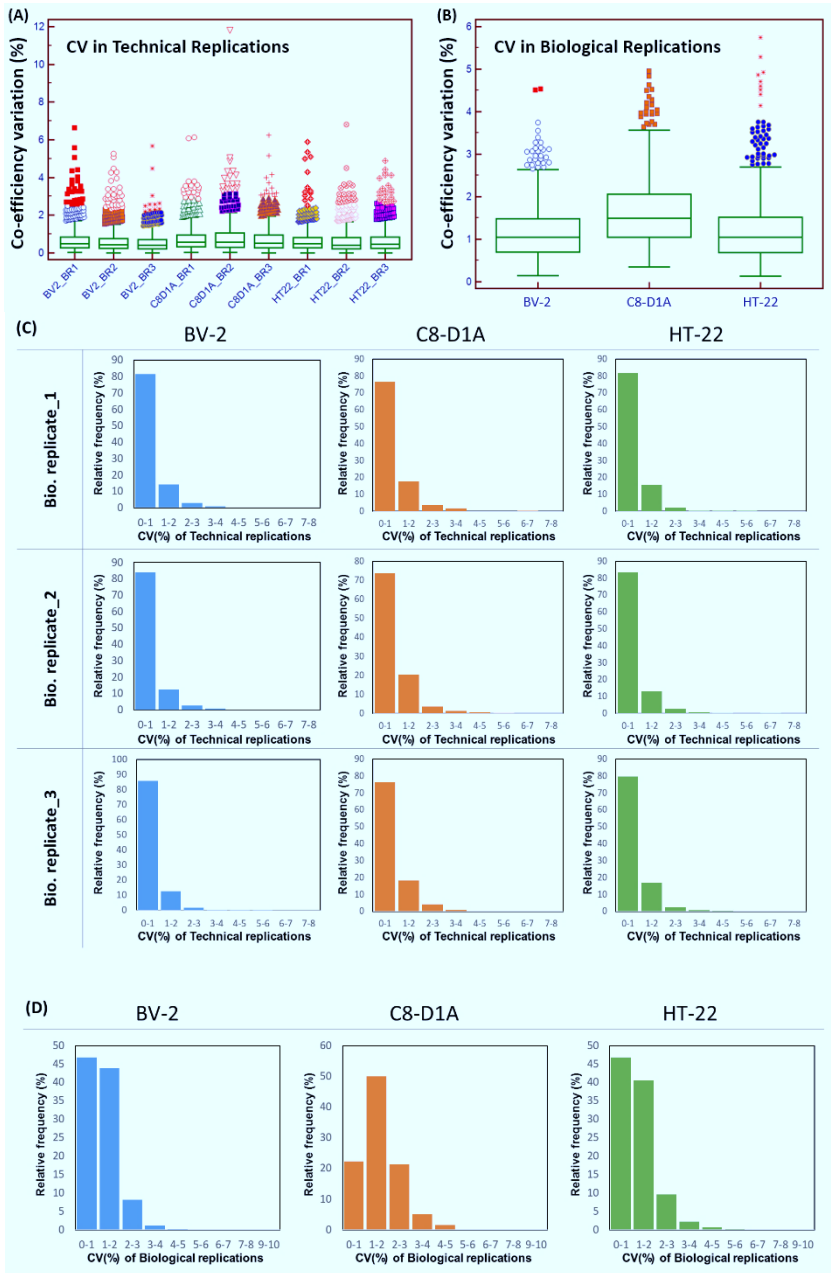

Figure 1-7. Precision of proteomic approaches

Intensity values of label-free quantitation by MaxQuant were transformed to base-2 logarithms, and the coefficient of variation (CV) values in the technical (A, C) and biological replicates (B, D) in the 3 cell lines were calculated, as shown in the box plots and histogram, respectively.

Label-free quantification of secretome for three cell lines

To define the CNS cell line-specific secretome, I performed label-free quantitation (LFQ) and a bioinformatics analysis using several data improvement tools [42]. First, I performed principal component analysis (PCA) to compare the proteomes of the CNS cell lines. The distance between the technical and biological replicates was much smaller than that between cell types, demonstrating that the secretome signatures of the 3 cell lines led to robust segregation (Figure 1-8).

The secreted proteins were quantified in pairwise manner (Figure 1-1). As a result, application of the quantitation criteria (50% detection and p-value < 0.05) in comparison sets 1 (BV2 versus C8D1A), 2 (C8D1A versus HT22), and 3 (BV2 versus HT22) yielded 848, 763, and 1044 quantified proteins, respectively (Figure 1-9A). Further, these lists were filtered by analysis using SignalP, SecretomeP, Exocarta, and TMHMM. After removing the unannotated proteins using the bioinformatics tools and filtering with criteria (2-fold change in intensity between at least 2 biological replicates), 509, 418, and 596 proteins were considered as differentially expressed secretion proteins (DESPs) in 3 comparisons, respectively (Figure 1-9B).

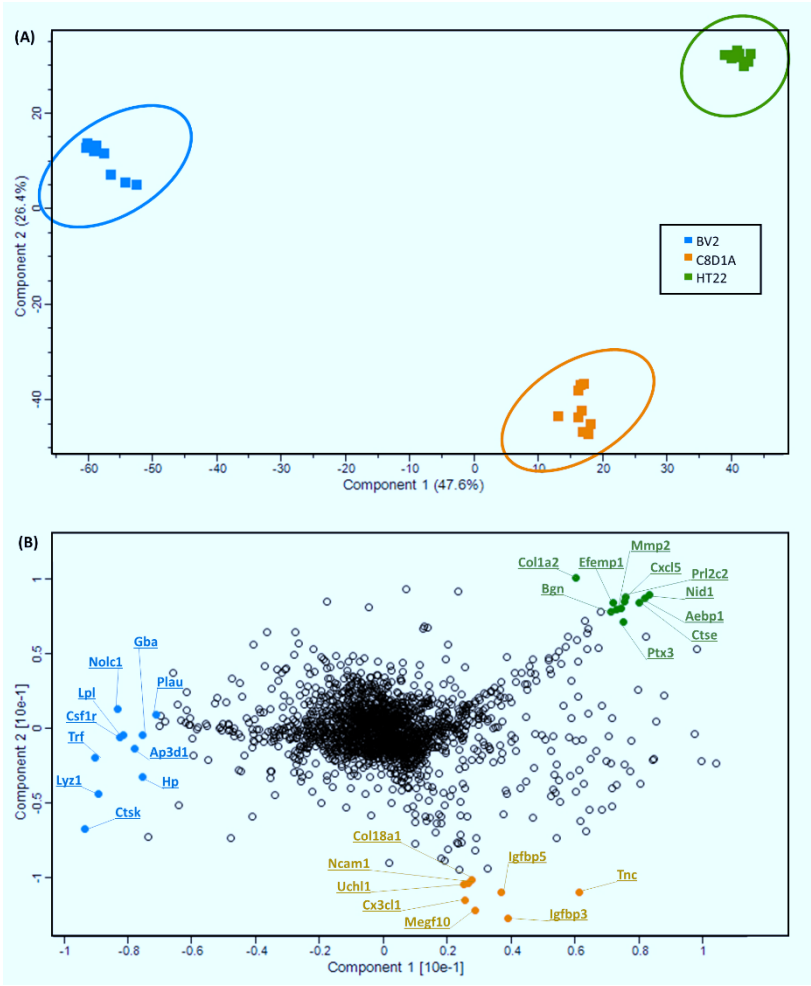

Figure 1-8. Principal component analysis (PCA)

(A) PCA of protein expression values in the cell lines. Components 1 and 2 account for 74% of the data variation. (B) Proteins driving the separation are colored according to the PCA plot above.

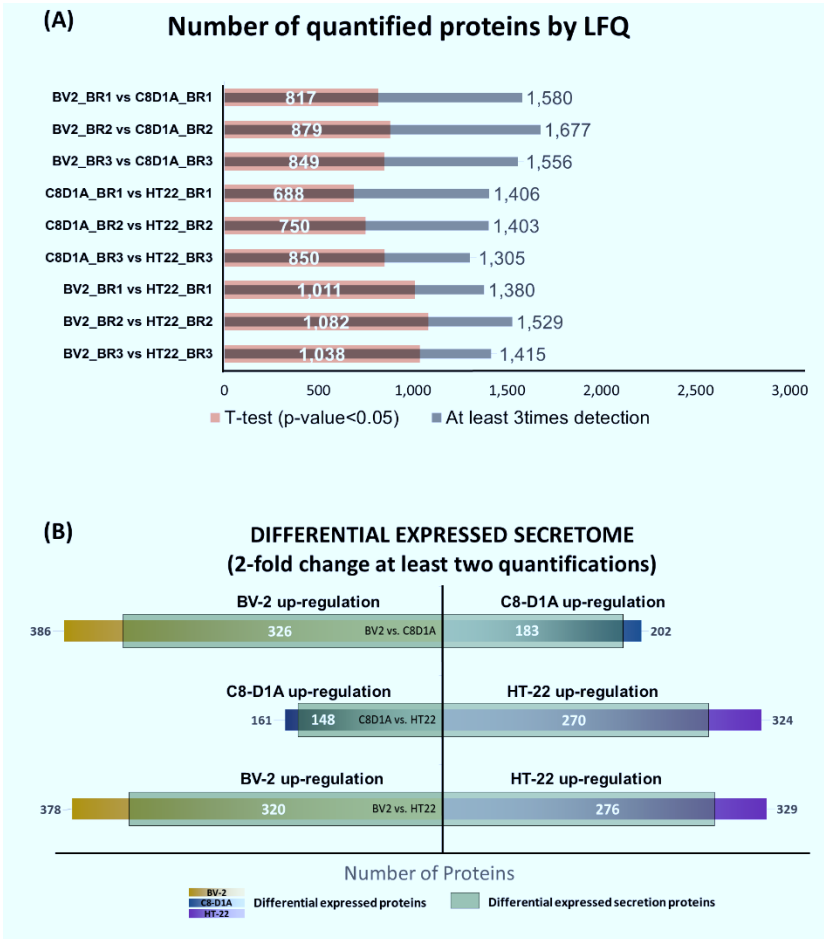

Figure 1-9. Label-free quantitation of identified secretion proteins

(A) Number of proteins quantified based on 50% detection and p-value < 0.05 in the 9 comparison sets. (B) Number of differentially expressed secretion proteins (DESPs) quantified using the filter criteria (2-fold change in at least 2 of 3 biological replicates) in the 3 comparison sets.

Clustering analysis and validation

The LFQ values of the proteins that were identified from the 3 cell lines were analyzed by ANONA to determine the trends of changes in abundance in the secretome. The heat map identified proteins with statistically significant changes between cell lines (FDR < 0.05) after ANOVA, z-score normalization, and hierarchical clustering. The heat map and hierarchical clustering indicated that cells with disparate characteristics can be distinguished by their specific secreted proteome patterns. Particularly, two-way hierarchical clustering created 3 clusters of cell types and 6 clusters of protein expression patterns in the 3 cell lines (Figure 1-10). The clustering results showed clear separation of the cell lines and the correct grouping of technical and biological replicates in each cell line. Furthermore, western blot analysis for validation of the quantified proteins showed the same aspects as the LFQ values of all correlated protein (Figure 1-11).

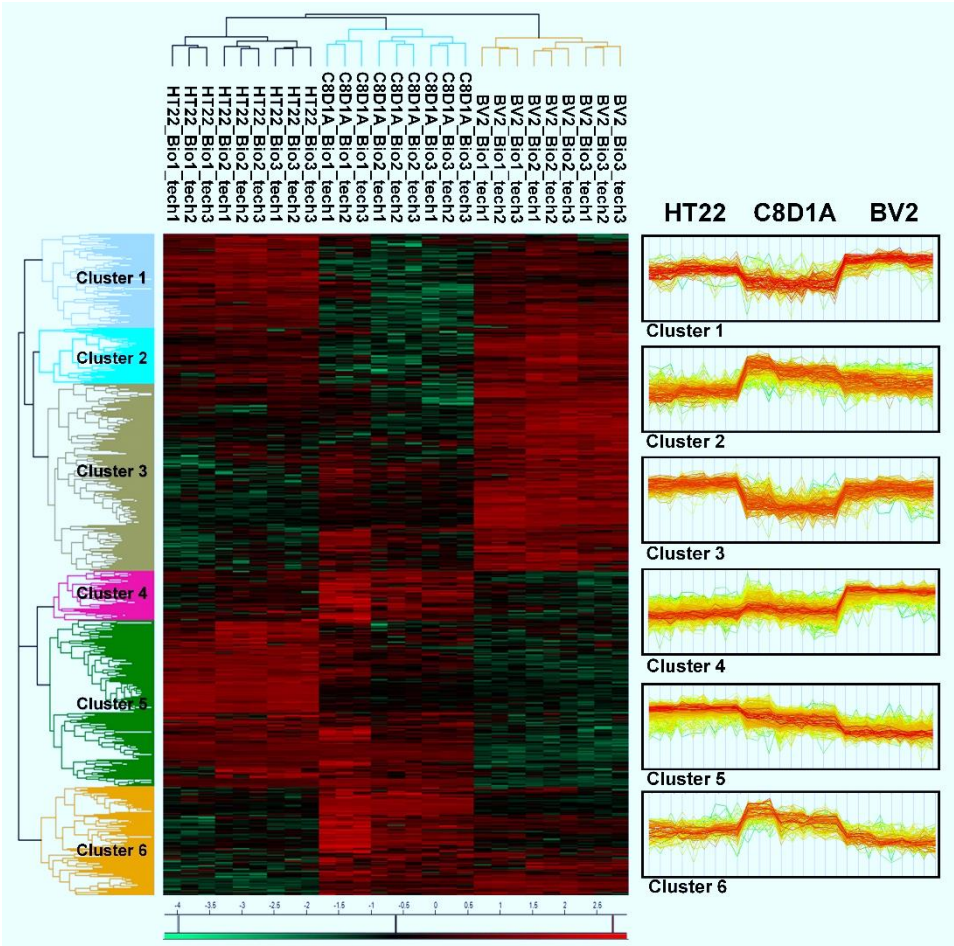

Figure 1-10. Cluster analysis.

Heat map and hierarchical clustering of differentially expressed secretion proteins (DESPs) after ANOVA of secreted proteins in the 3 cell lines. The six types of hierarchical clusters show that the level of DESPs can be classified based on their specific patterns.

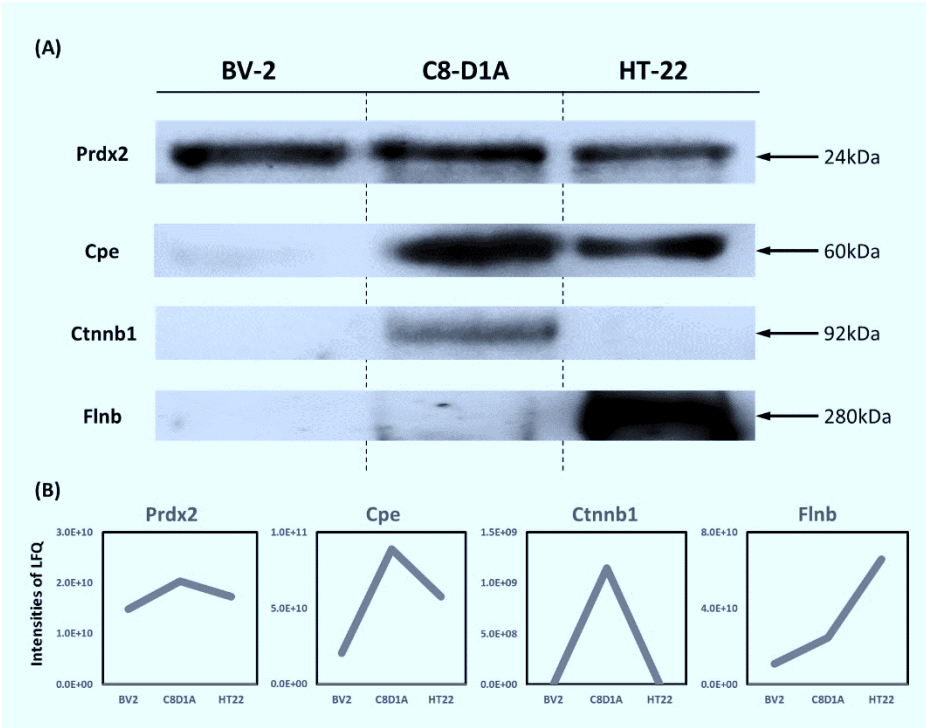

Figure 1-11. Western blot for validation of label-free quantitation

(A) Immunoblotting for validation of label-free quantitation data. Four randomly selected proteins were subjected to western blot analysis. (B) The graphs describe the patterns of the intensities of proteins corresponding to the results of the immune blots.

Gene ontology and pathway analysis

To determine the altered biological processes and pathways that might characterize the 3 cell lines, I analyzed the DESPs with regard to GO terms and KEGG pathway, based on the category of protein expression clustering (Table 1-1 and Figure 1-12). Notably, the 3 cell lines displayed secreted protein clusters that

were typical of the original functions of the cell type [5]. For example, clusters of highly expressed proteins in HT22 cells (clusters 3 and 5) were enriched for the GO BP terms “Cellular protein localization” (p-value < 1.13E-36) and “Cell adhesion” (p-value < 4.5E-08). Clusters of highly expressed proteins in C8D1A cells (clusters 2 and 6) were enriched for the GO BP terms “Generation of precursor metabolites and energy” (p-value < 3.58E-06) and “Extracellular structure organization” (p-value < 1.46E-04). Finally, clusters of highly expressed proteins in BV2 cells (clusters 1 and 4) were enriched for the GO BP terms “Vesicle-mediated transport” (p-value < 1.00E-03) and “Translation” (p-value < 1.13E-36).

Interestingly, KEGG pathway analysis showed that DESPs are closely related to functions that are mediated by neurons, astrocytes, and microglia, according to each expression cluster (Table 1-1). For example, many proteins in cluster 4 were enriched in lysosomes (32 proteins), which are linked the function of microglia as immune defense cells in the CNS [2-3, 5]. Also, several proteins in cluster 5 that were enriched with regard to focal adhesion (28 proteins), ECM-receptor interaction (16 proteins), and adherens junction (8 proteins) are involved in synaptic transmission, plasticity, and development in neurons [43]. In cluster 2, many glycolytic proteins were enriched in glycolysis/gluconeogenesis (10 proteins) and the citrate cycle (7 proteins), which are associated with astrocyte-meditated brain energy metabolism [1-3].

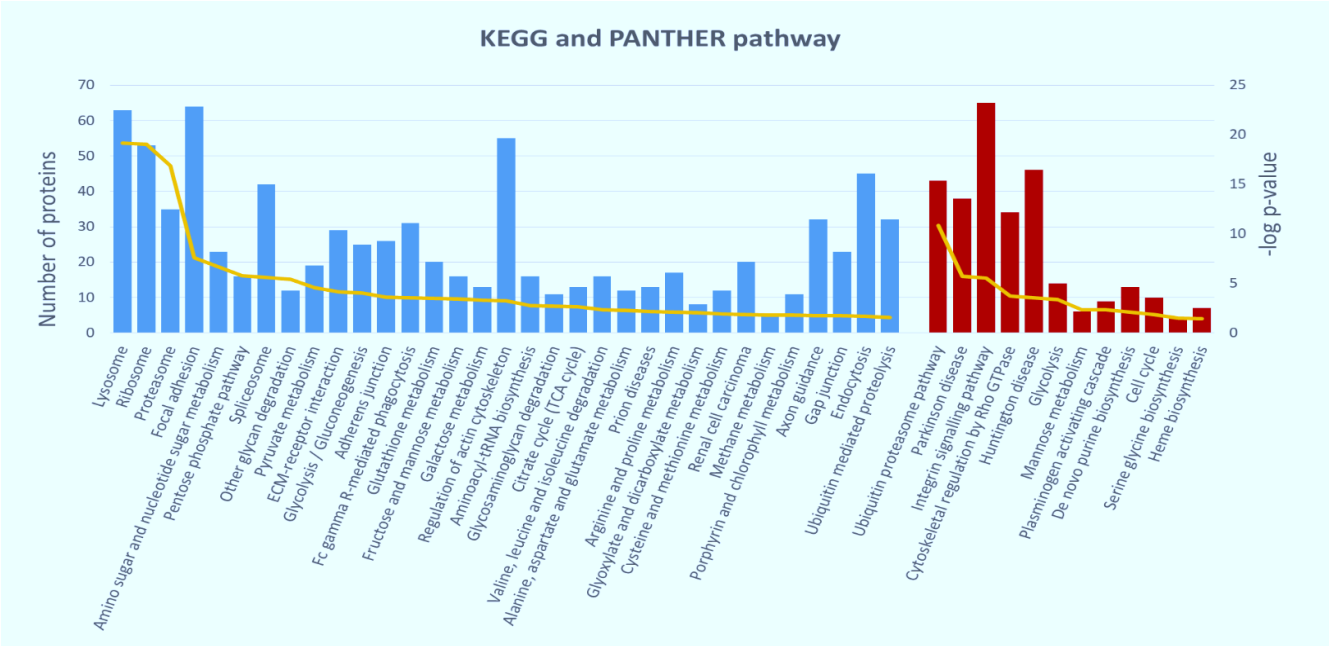

Figure 1-12. Pathway analysis

Pathway analysis with KEGG and PANTHER databases was performed against putative secreted proteins that were significant by ANOVA between secretome of the 3 cell lines. Number of proteins is annotated against their functions. Yellow line indicates the negative logarithm p-value of the Benjamini-Hochberg FDR; hence, the annotated pathways can be significant

Table 1-1. Summary of GO terms and KEGG pathway analysis

TOP5 of GO BP terms	Count	p-value	TOP5 of KEGG Pathway	Count	p-value
Cluster 1					
Translation	12	8.01E-06	Lysosome	8	6.60E-05
Protein folding	7	1.94E-04	Aminoacyl-tRNA biosynthesis	5	4.48E-04
tRNA aminoacylation for protein translation	5	2.37E-04	One carbon pool by folate	3	8.26E-03
Cellular protein localization	9	8.13E-04	Oocyte meiosis	5	1.74E-02
Vesicle-mediated transport	11	1.00E-03	Tight junction	5	2.83E-02
Cluster 2					
Generation of precursor metabolites and energy	15	3.58E-06	Glycolysis/Gluconeogenesis	10	6.032E-06
Cellular component morphogenesis	17	5.78E-06	Citrate cycle (TCA cycle)	7	2.516E-05
Coenzyme metabolic process	11	9.47E-06	Pyruvate metabolism	7	1.31E-04
Alcohol catabolic process	8	1.32E-05	Arginine and proline metabolism	7	5.52E-04
Cofactor metabolic process	12	1.36E-05	Fructose and mannose metabolism	6	7.14E-04
Cluster 3					
Cellular protein localization	14	1.13E-36	Proteasome	13	4.001E-12
Intracellular transport	16	4.68E-09	Terpenoid backbone biosynthesis	4	1.24E-03
Vesicle-mediated transport	15	5.04E-06	Valine, leucine, and isoleucine degradation	4	3.59E-02
Ribonucleoside monophosphate biosynthetic process	4	4.90E-05	Lysosome	6	4.00E-02
Protein localization	19	1.06E-04			
Cluster 4					
Translation	58	1.13E-36	Ribosome	33	2.574E-25
Translational initiation	11	4.68E-09	Lysosome	32	8.282E-20
tRNA aminoacylation	9	5.04E-06	Other glycan degradation	8	4.297E-07
Regulation of cytoskeleton organization	11	6.00E-05	Glycosaminoglycan degradation	8	7.508E-06
RNA splicing	15	6.17E-05	Aminoacyl-tRNA biosynthesis	9	6.982E-05
Cluster 5					
Cell adhesion	31	4.5E-08	Focal adhesion	28	2.68E-13
Vasculature development	20	7.91E-08	ECM-receptor interaction	16	1.48E-09
Blood vessel development	19	2.74E-07	Proteasome	7	1.07E-03
Extracellular structure organization	12	6.00E-05	Adherens junction	8	2.90E-03
Regulation of cell-substrate adhesion	7	6.17E-05	Pathways in cancer	18	3.01E-03
Cluster 6					
Extracellular structure organization	7	1.46E-04	Proteasome	5	3.52E-04
Macromolecule catabolic process	12	6.90E-04			
Proteolysis involved in cellular protein catabolic	10	2.16E-03			
Cell adhesion	10	3.01E-03			
Proteolysis	14	3.16E-03			
Skeletal system development	6	1.85E-02			

DISCUSSION

This report is the most comprehensive secretome study of murine neurons, astrocytes, and microglia to date, in which 2795 protein groups and 2125 putative secreted proteins were identified in 27 LC-MS/MS runs. Hundreds of DEPs and DESPs were discovered in the cell lines by LFQ approach. In addition, many PTMs were identified in the secreted proteins. Moreover, our datasets in CMs of 3 cell lines have provided exclusively secreted proteins that have not been reported to date. Our proteome covered 58% to 94 % of proteome that obtained from previous proteomic studies using astrocyte, microglial, and neuron primary cells (Figure 1-13). It suggests that our data is appropriate for the applications as *in vitro* model alternative to *in vivo* model. Specifically, I identified 49 proteins, including cytokines, hormones, and growth factors, 27 of which were quantified as DESPs, implicating them as important modulators of communication between the nervous and immune systems (Table 1-2).

Further, extensive profiling with our secretome approach provided standard reference libraries of secreted proteins in cultured neurons, astrocytes, and microglia, which will be invaluable for future functional studies of the molecular mechanisms of cell-cell communication in the CNS and brain. Thus, our approach can be used to perform in-depth quantitative proteomics studies of brain functions and the pathogenesis of neurodegenerative diseases with deep proteomic coverage. Improving the quantitation of the DESPs, the HCD spectra libraries from our large secretome datasets can be used to perform targeted proteomic analyses, including multiple reaction monitoring (MRM) and parallelreaction monitoring (PRM),

constituting a valuable resource for targeted quantitative studies of proteins that are related to cell-cell communication and dysfunction in the response to many CNS pathologies.

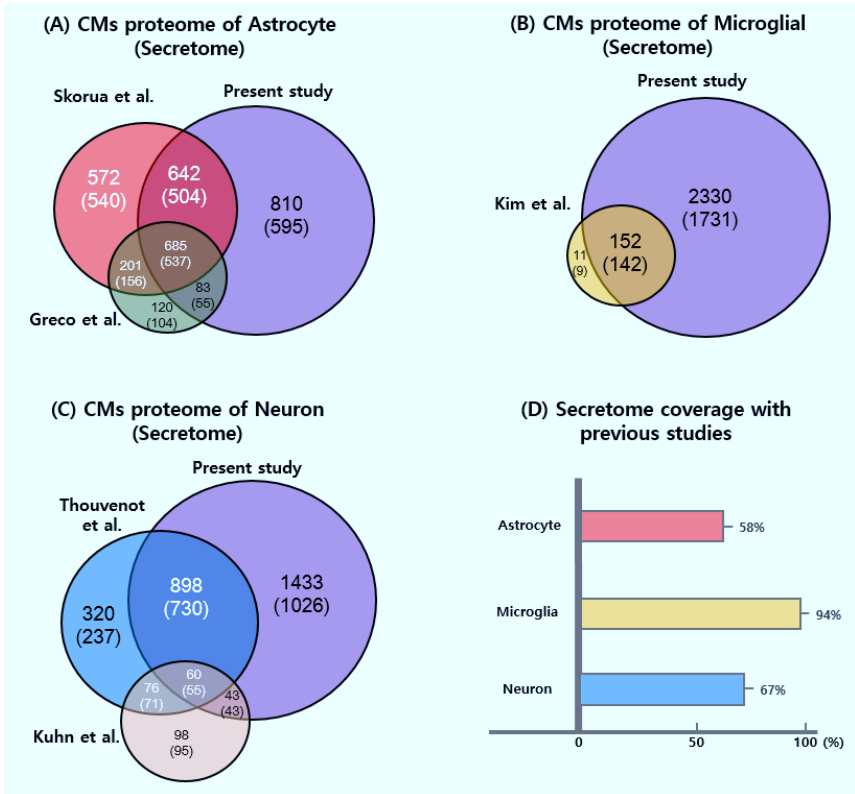

Figure 1-13. Comparison our data with others reported in the literature.

Identified and putative secreted proteins from our dataset were compared with other studies in CMs of (A) astrocyte [7, 44], (B) microglial [45], and (C) neuron [46-47]. The number in parentheses indicates number of putative secretion proteins analyzed by tools such as SignalP, SecretomeP, TMHMM, or Exocarta. (D) The secretome coverage indicates portion of secreted proteins identified from this study compared to previous proteomic studies of primary CNS cells.

Table 1-2. Summary of cytokines, hormones, and growth factors

Gene Name	Protein Name	Molecular Function	Set.1 (BV-2 vs. C8-D1A)	Set.2 (C8-D1A vs. HT-22)	Set.3 (BV-2 vs. HT-22)
Ccl5	C-C motif chemokine 5	Cytokine	-	-	-
Ccl4	C-C motif chemokine 4	Cytokine	BV2 on	-	BV2 on
Cxcl1	Growth-regulated alpha protein	Cytokine	-	HT22 on	HT22 on
Ccl3	C-C motif chemokine 3	Cytokine	BV2 up	-	BV2 on
Cxcl2	C-X-C motif chemokine 2	Cytokine	-	-	-
Cxcl10	C-X-C motif chemokine 10	Cytokine	-	HT22 on	HT22 up
Ccl7	C-C motif chemokine 7	Cytokine	BV2 up	HT22 up	HT22 up
Ccl8	C-C motif chemokine 8	Cytokine	-	HT22 on	HT22 on
Pf4	Platelet factor 4	Cytokine	BV2 on	-	BV2 on
Ccl20	Uncharacterized protein	Cytokine	-	-	-
Mif	Macrophage migration inhibitory factor	Cytokine	-	-	-
Cxcl5	C-X-C motif chemokine 5	Cytokine	-	HT22 on	HT22 on
Ccl2	C-C motif chemokine 2	Cytokine	-	HT22 up	HT22 up
Lif	Leukemia inhibitory factor	Cytokine	-	-	-
Csf3	Granulocyte colony-stimulating factor	Cytokine	-	-	-
Tnfsf9	Tumor necrosis factor ligand superfamily member 9	Cytokine	-	-	-
Spp1	osteopontin isoform 2 precursor	Cytokine	C8D1A up	C8D1A up	BV2 up
Aimp1	aminoacyl tRNA synthase complex-interacting multifunctional protein 1	Cytokine	-	-	-
Cx3cl1	Fractalkine	Cytokine	C8D1A on	C8D1A on	-
Nampt	Nicotinamide phosphoribosyltransferase	Cytokine	BV2 up	-	BV2 up
Csf1	Isoform 1 of Macrophage colony-stimulating factor 1	Cytokine	C8D1A up	HT22 up	HT22 up
Grn	granulins	Cytokine	BV2 up	HT22 up	-
Bmp1	bone morphogenetic protein 1 precursor	Cytokine	C8D1A on	C8D1A up	HT22 on
Igf2	insulin-like growth factor II isoform 1 preproprotein	Hormone	C8D1A on	C8D1A up	HT22 up
Prl2c2	Prolactin-2C2	Hormone	-	HT22 on	HT22 on
Stc2	Stanniocalcin-2	Hormone	-	-	-
Metrnl	Isoform 1 of Meteorin-like protein	Hormone	-	HT22 up	-
Inhba	Inhibin beta A chain	Hormone	-	-	-
Copa	Uncharacterized protein	Hormone	-	-	-
Gmfb	Glia maturation factor, beta	GF	-	-	-
Igf1	insulin-like growth factor I isoform 2 preproprotein	GF	-	C8D1A on	BV2 on
Btc	Probetacellulin	GF	-	-	-
Manf	Uncharacterized protein	GF	-	-	-
Timp1	Metalloproteinase inhibitor 1	GF	C8D1A on	C8D1A up	HT22 on
Hdgfrp3	Isoform 2 of Hepatoma-derived growth factor-related protein 3	GF	-	-	HT22 on
Gfer	FAD-linked sulfhydryl oxidase ALR	GF	-	-	-
Artn	Isoform 1 of Artemin	GF	-	-	-
Pdgfa	Platelet-derived growth factor alpha	GF	C8D1A on	C8D1A on	-
Hdgf	Hepatoma-derived growth factor	GF	-	-	-
Pdgfb	Platelet-derived growth factor subunit B	GF	-	-	-
Efemp1	Uncharacterized protein	GF	-	HT22 on	HT22 on
Nov	Protein NOV homolog	GF	C8D1A on	C8D1A on	-
Vegfa	Isoform L-VEGF-1 of Vascular endothelial growth factor A	GF	-	HT22 on	HT22 on
Figf	Vascular endothelial growth factor D	GF	-	-	-
Tgfb1	Transforming growth factor beta-1	GF	-	C8D1A up	-
Tgfb2	Transforming growth factor beta-2	GF	-	-	-
Efemp1	EGF-containing fibulin-like extracellular matrix protein 1	GF	-	HT22 on	HT22 on
Hgf	Isoform Long of Hepatocyte growth factor	GF	-	-	-
Thbs4	Thrombospondin-4	GF	-	-	-

Chapter II

Subtitle: Quantitative proteomics reveal temporal proteomic changes in signaling pathways during BV2 mouse microglial cell activation

METERIALS AND METHODS

Cell line culture and treatments

BV2 mouse microglial cells were cultured in DMEM, containing 10% FBS and 1% penicillin and streptomycin. A 100-mm dish was seeded with $1x10^6$ cells. After a 24-hr incubation at 37°C with 5% CO_2, serum deprivation was performed with serum-free media, and the cells were allowed to adjust for at least 4 hr. In the control sample, pellets were scraped and washed 3 times with 1x DPBS, and the conditioned media was collected and concentrated on 3 kDa conical filters for 24 hr (Amicon Ultra, Merck Millipore, Darmstadt, Germany) to a volume of approximately 200 µl [48].

BV2 cells were plated in a 100-mm dish and exposed to 1 of 2 stimuli for 24 hrs: 1 µg/ml Escherichia coli LPS or 10 ng/ml IFN-γ that was dissolved in serum-free DMEM. In case of the targeted analysis stage, BV2 cells were activated with 1 µg/ml LPS, 10 ng/ml IFN-γ, or 1 µg/ml LPS plus 10 ng/ml IFN-γ for 6, 12, 24, and 48 hr. At each time point, the conditioned media and pellet were harvested as in the control sample. All treatments were performed in triplicate.

Protein isolation and digestion

Cell pellets were lysed at room temperature in lysis buffer (4% SDS, 1 mM DTT, 0.1 M Tris-Cl, pH7.4) with 1 min of sonication. Conditioned media was added to the lysis buffer (4% SDS, 2 mM DTT, 0.1 M Tris-Cl), and the lysates were boiled and centrifuged at 15,000 rpm for 10 min. The concentration of the proteins in the lysates was measured using a BCA assay kit (Thermo Fisher Scientific, IL, USA). Then, 200 μg of the protein sample was digested by filter-aided sample preparation (FASP) with slight modifications [49]. The proteins were loaded onto a 30 K spin filter (Millipore, Billerica, MA, USA), and the buffer was exchanged with UA solution (8 M urea in 0.1 M Tris-Cl, pH 8.5) by centrifugation. After triple UA exchange, the reduced cysteines were alkylated with 0.05 M iodoacetamide (IAA) in UA solution for 30 min at room temperature in a dark room. I exchanged the UA buffer to 40 mM ammonium bicarbonate (ABC) and digested the samples with trypsin (enzyme-to-substrate ratio of 1:100) at 37°C for 18 hr. For of the construction library and the targeted analysis, the digested peptides were acidified with trifluoroacetic acid and cleaned using homemade C18 Stage-Tip columns.

Stable-isotope dimethyl labeling and cleaning of peptides

Dimethyl triplex labeling was performed according to standard protocols with several modifications [50]. Digested peptides were loaded onto a 200-μl homemade C18 Stage-Tip column that was packed with POROS 20 R2 resin. The peptides were then tagged with stable-isotope dimethyl labels, comprising 3 mixtures: regular formaldehyde and cyanoborohydride (28-Da shift, designated ‘light label’), deuterated formaldehyde and regular cyanoborohydride (32-Da shift,

designated ‘intermediate label’), and deuterated and ^{13}C labeled formaldehyde with cyanoborodeuteride (36-Da shift, designated ‘heavy label). I flowed the dimethyl labels intermittently through the column 5 times for 10 mins. The labeled peptides were then washed with loading buffer that contained 0.1% TFA. Cleaned peptides were eluted and dried on a vacuum concentrator.

Three biological replicates were established for each treatment group: 2 for the “forward” experiment and 1 for the “reverse” experiment. For the forward experiment, untreated control peptides were labeled with the light label, whereas peptides from cells that were stimulated with LPS or LPS+IFN-γ were labeled with the intermediate or heavy label, respectively. For the reverse experiment, LPS treated samples were tagged with heavy dimethyl labels, and the control and LPS+IFN-γ treated samples were tagged with light and intermediate dimethyl labels, respectively.

Peptide fractionation with high-pH reverse phase fractionation

Dimethyl-labeled peptides were fractionated per an established StageTip-based high-pH reverse phase protocol with some modifications [6]. Dimethyl-labeled peptides and desalted peptides were resolved in 200 µl loading buffer (10 mM ammonium formate, pH 10 and 2% acetonitrile) and loaded onto 200-µl yellow tips that were packed with C18 Empore disk membranes (3 M, Bracknell, UK) and POROS 20 R2 resin (Invitrogen, Carlsbad, CA). Loaded peptides were eluted with ACN gradient buffer solution at pH 10 in 13 fractions. The fractions were dried on a speed vacuum concentrator and stored at -80°C pending the LC-MS analysis.

Mass spectrometric analysis of dimethyl labeling

Peptides were separated on a Nanoflow Easy-nLC 1000 (Proxeon Biosystems, Odense, Denmark) that was equipped with a trap column (100 Å, 3-μm particle, 75 μm x 2 cm) and an analytical column (100 Å, 1.8-μm particle, 50 mm x 15 cm). A gradient that ranged from 5% to 30% acetonitrile was run at a fixed flow rate of 300 nl/min for 180 min and 60 min for the relative quantitation and targeted analysis, respectively. Eluted peptides were ionized at the tip of the column at a spray voltage of 2.00 kV. Ionized peptides were analyzed on a quadrupole-orbitrap mass spectrometer (Q-Exactive, Thermo Fisher Scientific, San Jose, CA, USA).

MS1 spectra were measured in data-dependent acquisition (DDA) mode at a resolution of 70,000 with an m/z range of 300 to 1800 and a target automatic gain control (AGC) of 3.0 x E6 with 100-ms maximum fill times. The 20 most abundant ions were selected with an isolation window of 2 m/z, fragmented by higher-energy collisional dissociation (HCD) with a normalized collision energy of 30 and a resolution of 17,500 at 100 m/z. The dynamic exclusion of sequenced peptides was fixed to 30 s to restrict repeated sequencing. Each sample was analyzed in triplicate for technical replicates.

Mass spectrometry for label-free PRM analysis

The experiments were performed on a quadrupole mass filter that was connected to a benchtop orbitrap mass spectrometer in parallel reaction monitoring (PRM) mode with an isolation width of 2 m/z, a target AGC value of 1.0 x E6, and a maximum injection time of 100 ms. To optimize the PRM analyses, the PRM event used a resolution of 35,000 or 70,000 on the orbitrap. Ion

activation/dissociation was performed with a higher-energy c-trap dissociation of 25, 27, or 30. For regular PRM analyses, the PRM event used a resolving power of 35,000 with a normalized collision energy of 27 on the orbitrap. PRM scans were triggered by scheduled targeting precursor ions that were selected for endogenous peptides in ±5-min and ±1.5-min elution windows for the evaluation of detectability and the targeting method, respectively

Raw data search

Raw MS files for the dimethyl-labeled quantification were processed using the Andromeda search engine, the built-in peptide identification algorithm in MaxQuant (ver. 1.3.0.5), to match the spectra against the UniprotKB FASTA database (74,540 entries, version from June 2014). MS/MS searches were performed with the following parameters: peptide length of at least 6 amino acids, fixed carbamidomethylation modification, variable methionine oxidation, and variable N-terminal acetylation. The tolerance was set to 6 ppm and 20 ppm for main search and first search, respectively. A false discovery rate (FDR) of 1% was applied to all protein and peptide searches. The retention times of all analyzed samples were linearized with the "Match between runs" feature of MaxQuant, which allows identified peptides to be transferred in the absence of sequencing with a retention window of 2 min. Only for the dimethyl labeled quantification were 3 multiplicities selected with stable-isotope dimethyl labeling (control: +28 Da, intermediate: +32 Da, heavy: +36 Da) at the lysine and N-terminus. All proteins were filtered for common contaminants, such as keratins.

Prediction tools for putative secreted proteins

Proteins that were detected in conditioned media were filtered to predict secreted proteins using SignalP 4.1 (http://www.cbs.dtu.dk/services/SignalP/), SecretomeP 2.0 (http://www. cbs.dtu.dk/services/ SecretomeP/), and the TMHMM server 2.0 (http://www.cbs.dtu.dk/services/TMHMM/) and by comparison with the Exocarta database (http://www.exocarta.org). The FASTA forms of the identified proteins were exported and used for this analysis. The resulting protein lists were submitted to the SignalP 4.1 server. 'Eukaryotic organism group' and a cutoff value of 0.45 were used as prediction parameters. The SecretomeP 2.0 server was used to determine whether the proteins were non-classically secreted, with the organism 'mammal' and a threshold score of 0.5 as parameters. The TMHMM server 2.0 was used with the FASTA forms to predict transmembrane helices in the proteins. The resulting dataset was compared with exosomal proteins from Exocarta.

Detectability of label-free PRM analysis

The necessary information on the target peptides, such as RT, precursor m/z, and precursor charge, was extracted from the reference spectral libraries to initiate the PRM. To match the raw data from the PRM, iRT peptides that contained heavy isotopes ($_{13}C_6$, $_{15}N_7$ in Arg or Lys) were spiked into each sample at equal amounts (25 fmol). The elution times of the 15 iRT peptides in each sample were used to calibrate and align the retention times of the target peptides. (Thermo Fisher Scientific, IL, USA). Applying linear regression to the elution times corrected the time shifts that were caused by the changes to the system parameters and the long intervals between analyses [51]. The adjusted elution times of each peptide were used

to determine the centers of the monitoring windows more accurately for the scheduled LC-MS/MS analyses. MS analysis was performed without scheduling of retention time for the detectability check. The assigned peptides were manually accepted only if they satisfied the empirically defined criteria: presentation spectrum in the, non-redundant peptide, selected top 5 or fewer product ions, and CVs of retention times < 5%.

Reproducibility of label-free PRM analysis

Detectable peptides were embedded into a single analyst inclusion list of the method file. The list contained 525 and 604 peptides for the WCP and SEC groups, respectively. The peptides were analyzed in windows of 4 minutes with 5 technical replicates for each run. To check the reproducibility of each run, high-purity (>98%) stable-isotope-labeled b-galactosidase peptide (GDFQFNISR, AQUA ultimate, Thermo Fisher Scientific, IL, USA), with $_{13}C_6$, $_{15}N_7$ in Arg, was spiked into PRM samples. Extracted-ion chromatograms (XICs) of the b-galactosidase peptide were used to normalize the results with regard to the variation between runs. Normalized XICs of select product ions were calculated using Skyline against target peptides. Peptides with CVs < 20% in 5 replicates under at least 2 conditions were included in the list of target peptides for the individual PRM analysis.

In-house spectral library for PRM analysis

A spectral library with high-quality reference MS/MS spectra is necessary to identify false positives in MS/MS spectra that are obtained in the PRM, because all fragments of the targeted peptide were acquired in the PRM analysis. Comparing spectra with the annotated reference MS/MS spectra confirms the correct identity of the peptides in the targeted analysis. Two search engines were used to increase the spectral resources in constructing the PRM library. The spectra were first identified using the Andromeda search engine in MaxQuant. The parameters in the discovery stage were used, except for those that pertained to the labeled quantification. The built-in SequestHT search algorithm in Proteome Discoverer (ver 1.4, Thermo Fisher Scientific, San Jose, CA, USA) was used to construct the second library. A microglia-specific library of 76,910 peptides was constructed—corresponding to 6329 proteins and 914,829 MS/MS spectra—identified from 12 pre-fractionated pooled matrix samples.

Target protein selection and in silico fragmentation

Target selections in the whole cell proteome (WCP) and secretome (SEC) groups were processed as shown in Figure 2-6 A. Normalized ratios from MaxQuant were filtered statistically in 2 steps: (1) Two paired groups were compared by their significance B values, which were calculated for the protein subsets that were obtained, based on intensity, with a Benjamini-Hochberg FDR < 5%. (2) ANOVA with p-value<0.05 was then applied to proteins that passed the first step to select significantly differentially expressed proteins (DEPs) or differentially expressed secreted proteins (DESPs) in the 3 conditions.

To compare our whole-cell lysate data with earlier studies on the BV2 proteome and transcriptome, KEGG pathway analysis was performed using *Mus musculus* as the reference with default settings on the DAVID bioinformatics website (Ver 6.7, https://david-d.ncifcrf.gov/) with DEPs. Protein-protein interaction networks were searched with associated proteins in the KEGG pathways using Cytoscape and the STRING database [52-53].

For the label-free PRM method, endogenous peptides must first be selected for quantifiable surrogates of a target protein. Because multiple MS/MS data points for the selected precursor are acquired throughout the elution profile, the peptide should be stoichiometric and specific for the target protein. The mass range of the quadrupole orbitrap instrument was suitable for m/z values of peptides with 6 to 25 amino acids. The selected peptide should be unique to the target protein. Unique peptides were identified, based on the MaxQuant results. A double or triple charge state of a peptide was preferred to optimize the measurable m/z range. The signals of the less than five most intense product ions for each precursor were selected, based on being matched in the library to a portion of the product ion on normalization of the peak areas to total peak areas.

Target peptide quantification and processing of longitudinal datasets

Raw files from the longitudinal PRM analysis were processed using Skyline (ver. 3.5.0), an open source software for quantitative proteomic analysis [54]. Because reproducibility of the peptide elution time is critical when the sample size is large, commercial iRT peptides were added to the sample before data were acquired. Peak integration was performed by manually drawing a demarcation line, based on the RT

prediction. After a .csv file that contained variables, such as protein name, sequence of peptide, charge, condition, and the normalized extracted-ion chromatogram (XIC) of the peak area, was exported, it was imported into MSstats (ver. 3.3.4), an R package that is used for the relative quantification of proteins and peptides. The data were processed using a $\log_2$ scale and then normalized to equalized medians. A linear mixed model was used to calculate the degree of statistical significance of the integrated peak area between the 3 conditions. Twelve comparisons of the 3 conditions were made simultaneously.

NO assay of conditioned media from activated microglia

Nitric oxide assay was performed on the conditioned media of activated microglia using Griess reagent [55]. Griess reagent (50 μl) was mixed with NaNO (0-100 μM) to create a standard NO curve. After a 15-min incubation, the absorbance was measured at 540 nm, and the nitric oxide that was generated from activated cells was measured.

Immunoblotting analysis

Whole-cell lysates were prepared in RIPA lysis buffer (Tris-Cl pH 7.4, 1% NP-40, 1 mM EDTA, 8 M urea, and 150 mM NaCl) that contained protease inhibitor cocktail (PMSF). Proteins (30 μg, as measured by BCA assay) were separated by 12% SDS-PAGE and transferred to polyvinylidene fluoride (PVDF) membranes (Hybond-P, GE Healthcare, PA, USA). Membranes were blocked with 5% BSA and incubated for 2 hours with primary antibody to β-actin or iNOS (1:1000 dilution;

Sigma-Aldrich, Louis, MO, USA) for 18 hours at 4°C. The membranes were then washed 5 times with Tris-buffered saline and Tween-20 (TBS-T) before being incubated in horseradish peroxidase-conjugated secondary antibodies for 2 hr. Detection solution (West-Q chemiluminescent substrate Kit-plus, GenDEPOT, Barker, TX, USA) was used to develop the membranes, and the signals were quantified on an LAS-4000 (Fujifilm, Japan).

RESULTS

Activation status of murine microglia cell line

Prior to the mass spectrometric analysis, the status of activated microglia was assessed and confirmed in whole-cell proteome (WCP) and conditioned media collection (CMC) samples by NO assay and immunoassay of inducible nitric oxide synthase (iNOS), respectively (Figure 2-1). LPS/IFN-γ treated microglia expressed more iNOS than cells that were stimulated with LPS alone. Secretion of NO also rose with the combination treatment. In longitudinally collected samples, NO and iNOS levels increased at each time point. These results demonstrate that LPS and IFN-γ effect the production of nitric oxide through inducible nitric oxide synthase and synergize in activating this murine microglial cell line compared with either individual compound. To determine the mechanisms that affect the intracellular and intercellular environments during microglial activation, experiments were conducted to quantify and verify the changes in total protein levels, based on mass spectrometry (Figure 2-2).

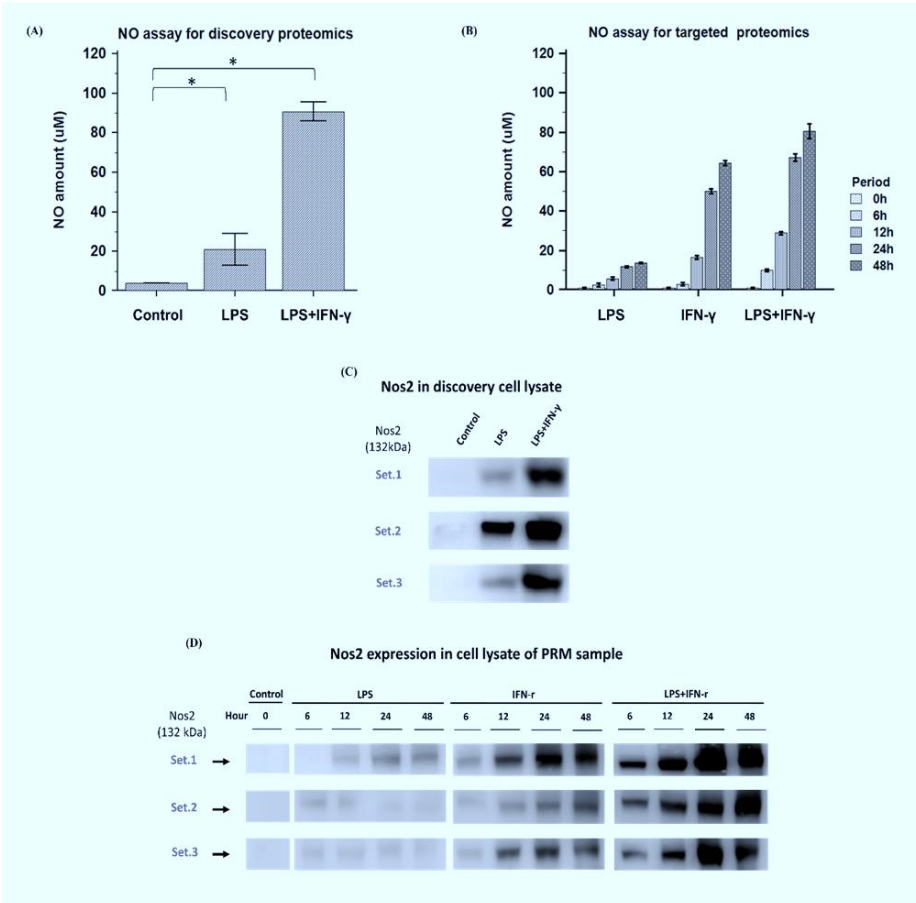

Figure 2-1. Confirmation of differential expression of iNOS and nitric oxide in activated microglia model.

(A) NO assay and (C) immunoblotting were performed to measure nitric oxide in conditioned media and iNOS in whole-cell lysate collected from 3 treatment groups: control, LPS, and LPS plus IFN-γ. These samples were used for the discovery step. Longitudinal samples were collected for 6, 12, 24, and 48 hr from control, LPS treated, IFN-γ treated, and LPS plus IFN-γ treated groups. (B) NO assay and (D) immunoblotting were performed with all collected samples that were prepared for PRM analysis.

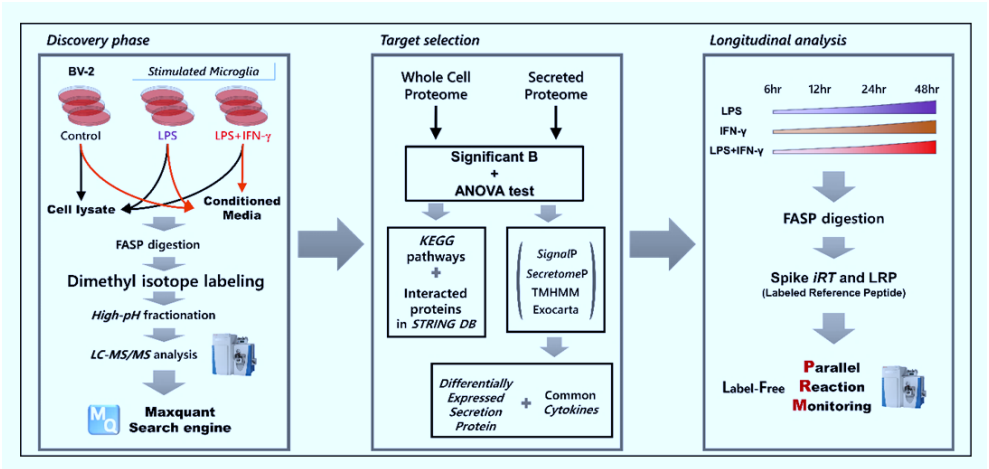

Figure 2-2. Systematic workflow of proteomic analysis for whole-cell and secreted proteomes in activated microglia cell line.

A single platform workflow enabled both global proteomics and targeted proteomics in this study. In-depth quantitative proteomic analysis discovered intracellular and extracellular proteins of activated BV2 microglia cells in large scale. A number of filtration criteria starting with a pairwise statistical testing and bioinformatics analysis were utilized to select target proteins. The longitudinal validation studies contained biological and technical triplicates using label-free PRM approach.

Characterization of proteome identified in discovery phase

To examine the global protein expression profiles on activated BV2 microglia cells, quantitative proteomics was performed by stable-isotope dimethyl labeling. Based on the discovery analysis, 5492 protein groups were identified in the WCP, of which 4748 proteins were quantified in the LPS or LPS/IFN-γ treated group across the 3 biological replicates (Figure 2-3A). From the corresponding CMC, 4938 protein groups were identified, and 3558 proteins were quantified in the LPS and LPS/IFN-γ treated groups in biological triplicate (Figure 2-3B). Specifically, to predict the putative secretome, 3558 quantifiable proteins in CMC were examined by sequence analysis with SignalP, SecretomeP, Exocarta, and TMHMM [48] (Figure 2-3C). As a result, 2387 proteins (67.09% of quantified proteins) were expected to be released by classical or non-classical secretion from activated cells and were thus collectively termed the secretome (SEC). The quantified proteins in the WCP and the putative secreted proteins in CMC were designated the WCP and SEC groups, respectively.

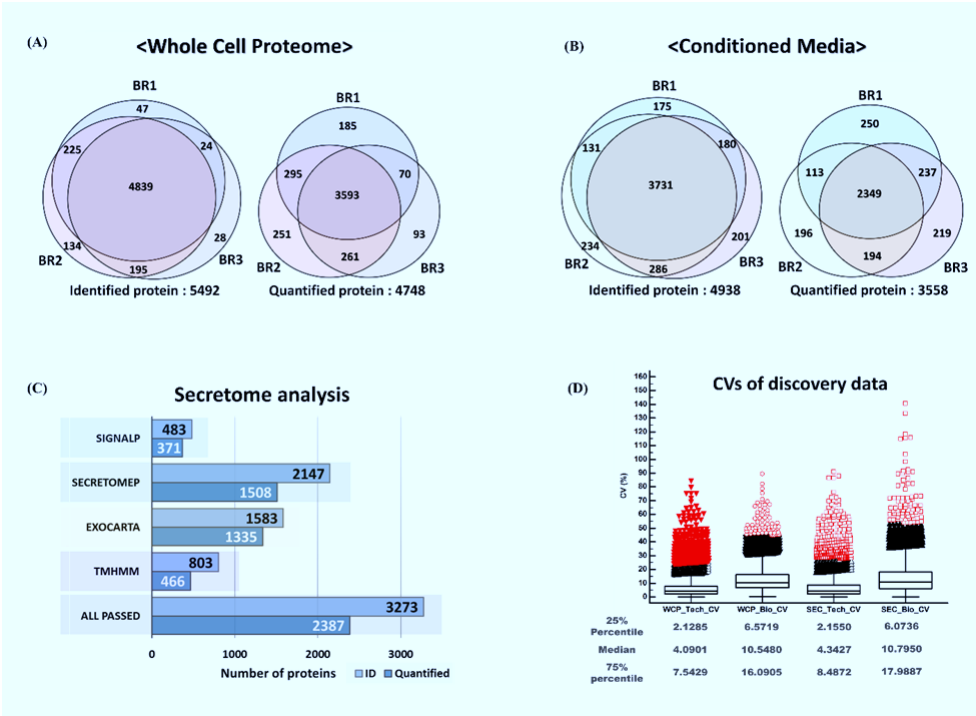

Figure 2-3. Identification and quantification for dimethyl labeling.

Venn diagram of identified and quantified proteins in (A) whole-cell proteome and (B) conditioned media from dimethyl-labeled discovery proteomics. Proteins that had a minimum ratio count of two were selected as quantified proteins. (C) Four bioinformatics tools, SignalP, SecretomeP, Exocarta, and TMHMM were used for the prediction of putative secreted proteins. The number in each box indicates the amount of putative secreted proteins from the prediction tools. (D) Box-plots and minimum to maximum whiskers representing the CV values of technical and biological replicates in the WCP and SEC groups for the discovery data. Box and whisker plots with statistical summaries were calculated in MedCalc (Ver. 12.3.0.0).

Global protein quantification in activated microglia

Principal component analysis (PCA) was performed to compare the proteomes of normal microglia and each group of activated microglia. The distance between each group was 80.3% for the WCP group and 75.3% for the SEC group. These values were calculated, based on the sum of the components from the analysis (Figure 2-4 A, B). To evaluate the reproducibility and quality of the dimethyl labels, their coefficient of variation (CV) and Pearson correlation values were calculated. The median CVs between the technical and biological replicates of the quantification of dimethyl labeling for the WCP group were 4.09% and 10.54%, respectively. For the SEC group, the CVs were 4.33% and 10.79%, respectively (Figure 2-3D). The median CVs in all samples were below 20%, indicating that the quantification of dimethyl labeling had high reproducibility. Forward and reverse labeling was performed in each group to reduce potential errors. By Pearson correlation analysis of the forward and reverse experiments under each condition, there was significant correlation, with R values of 0.823 and 0.843 for the LPS and LPS/IFN-γ treatments in the WCP group, respectively. For the SEC group, these values were 0.87 and 0.913, respectively (Figure 2-4 C, D).

On examination of the dimethyl isotope labeling across biological and technical triplicates, I observed high correlation between the control and LPS treated groups (0.92-0.96). In contrast, the correlation was low between the control and combination treatment group (0.86-0.91, Figure 2-5). This difference indicates that the dimethyl isotope labeling of peptides was performed properly in the forward and reverse experiments.

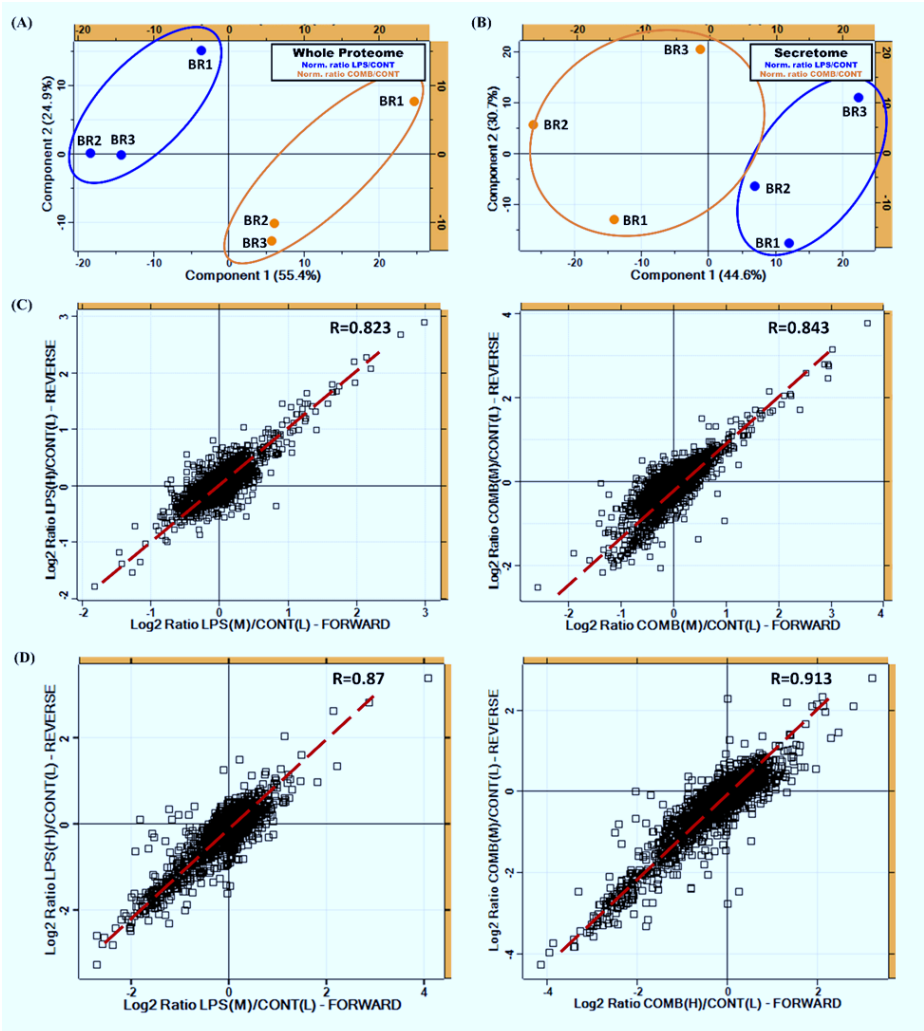

Figure 2-4. Assessment of global proteomics

Principle components analysis (PCA) of the (A) whole-cell proteome and (B) secretome in the dimethyl-labeled quantitative analysis revealed that each ratio of biological labeling was similar, except for the reverse labeling of a third biological replicate. Components 1 and 2 accounted for 80.3% and 75.3% of the variation in data in the WCP and SEC groups, respectively. PCA test was performed in Perseus (Ver. 1.5.0.8). Correlations between the forward and reverse labeling of dimethyl isotopes were analyzed for the (C) WCP and (D) SEC groups.

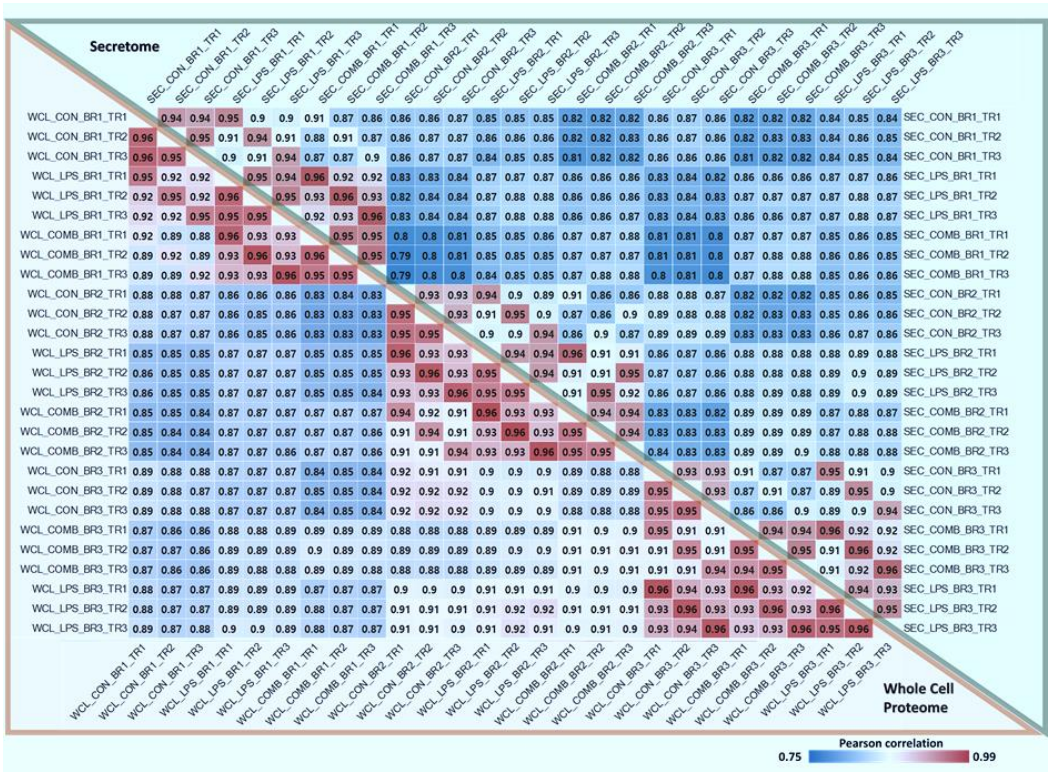

Figure 2-5. Heatmap of pairwise correlation values for discovery data

The numbers in orange or green triangle represent pairwise Pearson correlation values for WCP or SEC groups, respectively. Pearson correlation coefficients between samples in the discovery data were calculated using Perseus, and the heatmap was visualized in Excel.

Significance of proteome between treatment groups

To identify differentially expressed proteins (DEPs), a pairwise comparison analysis was performed for each treatment group. Expression levels of whole-cell and secreted proteins in the LPS and LPS/IFN-γ treated groups were measured and compared with that of unactivated microglia. The statistical analysis for significant expression and secreted proteins was performed as described in Figure 2-6 A.

For the WCP group, significantly expressed proteins were determined by significance B analysis (Benjamini-Hochberg FDR<0.05) and pairwise comparison 257 proteins in control versus LPS treated cells and 264 proteins from LPS/IFN-γ treated cells were significant. Subsequently, ANOVA was performed for proteins that were significantly expressed in at least 2 of the 3 pairwise comparisons for each condition. Total of 202 proteins were considered DEPs between the 3 groups, with *p-value* < 0.05.

Using 202 DEPs from the discovery stage, KEGG pathway enrichment was performed to classify functions that were associated with the activation of microglia (Figure 2-7 A). Five distinct pathways that were related to microglial activation were selected: glycolysis and gluconeogenesis; antigen processing and presentation; Toll-like receptor signaling; natural killer cell-mediated cytotoxicity; and alanine, aspartate, and glutamate metabolism. To analyze proteins that were involved in these pathways and DEPs, direct and indirect information on protein-protein interactions (PPIs), based on the STRING database, was used to select additional target proteins (Figure 2-6 B). Ultimately, 319 proteins were chosen as initial target proteins from the PPI network for targeted proteomic analysis.

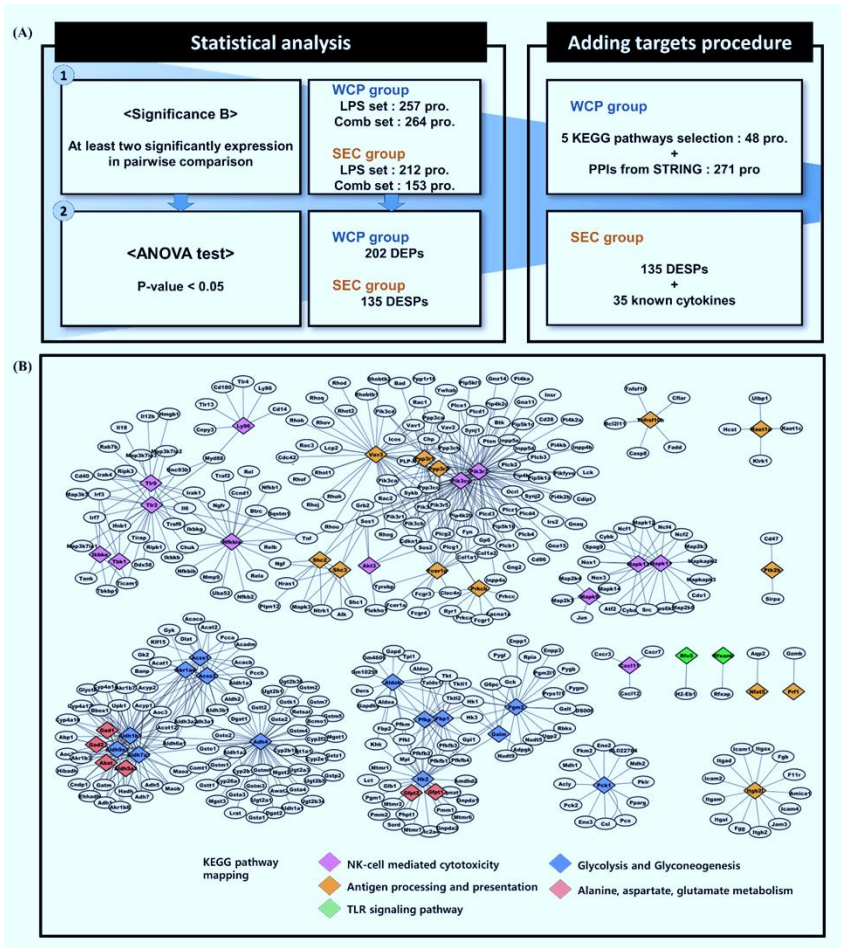

Figure 2-6. Scheme for target protein selection

(A) Criteria for target proteins in the global proteomics analysis are described in the flowchart. Two statistical analysis methods, significance B and ANOVA, were performed using Perseus. (B) Additional target candidates were collected using the STING database, which describes interacting or bound proteins. The protein-protein interaction (PPI) network was imported into Cytoscape, ver 3.4.0, and the proteins were visualized and mapped into KEGG pathways. Significantly differentially expressed proteins (diamond box in the figure) were enriched in 5 KEGG pathways related to the immune response and metabolism.

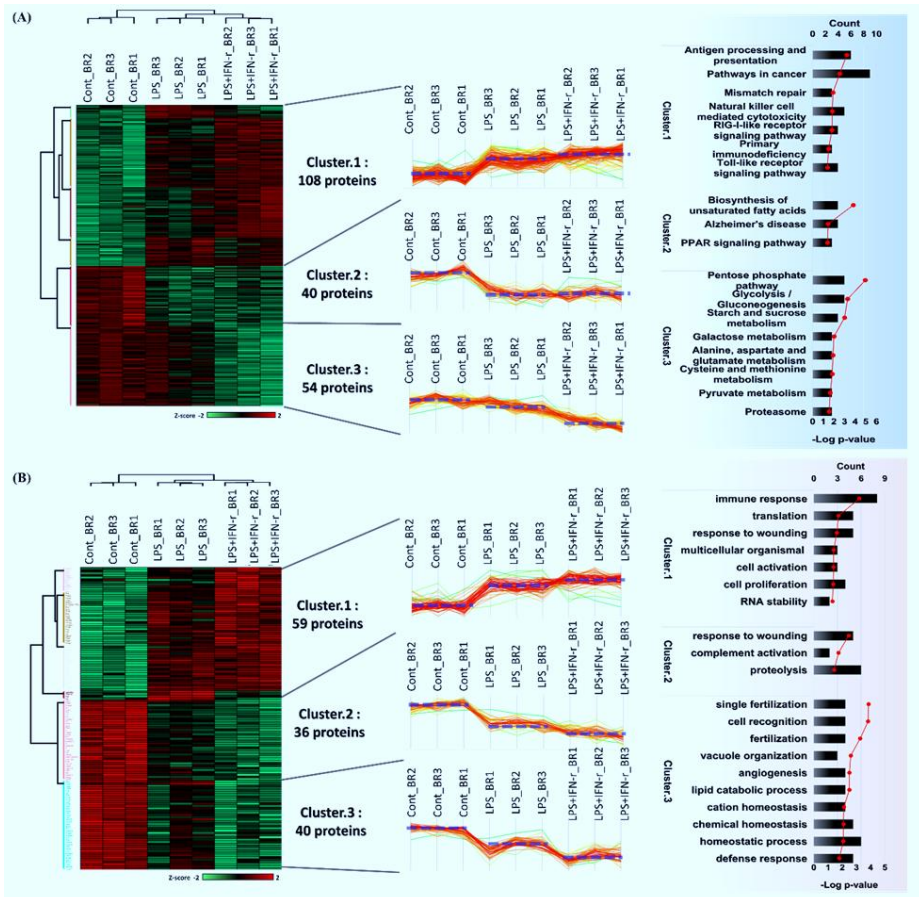

Figure 2-7. Statistical analysis and bioinformatics.

Hierarchical heatmap clusters of significant proteins from ANOVA across 3 treatment groups were analyzed in Perseus (Ver. 1.5.0.8); 202 and 135 proteins were included in the (A) WCP and (B) SEC groups, respectively, with a Benjamini-Hochberg FDR <0.05. DEPs and DESPs were analyzed for gene ontology and KEGG pathway annotation on the DAVID website. Minus $\log_2$ *p-values* with count of enriched proteins were drawn using Excel (BR: biological replicate).

The SEC group was processed in the same manner as the WCP group. By significance B analysis, 212 and 153 proteins were significant by pairwise comparison in control versus LPS and control versus LPS/IFN-γ treated groups, respectively. By ANOVA of the 3 groups, 135 secreted proteins were significantly differently expressed secreted proteins (DESPs). Because the KEGG pathway analysis of DESPs identified the enrichment of 2 pathways, “nicotinate and nicotinamide metabolism” and “ribosome”, I designated 135 DESPs as target proteins, with an additional 35 cytokines that mediate cell-cell communication but were not quantified in the dimethyl labeling proteomic analysis. These cytokines included common cell surface markers on activated microglia and small inducible cytokines, such as tumor necrosis factor and C-C motif chemokine ligands. In conclusion, 170 putative secreted proteins were defined as initial target proteins for the PRM analysis. Consequently, PRM analysis was used to validate the quantification of target proteins from discovery-based proteomics studies and to trace temporal proteome and secretome of targeted proteins during microglial activation.

Selection of target peptides

To select target peptides from initial target proteins, Skyline was processed with the necessary information from the spectral library**.** The number of target peptides was 1086 and 1088, corresponding to 319 and 170 proteins, for the WCP and SEC groups, respectively. RT alignment was performed by spiking with the iRT SIS peptide, and matching elution times for the selected peptide and predicted retention times based on iRT score from the Skyline calculation were the criteria to pare the number of undetectable peptides (Figure 2-8 A). After optimization of the resolving power and collision energy for MS2 for the quality control, an intra-technical assay with 5 replicates in each group was performed to select target peptides that had a CV < 20% (Figure 2-8 B, C) by increasing the quantitative reliability, I hoped to improve the reliability of the target screen. Using these criteria, 347 and 464 target peptides, corresponding to 217 and 146 proteins of the whole-cell proteome and secretome, respectively, were selected for the longitudinal activation of microglia (Table 2-1).

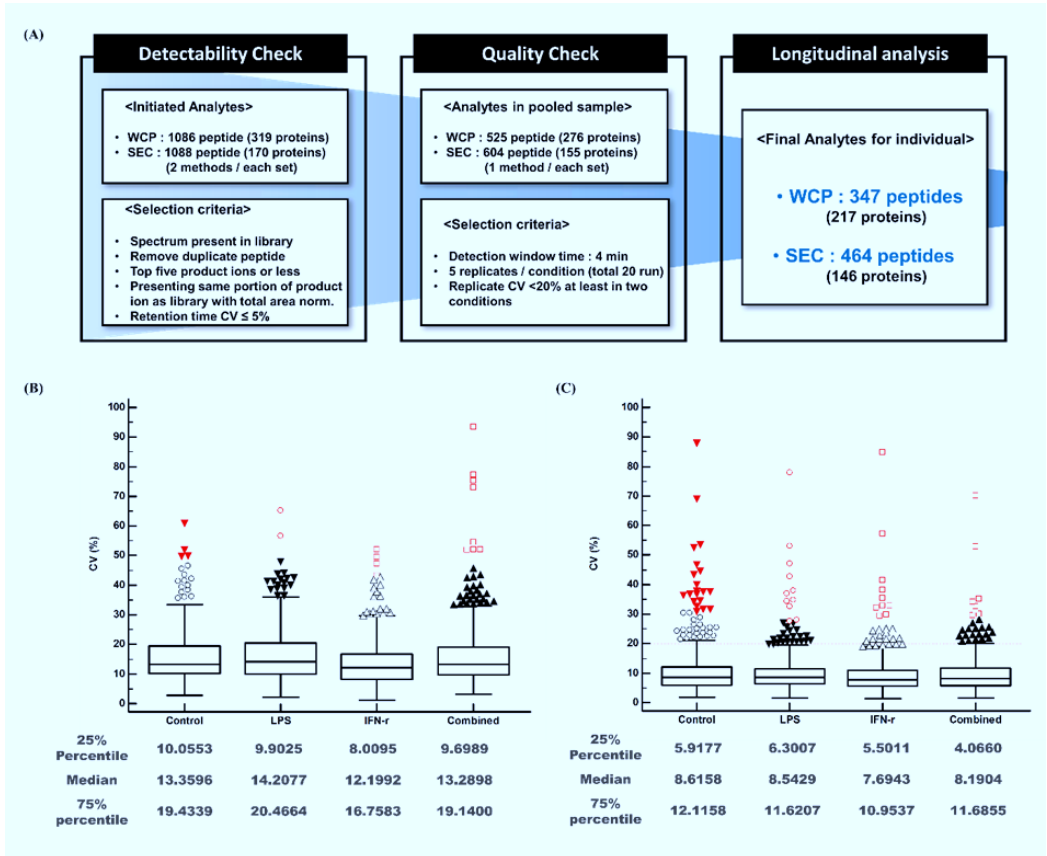

Figure 2-8. Filter criteria of targeted peptides for label-free PRM

Filter criteria were applied sequentially to select quantifiable target peptides for label-free PRM analysis (A). To check the quality of the analyte peptide, the CVs of 5 replicates in each treatment group were measured in the (B) WCP and (C) SEC groups. Box and whisker plots with statistical summaries were calculated in MedCalc (Ver. 12.3.0.0). The red dashed line is the cut-off value (20%) for final target peptides.

Table 2-1. List of target proteins and corresponding peptides

#	Protein Accession	Gene name	Sources	Peptide Sequence	Precursor Charge	Product ions
1	Q5SWU9	Acaca	STRING DB	LPELLLK	2	b4, b3, y5, y6
				TFEDFVR	2	y3, y4, y5
				LGGIPVGVVAVETR	2	y5, y7, y8, y10
2	Q8R5C9	Acacb	STRING DB	FGAYIVDGLR	2	b3, y3, y5, y6
3	P45952	Acadm	STRING DB	GIAFEDVR	2	b5, y4, y5, y6
				ENVLIGEGAGFK	2	y3, y5, y7, y9
4	Q8QZT1	Acat1	STRING DB	GATPYGGVK	2	y3, y4, y6
				FASEITPITISVK	2	y3, y5, y7, y8
5	Q8CAY6	Acat2	STRING DB	VAVLSQNR	2	y4, y5, y6
				ELGLNPEK	2	y3, y6
6	P56376	Acyp1	STRING DB	GTVQGQLQGPVSK	2	y5, y7, y9
7	P28474	Adh5	Glycolysis / Gluconeogenesis	AGDTVIPLYIPQC[+57]GEC[+57]K	2	b5, y5, y7, y11
				IDPSAPLDK	2	b3, y3, y4, y6
8	Q8VDL4	Adpgk	STRING DB	LGPAPVPVGPLSPESR	2	b3, y8, y10, y12
				LLQALGLSPGSGK	2	y5, y6, y8, y9
				VAGTQAC[+57]ATETIDTNR	2	y3, y8, y9, y10
9	Q9JII6	Akr1a1	Glycolysis / Gluconeogenesis	ALGLSNFNSR	2	y4, y6, y8
				GLEVTAYSPLGSSDR	2	b3, y8, y9, y11
10	P45376	Akr1b1	STRING DB	NLVVIPK	2	b3, y3, y5
11	Q62148	Aldh1a2	STRING DB	YYAGWADK	2	y3, y4, y5, y6
12	P47738	Aldh2	Glycolysis / Gluconeogenesis	GYFIQPTVFGDVK	2	b3, y4, y5, y8
13	P47740	Aldh3a2	Glycolysis / Gluconeogenesis	YLAPTILTDVDPNSK	2	b4, y4, y8, y9
				NVDEAINFINDR	2	y3, y5, y6, y10
14	Q80VQ0	Aldh3b1	Glycolysis / Gluconeogenesis	LVPALQNAITR	2	y6, y7, y8, y9
15	Q9EQ20	Aldh6a1	STRING DB	AISFVGSNQAGEYIFER	2	y7, y8, y12, y13
16	Q9DBF1	Aldh7a1	Glycolysis / Gluconeogenesis	FQDEEEVFEWNNEVK	2	b3, y6
17	Q9JLJ2	Aldh9a1	Glycolysis / Gluconeogenesis	VEPVDASGTEK	2	y4, y5, y6, y7
				C[+57]QVLLEAAR	2	y5, y6, y7
				ISFTGSVPTGVK	2	y5, y8, y9
18	P05064	Aldoa	Glycolysis / Gluconeogenesis	QLLLTADDR	2	y4, y5, y6, y7
				GVVPLAGTNGETTTQGLDGLSER	3	y5, y6, y8
19	Q91Y97	Aldob	Glycolysis / Gluconeogenesis	VLAAVYK	2	y3, y5
20	P05063	Aldoc	Glycolysis / Gluconeogenesis	TPSALAILENANVLAR	2	y8, y10, y11
21	Q8JZV7	Amdhd2	STRING DB	VLPQIPVK	2	y3, y4, y5, y6
22	P35991	Btk	STRING DB	LSYYEYDFER	2	y4, y5, y6, y7
23	O89110	Casp8	Toll-like receptor signaling pathway	LSEEVSELELR	2	y6, y7, y8, y9
				EASIYDLTSYFTGSK	2	y4, y5, y8, y11
24	P10810	Cd14	Toll-like receptor signaling pathway	VFPALSTLDLSDNPELGER	3	y4, y6, y7, y9
				GLISALC[+57]PLK	2	y3, y4, y7, y8
25	P27512	Cd40	Toll-like receptor signaling pathway	GTSQTNVIC[+57]GLK	2	y4, y5, y7, y8
26	P60766	Cdc42	STRING DB	TC[+57]LLISYTTNK	2	b3, y4, y6, y7
27	P61022	Chp1	STRING DB	IPELAINPLGDR	2	y6, y8, y9, y10
28	Q60680	Chuk	STRING DB	IIDLGYAK	2	y4, y5
29	Q9JKF4	Clec6a	STRING DB	WQWIDDTPFSQNVR	2	y7, y8, y10, y12
30	Q01149	Col1a2	STRING DB	GFPGTPGLPGFK	3	b3, y3, y4
31	O88587	Comt	STRING DB	AVYQGPGSSPVK	2	b3, y3, y7, y8
32	Q80X68	Csl	STRING DB	GLVYETSVLDPDEGIR	3	y4, y5, y6, y7
				GYSIPEC[+57]QK	2	b3, y3, y4, y5
33	Q61462	Cyba	STRING DB	LFGPLTR	2	y3, y4, y5
34	Q61093	Cybb	STRING DB	YSIALSDIGDNENEEYLNFAR	3	y6, y7
				NPEGGLYVAVTR	2	y5, y6, y9, y10
				QSISNSESGPR	2	y4, y6, y7, y8
35	Q6Q899	Ddx58	STRING DB	IESFVVEDIVSGVQNR	2	y7, y8, y10, y11
36	Q9Z2A7	Dgat1	STRING DB	TSVGDGYWDLR	2	y6, y8, y9

Continue..

37	Q8BMF4	Dlat	Glycolysis / Gluconeogenesis	DVPLGAPLC[+57]IIVEK	2	y3, y4, y8, y10
				GLETIASDVVSLASK	2	b4, y5, y9, y10
38	P17183	Eno2	Glycolysis / Gluconeogenesis	AAVPSGASTGIYEALELR	2	b3, y5, y7, y10
39	P21550	Eno3	Glycolysis / Gluconeogenesis	GVPLYR	2	y3, y4
40	P20491	Fcer1g	Natural killer cell mediated cytotoxicity	ADAVYTGLNTR	2	b3, y5, y6, y7
				SQETYETLK	2	y3, y5, y6, y7
41	P26151	Fcgr1	STRING DB	ELFTTPVLR	2	y4, y5, y6, y7
42	P08508	Fcgr3	STRING DB	LDPPWIQVLK	2	y5, y6, y7, y8
43	Q8R2R4	Fcgr4	STRING DB	VLEEDSVTLR	2	y5, y6, y8
44	P39688	Fyn	Natural killer cell mediated cytotoxicity	GSLLDFLK	2	y3, y4, y5, y6
45	P16858	Gapdh	STRING DB	VIPELNGK	2	y3, y5, y6
46	Q9D964	Gatm	STRING DB	)C[+57]PVSSYNEWDPLEEVIVGF	3	y5, y6, y7, y9
				AENAC[+57]VPPFTVEVK	2	b4, b3, y7, y8
				FVTTEFEPC[+57]FDAADFIR	3	y3, y6, y7, y8
47	P47856	Gfpt1	Alanine, aspartate and glutamate metabolism	VIFLEDDDVAAVVDGR	2	y8, y9, y10, y11
				C[+57]QNALQQVVAR	2	y5, y6, y7, y8
48	Q9Z2Z9	Gfpt2	Alanine, aspartate and glutamate metabolism	GYDVDFPR	2	y3, y6
49	Q9WU65	Gk2	STRING DB	FLVFNSK	2	y4, y5
50	P23780	Glb1	STRING DB	TVAEALGILC[+57]PNGPVK	2	y6, y7, y8, y10
51	P30677	Gna14	STRING DB	FVFAAVK	2	y3, y4, y5
52	P21279	Gnaq	STRING DB	VSAFENPYVDAIK	2	y4, y7, y8
53	P63213	Gng2	STRING DB	EDPLLTPVPASENPFR	3	y6, y7, y8
54	Q9JK38	Gnpnat1	STRING DB	VEDVVVSDEC[+57]R	2	b3, y6, y7
55	P06745	Gpi	Glycolysis / Gluconeogenesis	TLASLSPETSLFIIASK	3	y3, y4, y5, y6
				EWFLEAAK	2	y3, y4, y5
56	Q60631	Grb2	STRING DB	NQQIFLR	2	y3, y4, y5
57	P10649	Gstm1	STRING DB	YIATPIFSK	2	y3, y5, y6, y7
58	O09131	Gsto1	STRING DB	VPPLIASFVR	2	y5, y6, y7, y8
59	P46425	Gstp2	STRING DB	FEDGDLTLYQSNAILR	2	y6, y8, y9, y10
				SLGLYGK	2	y3, y4, y5
60	Q9WVL0	Gstz1	STRING DB	GIDYEIVPINLIK	2	b3, y4, y6, y7
				VITSGFNALEK	2	y3, y7, y8, y9
61	Q61425	Hadh	STRING DB	LLVPYLIEAVR	2	y5, y6, y7, y8
62	Q99L13	Hibadh	STRING DB	DLGLAQDSATSTK	2	b3, y3, y7, y9
63	P17710	Hk1	Glycolysis / Gluconeogenesis	GAALITAVGVR	2	y3, y4, y5, y8
64	O08528	Hk2	Glycolysis / Gluconeogenesis	AELLFQGK	2	y3, y4, y5, y6
				NVELVDGEEGR	2	y5, y6, y7, y9
65	Q3TRM8	Hk3	Glycolysis / Gluconeogenesis	GQDSPAPSVR	2	y4, y6, y7, y8
				VAEGSVQIINQVYSIPEC[+57]R	3	y4, y6, y10
66	P63158	Hmgb1	STRING DB	DIAAYR	2	y3, y4
67	Q61411	Hras	Natural killer cell mediated cytotoxicity	LVVVGAGGVGK	2	y5, y7, y8, y9
				QGVEDAFYTLVR	2	y6, y7, y8, y9
68	P13597	Icam1	Natural killer cell mediated cytotoxicity	GEEILSR	2	b3, y3, y4, y5
				LFC[+57]SLEGLFPASEAR	2	y6, y7, y9, y10
69	O88351	Ikbkb	Toll-like receptor signaling pathway	ALDDILNLK	2	y3, y4, y6, y7
				ALELLPK	2	y3, y4
70	Q9R0T8	Ikbke	Toll-like receptor signaling pathway	SLSC[+57]LGEELLK	2	y3, y4, y6, y7
				LLAFDLQDNNR	2	y3, y6, y7, y8
71	O88522	Ikbkg	Toll-like receptor signaling pathway	AQVTSLLGELQESQSR	2	y7, y9, y11, y12
72	Q9ES52	Inpp5d	STRING DB	DLPLATENPR	2	y5, y6, y7, y8
				LSLSETLFQR	2	y5, y7, y8
				QAPVPVLGPTPR	2	y5, y6, y8, y10
73	P81122	Irs2	STRING DB	ALTDLVSEGR	2	y4, y5
74	P24063	Itgal	Natural killer cell mediated cytotoxicity	TEFTFLDYVK	2	y5, y6, y7, y8
				LADVVVGAEGR	2	b4, y5, y6, y9
				LDLDFPR	2	y3, y4, y5

Continue..

75	P05555	Itgam	STRING DB	FQLELPVK	2	y3, y4, y5, y6
76	Q9QXH4	Itgax	STRING DB	IQYFGQSLSGGQDLTR	2	y3, y8, y10, y12
77	P11835	Itgb2	STRING DB	SIANPEFDQR	2	y6, y7, y8
				SAVGELSDDSSNVVQLIK	2	b3, y4, y5, y12
				YNSQVC[+57]GGSDR	2	y5, y6, y7, y9
78	P05627	Jun	Toll-like receptor signaling pathway	NSDLLTSPDVGLLK	2	b3, y4, y5, y7
79	Q60787	Lcp2	Natural killer cell mediated cytotoxicity	YQEESQVYLLGTGLR	2	y5, y8, y11, y13
80	Q9JHF9	Ly96	Toll-like receptor signaling pathway	FPISISSEPC[+57]IR	2	y4, y7, y8, y9
81	Q64133	Maoa	STRING DB	INVLVLEAR	2	y4, y5, y6, y7
				EIPVDAPWQAR	2	y5, y6, y7, y8
				NLPSVPGLLK	2	y5, y6, y7, y8
82	Q8BW75	Maob	STRING DB	ELGLETYK	2	b3, y3, y4, y6
83	P47809	Map2k4	Toll-like receptor signaling pathway	LC[+57]DFGISGQLVDSIAK	2	b3, y4, y5, y10
84	P47811	Mapk14	Toll-like receptor signaling pathway	TIWEVPER	2	b5, y4, y5, y6
85	Q63844	Mapk3	Natural killer cell mediated cytotoxicity /	GQPFDVGPR	2	y4, y5, y6, y7
				EIQILLR	2	y3, y4, y5
86	P14152	Mdh1	STRING DB	GEFITTVQQR	2	b3, y5, y6, y7
87	P08249	Mdh2	STRING DB	GYLGPEQLPDC[+57]LK	2	b5, y5, y6, y10
				GC[+57]DVVVIPAGVPR	3	b3, y4, y5, y6
				IQEAGTEVVK	2	y3, y6, y7, y8
88	Q91VS7	Mgst1	STRING DB	VFANPEDC[+57]AGFGK	2	y4, y5, y6, y9
89	Q924M7	Mpi	STRING DB	LPFLFK	2	b3, y3, y4, y5
90	P22366	Myd88	Toll-like receptor signaling pathway	SLLDAWQGR	2	y4, y5, y6, y7
91	Q09014	Ncf1	STRING DB	NNVADITGPIILQTYR	3	y4, y5, y6
				AGEEITQAQR	2	y4, y5, y6, y7
92	O70145	Ncf2	STRING DB	TPEIFR	2	y3, y4, y5
				AFVEGC[+57]AAK	2	y3, y5, y6, y7
93	P97369	Ncf4	STRING DB	AEALFDFTGNSK	2	b3, y5, y7, y8
				AGDVIFLLSK	2	b3, y3, y5, y6
				EDIALSYQDAEGDLVR	2	b3, y7, y11, y12
94	P25799	Nfkb1	Toll-like receptor signaling pathway	IC[+57]NYVGPAK	2	y4, y5, y7
				AGC[+57]VTGGEEIYLLC[+57]DK	2	y3, y4, y5, y12
95	Q9WTK5	Nfkb2	STRING DB	GGDEVYLLC[+57]DK	2	b3, y3, y4, y6
				ALLDYGVTADAR	2	y5, y7, y8, y9
				AGAAAPELLQALLR	2	b4, b3, y6, y9
96	Q8CIZ9	Nox1	STRING DB	NLLSFLR	2	y3, y4
97	Q9JKX6	Nudt5	STRING DB	SADAVSVIPVLQR	2	b3, y5, y6, y8
				VYAYGLALK	2	b3, y3, y5, y7
98	Q91ZA3	Pcca	STRING DB	SFGLPSIGR	2	b3, y5, y7
				FLSDVYPDGFK	2	y3, y5, y6, y9
99	Q99MN9	Pccb	STRING DB	DTSYLFITGPEVVK	2	y5, y6, y7, y9
				GFVDDIIQPSSTR	2	y5, y6, y7, y10
100	Q8BH04	Pck2	Glycolysis / Gluconeogenesis	DTVPLLAGGAR	2	y5, y6, y7, y8
				FDSEGQLR	2	y4, y5, y6
101	Q05920	Pc	STRING DB	GTPLDTEVPLER	2	y4, y5, y8
				ALAVSDLNR	2	y3, y5, y6, y7
102	P12382	Pfkl	Glycolysis / Gluconeogenesis	EQWWLNLR	2	y3, y4, y5, y6
103	Q9WUA3	Pfkp	Glycolysis / Gluconeogenesis	VYFIYEGYQGLVDGGSNIVEAK	3	b3, y4, y9, y10
104	Q9DAK9	Phpt1	STRING DB	NGYDC[+57]EC[+57]LGGGR	2	y6, y7, y8, y9
105	Q2TBE6	Pi4k2a	STRING DB	QLLLQFER	2	y3, y4, y5, y6
				VPFSQEIK	2	y3, y5, y6, y7
				SASESYTQSFQSR	2	y5, y6, y8, y9
106	Q8CBQ5	Pi4k2b	STRING DB	LVILDYIIR	2	y4, y5, y6, y7
107	E9Q3L2	Pi4ka	STRING DB	DFLVIPSPVLVK	2	b3, y5, y7, y8
				QYGDESTLAFQQAR	2	y6, y7, y12
108	Q8BTI9	Pik3cb	Natural killer cell mediated cytotoxicity / Toll-like receptor signaling pathway	EALELLDFNYPDQYVR	2	y4, y6, y9

Continue..

109	O35904	Pik3cd	Natural killer cell mediated cytotoxicity / Toll-like receptor signaling pathway	DALLNWLK	2	y4, y5, y6
110	Q9JHG7	Pik3cg	Natural killer cell mediated cytotoxicity / Toll-like receptor signaling pathway	GIDIPVLPR	2	b3, y5, y6, y7
111	P26450	Pik3r1	Natural killer cell mediated cytotoxicity / Toll-like receptor signaling pathway	VLSEIFSPVLFR	2	y5, y6, y7, y10
112	Q9Z1T6	Pikfyve	STRING DB	ELVNWLIR	2	y3, y4, y5, y6
113	O70172	Pip4k2a	STRING DB	FGIDDQDFQNSLTR	2	y4, y6, y9
114	Q80XI4	Pip4k2b	STRING DB	FGIDDQDYQNSVTR	2	y5, y6, y7, y10
115	P70182	Pip5k1a	STRING DB	DC[+57]LVLQSFK	2	y3, y4, y5
116	P53657	Pklr	STRING DB	VFLAQK	2	y3, y4
117	P52480	Pkm	STRING DB	GDYPLEAVR	2	y3, y4, y5, y6
118	Q62077	Plcg1	Natural killer cell mediated cytotoxicity	DEAFDPFDK	2	y3, y4, y6
119	Q8CIH5	Plcg2	Natural killer cell mediated cytotoxicity	SESSTEAYIR	2	y4, y5, y7, y8
				FDDVVQAIR	2	b3, y5, y6, y7
				TTVVNDNGLSPVWAPTQEK	2	y5, y6, y7, y9
120	P48453	Ppp3cb	Natural killer cell mediated cytotoxicity	LFEVGGSPANTR	2	b9, y5, y7, y9
121	Q32M04	Prps1l1	STRING DB	VTAVIPC[+57]FPYAR	2	b4, b3, y7, y8
122	O08586	Pten	STRING DB	IYNLC[+57]AER	2	b3, y4, y6
123	Q9QVP9	Ptk2b	Natural killer cell mediated cytotoxicity	NLLDAVDQAK	2	y4, y6, y7, y8
124	Q05144	Rac2	Natural killer cell mediated cytotoxicity	AVLC[+57]PQPTR	2	y3, y5, y6, y7
125	P60764	Rac3	Natural killer cell mediated cytotoxicity	AVLC[+57]PPPVK	2	y3, y4, y5, y6
126	P15307	Rel	STRING DB	GGDEIFLLC[+57]DK	2	y3, y4, y6, y7
				FVLNDWEAR	2	y4, y6, y7
				TTLIFQK	2	y3, y5
127	Q04207	Rela	Toll-like receptor signaling pathway	DGYYEADLC[+57]PDR	2	y5, y7, y8, y9
				VSGSC[+57]LGGDEIFLLC[+57]DI	2	y3, y4, y6, y11
128	Q04863	Relb	STRING DB	SAGSILGESSTEASK	2	b4, y7, y9, y10
				LTDGVC[+57]SEPLPFTYLPR	2	y7, y9, y12
129	P62746	Rhob	STRING DB	TC[+57]LLIVFSK	2	y3, y4, y5, y6
				QVELALWDTAGQEDYDR	2	y7, y8, y10, y11
130	P84096	Rhog	STRING DB	TVNLNLWDTAGQEEYDR	3	y4, y5, y7, y9
				YLEC[+57]SALQQDGVK	2	y3, y6, y7, y9
131	Q8BG51	Rhot1	STRING DB	ILLVGEPR	2	y4, y5, y6
				WIPLINER	2	y3, y4, y5, y6
				SFEYC[+57]AR	2	y4, y5
132	Q8JZN7	Rhot2	STRING DB	SAFLQAFLGNSLGEAR	2	b3, y8, y10, y11
133	Q8VDU1	Rhov	STRING DB	WLPEIR	2	y3, y4
134	Q60855	Ripk1	Toll-like receptor signaling pathway	TQIDVPLSLK	2	y3, y5, y6, y8
135	P47968	Rpia	STRING DB	FGGEVELR	2	b3, y4, y6
136	Q8C050	Rps6ka5	STRING DB	VGIENFELLK	2	y3, y6, y7
				VIDFGFAR	2	y4, y5, y6
137	P98083	Shc1	STRING DB	EAISLVC[+57]EAVPGAK	2	y3, y4, y8, y9
				ELFDDPSYVNIQNLDK	2	y7, y8, y11
138	P97797	Sirpa	STRING DB	EDVVFTC[+57]QVK	2	b3, y4, y5, y6
139	Q64442	Sord	STRING DB	VAIEPGVPR	2	y4, y5, y6, y7
140	Q62245	Sos1	Natural killer cell mediated cytotoxicity	QLTLLESDLYR	2	y3, y5, y7, y9
141	Q64337	Sqstm1	STRING DB	LTPTTPESSSTGTEDK	2	y7, y9, y11, y12
142	P05480	Src	STRING DB	GAYC[+57]LSVSDFDNAK	2	y3, y7, y8
				DAWEIPR	2	y3, y4, y5
143	P48025	Syk	STRING DB	DESEQTVLIGSK	2	y3, y4, y7, y8
				WYAPEC[+57]INYYK	2	y4, y6, y8, y9
144	Q8CHC4	Synj1	STRING DB	GFEANAPAFDR	2	y6, y7

Continue..

145	Q93092	Taldo1	STRING DB	LSSTWEGIQAGK	2	y3, y4, y6
				ALAGC[+57]DFLTISPK	2	y3, y5, y6
146	Q9WUN2	Tbk1	Toll-like receptor signaling pathway	TTEENPIFVTSR	2	y5, y7, y8, y9
				LSSSQGTIESSLQDISSR	2	y4, y5, y10, y11
147	P40142	Tkt	STRING DB	LDNLVAIFDINR	2	b3, y5, y7, y8
				IIALDGDTK	2	y4, y5, y6, y7
148	Q99MX0	Tktl1	STRING DB	LIESQIQTNK	2	y3, y4, y5, y8
149	Q6R5N8	Tlr13	STRING DB	ILEPNSFSGLTNLR	2	y6, y11
150	Q99MB1	Tlr3	Toll-like receptor signaling pathway	EFSPGC[+57]FQTIGK	2	y4, y8, y9
				LEPFIFDDQTSLR	2	y6, y8
151	Q9EQU3	Tlr9	Toll-like receptor signaling pathway	FVDLSDNR	2	b3, y4, y6
				AQSAVADWVYNELR	2	y7, y8, y9, y10
				TSFLLAQQR	2	y4, y5, y6, y7
152	P06804	Tnf	Natural killer cell mediated cytotoxicity / Toll-like receptor signaling pathway	GDQLSAEVNLPK	2	b3, y7, y8
153	P17751	Tpi1	STRING DB	VVFEQTK	2	y3, y4, y5
				VVLAYEPVWAIGTGK	3	y4, y5, y6, y7
				IIYGGSVTGATC[+57]K	2	y6, y10, y11
154	P62984	Uba52	STRING DB	EGIPPDQQR	2	y3, y4, y5, y6
155	Q91ZJ5	Ugp2	STRING DB	SFENSLGINVPR	2	y4, y6, y9
156	Q63886	Ugt1a1	STRING DB	IPQTVLWR	2	y4, y5, y6, y7
157	Q8VCW4	Unc93b1	STRING DB	SVGWGNIFQLPFK	2	y3, y4, y6, y9
158	P27870	Vav1	Natural killer cell mediated cytotoxicity	YC[+57]SQVESASK	2	y4, y6, y7, y8
				AGAEGILTNR	2	y3, y4, y6, y7
				SDGTYLVR	2	y3, y4, y5, y6
159	Q9R0C8	Vav3	Natural killer cell mediated cytotoxicity	VTWDSAQVFDLAQTLR	2	y3, y6, y8, y9
				EIIDLQQYK	2	y3, y5, y6, y7
				LQAETELINR	2	y4, y6, y7, y8
160	Q9CQV8	Ywhab	STRING DB	IEAELQDIC[+57]NDVLELLDK	2	b4, b3, y6, y10
				YLSEVASGENK	2	y5, y6, y7, y9
				TAFDEAIAELDTLNEESYK	3	y3, y4, y6
161	P04627	Araf	Natural killer cell mediated cytotoxicity	GLNQDC[+57]C[+57]VVYR	2	y3, y5, y6, y7
162	P70444	Bid	Natural killer cell mediated cytotoxicity	QELEVLGR	2	y4, y5, y6
163	P70677	Casp3	Natural killer cell mediated cytotoxicity	SVDSGIYLDSSYK	2	y4, y5, y7, y11
				SGTDVDAANLR	2	y5, y6, y7, y8
164	P18181	Cd48	Natural killer cell mediated cytotoxicity	TIFESEFK	2	y3, y4, y5, y6
				STFYTC[+57]QVSNPVSSK	2	y3, y5, y6, y7
165	P25446	Fas	Natural killer cell mediated cytotoxicity	SDAYQDLIK	2	y4, y5, y6, y7
166	P01580	Ifng	Natural killer cell mediated cytotoxicity	FEVNNPQVQR	2	y5, y6, y7, y8
167	Q60591	Nfatc2	Natural killer cell mediated cytotoxicity	ATIDC[+57]AGILK	2	y4, y6, y7
168	P35235	Ptpn11	Natural killer cell mediated cytotoxicity	YPLNC[+57]ADPTSER	2	y8, y9
				VGQALLQGNTER	2	y6, y7, y9
169	P29351	Ptpn6	Natural killer cell mediated cytotoxicity	GEPWTFLVR	2	y4, y5, y6, y7
				DSNIPGSDYINANYVK	2	b3, y6, y8, y12
				GLDC[+57]DIDIQK	2	y4, y5, y6, y8
170	P04441	Cd74	Antigen processing and presentation	LTITSQNLQLESLR	2	y6, y8, y10, y11
				SGPLEYPQLK	2	y4, y5, y6, y7
171	Q9R233	Tapbp	Antigen processing and presentation	FIPFPASAK	2	y3, y5, y6, y7
				SLSPEQNC[+57]PR	2	y4, y5, y6, y7
172	P01887	B2m	Antigen processing and presentation	TPQIQVYSR	2	y4, y5, y6, y7
173	Q01147	Creb1	Antigen processing and presentation	VAVLENQNK	2	y4, y5, y7
				TLIEELK	2	b4, y3, y4
174	P35564	Canx	Antigen processing and presentation	GSLSGWILSK	2	y3, y4, y6, y7
175	P14211	Calr	Antigen processing and presentation	EQFLDGDAWTNR	3	b3, y3, y4
				QIDNPDYK	2	y3, y4, y6
176	P10605	Ctsb	Antigen processing and presentation	EQWSNC[+57]PTIGQIR	2	y4, y7, y8, y9
				GSC[+57]GSC[+57]WAFGAVEAI	3	y5, y6, y9, y10

Continue..

177	P06797	Ctsl	Antigen processing and presentation	ENGGLDSEESYPYEAK	3	b5, y4, y7, y8
178	O70370	Ctss	Antigen processing and presentation	YIQLPFGDEDALK	2	b3, y3, y5, y9
				NSWGLNFGDQGYIR	2	y5, y8, y11
179	Q61696	Hspa1a	Antigen processing and presentation	DAGVIAGLNVLR	2	b3, y6, y7, y8
180	P20029	Hspa5	Antigen processing and presentation	ITPSYVAFTPEGER	3	y3, y4, y5, y7
				LTPEEIER	2	y3, y4, y5, y6
181	P11499	Hsp90ab1	Antigen processing and presentation	YESLTDPSK	2	b3, y3, y4, y7
				IDIIPNPQER	2	b3, y4, y6, y7
				ADLINNLGTIAK	2	b3, y5, y8, y9
182	P01898	H2-Q10	Antigen processing and presentation	WASVVVPLGK	2	y3, y4, y5, y8
183	Q9ESY9	Ifi30	Antigen processing and presentation	VSLYYESLC[+57]GAC[+57]R	2	y5, y7, y8, y9
184	O89017	Lgmn	Antigen processing and presentation	DYTGEDVTPENFLAVLR	2	y9, y10
				ESSYAC[+57]YYDEER	2	y5, y6, y7, y8
185	P63139	Nfyb	Antigen processing and presentation	EQDIYLPIANVAR	2	b3, y7, y9, y11
186	P70353	Nfyc	Antigen processing and presentation	VQELPLAR	2	b3, y5, y6
187	P61290	Psme3	Antigen processing and presentation	SNQQLVDIIEK	2	y3, y4, y5, y6
				TVESEAASYLDQISR	2	y4, y6, y8, y10
				LIISELR	2	y3, y4, y5
188	P27773	Pdia3	Antigen processing and presentation	DGEEAGAYDGPR	2	y3, y7, y8, y9
				DLLTAYYDVDYEK	3	y3, y4, y6
189	P63017	Hspa8	Antigen processing and presentation	GTLDPVEK	2	y3, y4, y5, y6
				VC[+57]NPIITK	2	y3, y5, y6
190	P21958	Tap1	Antigen processing and presentation	SFANEEGEAQK	2	y3, y5, y6, y9
				GLVEFQDVSFAYPNQPK	3	y4, y5, y6, y7
				ENIAYGLNR	2	y4, y5, y6, y7
191	P36371	Tap2	Antigen processing and presentation	ALVGGTASTSVVR	2	y6, y10, y11
				EAVGGLQTVR	2	y4, y6, y7, y8
192	P17515	Cxcl10	Toll-like receptor signaling pathway	LEIIPASLSC[+57]PR	2	b3, y6, y7, y8
193	P18340	Cxcl9	Toll-like receptor signaling pathway	QFAPSPNC[+57]NK	2	y3, y5, y6, y7
194	P56477	Irf5	Toll-like receptor signaling pathway	DFQLFYDGPR	2	y3, y5, y6, y7
				FYTNQLLDVLDR	2	y5, y6, y9, y10
195	Q8CF89	Tab1	Toll-like receptor signaling pathway	YGYTDIDLLSAAK	2	y4, y5, y7, y9
196	P10923	Spp1	Toll-like receptor signaling pathway	GDSLAYGLR	2	y3, y4, y5, y7
197	Q9QZ06	Tollip	Toll-like receptor signaling pathway	QGQVEDEWYSLSGR	2	y5, y6, y10
198	P58681	Tlr7	Toll-like receptor signaling pathway	NLQELDLSQNYLAR	2	y7, y8, y9, y10
				SLTTLILK	2	y3, y4, y5, y6
199	O08749	Dld	Glycolysis / Gluconeogenesis	GIEIPEVR	2	b3, y4, y5, y6
				IDVSVEAASGGK	2	y4, y6, y7, y9
				FPFAANSR	2	y4, y5, y6, y7
200	P00342	Ldhc	Glycolysis / Gluconeogenesis	LVIITAGAR	2	y4, y5, y6, y7
				VIGSGC[+57]NLDSAR	2	y3, y4, y8, y10
201	P09411	Pgk1	Glycolysis / Gluconeogenesis	AAVPSIK	2	y3, y4, y5
				YSLEPVAAELK	2	y4, y5, y7, y8
				VLPGVDALSNV	2	b7, y3, y9
202	Q9DBJ1	Pgam1	Glycolysis / Gluconeogenesis	ALPFWNEEIVPQIK	3	y3, y4, y5, y6
203	P17182	Eno1	Glycolysis / Gluconeogenesis	DATNVGDEGGFAPNILENK	3	y3, y4, y6, y7
				EALELLK	2	b3, y4, y5
				SC[+57]NC[+57]LLLK	2	y3, y4, y5, y6
204	P35486	Pdha1	Glycolysis / Gluconeogenesis	LEEGPPVTTVLTR	2	y6, y8, y9, y10
				'GGNGIVGAQVPLGAGIALAC[+5	3	y3, y5, y9, y11
				LPC[+57]IFIC[+57]ENNR	2	y5, y6, y7, y8

Continue..

205	P54822	Adsl	Alanine, aspartate and glutamate metabolism	NAFDLLLPK	2	b3, y3, y5, y6
206	P28650	Adssl1	Alanine, aspartate and glutamate metabolism	VVDLLATDADIVSR	2	b3, y6, y8, y9
207	P46664	Adss	Alanine, aspartate and glutamate metabolism	VGIGAFPTEQDNEIGELLQTR	3	y4, y5, y7, y8
				FIEDELQIPVK	2	y3, y4, y9
208	P16460	Ass1	Alanine, aspartate and glutamate metabolism	FELTC[+57]YSLAPQIK	2	y4, y5, y7, y8
				NQAPPGLYTK	2	b3, y3, y6
209	Q61024	Asns	Alanine, aspartate and glutamate metabolism	GLVSLK	2	b4, y3, y4
				ETFEDC[+57]NLLPK	2	y3, y6, y7, y9
				EAFSDGITSVK	2	y4, y6, y7, y8
210	Q8C196	Cps1	Alanine, aspartate and glutamate metabolism	EIEYEVVR	2	y3, y4, y5, y6
211	B2RQC6	Cad	Alanine, aspartate and glutamate metabolism	TLGVDLVALATR	2	b3, y7, y8, y10
				LFVEALGQIGPAPPLK	3	y3, y4, y6, y7
212	P26443	Glud1	Alanine, aspartate and glutamate metabolism	YSTDVSVDEVK	2	y4, y6, y8, y9
				VYEGSILEADC[+57]DILIPAASEK	3	y3, y6, y7, y8
				IIAEGANGPTTPEADK	2	y5, y6, y8, y9
213	P05202	Got2	Alanine, aspartate and glutamate metabolism	EYLPIGGLAEFC[+57]K	2	y3, y8, y9, y10
				FVTVQTISGTGALR	3	b3, y4, y6, y7
214	Q8BGT5	Gpt2	Alanine, aspartate and glutamate metabolism	LFLLADEVYQDNVYSPDC[+57]R	3	b3, y4, y5, y6
215	Q8QZR5	Gpt	Alanine, aspartate and glutamate metabolism	ALELEQELR	2	y3, y4, y7
				LLVAGEGR	2	y4, y5, y6
				LTEQVFNEAPGIR	2	y4, y5, y7
216	D3Z7P3	Gls	Alanine, aspartate and glutamate metabolism	DSPGETDAFGNSEGK	2	y6, y7, y8, y10
				VADYIPQLAK	2	b3, y3, y5, y8
217	P05201	Got1	Alanine, aspartate and glutamate metabolism	VGGVQSLGGTGALR	2	b3, y9, y10

Precision and accuracy of longitudinal label-free PRM

The longitudinal effects (6, 12, 24, and 48 hours) of LPS, IFN-γ, and LPS/IFN-γ on the WCP and SEC in BV2 cells were analyzed using the final 217 and 146 target proteins in PRM mode, which was performed on the same mass spectrometric system as in the discovery stage. One hundred seventeen raw files for the WCP and SEC groups were imported into Skyline for manual peak integration. A plot was generated and exported using the normalized XIC peak areas of the precursors and LRP. Fourteen of 15 iRT peptides were detected in the WCP group, versus 10 iRT for the SEC group. The average CV of the elution time for the detected iRT peptides between 234 runs was 0.43%. The average CVs of normalized XIC peak areas for the WCP and SEC groups between 117 runs were 20.85% and 24.27%, respectively (Table 2-2).

Table 2-2. Variation of label-free PRM analysis

#	iRT peptide	CVs (%) of Retention Time	CVs (%) of normalized XIC for WCL	CVs (%) of normalized XIC for SEC
1	GILFVGSGVSGGEEGAR	0.13	13.89	20.16
2	ELASGLSFPVGFK	0.15	22.05	17.23
3	NGFILDGFPR	0.24	18.06	19.18
4	LTILEELR	0.23	20.28	20.57
5	GLILVGGYGTR	0.14	17.90	14.72
6	ELGQSGVDTYLQTK	0.17	18.69	16.89
7	SAAGAFGPELSR	0.25	15.00	19.12
8	TASEFDSAIAQDK	0.26	16.86	N.D
9	IGDYAGIK	0.05	27.01	N.D
10	DIPVPKPK	1.14	33.88	30.23
11	GISNEGQNASIK	1.50	29.19	27.73
12	SFANQPLEVVYSK	1.09	15.94	N.D
13	LSSEAPALFQFDLK	0.15	22.43	N.D
14	HVLTSIGEK	0.46	N.D	33.69
15	SSAAPPPPPR	0.38	43.53	N.D

The variability in repeat measurements of the same targeted peptides was defined as the technical CVs, whereas that across biological replicates was expressed as the biological CVs. Technical CVs were calculated as described in the methods section with each normalized XIC peak area of the targeted peptides, and biological CVs were determined with the mean CVs of normalized XIC peak areas in technical triplicates. The median CVs of target peptides in the WCP group were 6.07% and 9.09% for technical and biological replicates, and those of the SEC group were 5.02% and 14.25%, respectively. As shown in Figure 2-9 A, the values were less than 20%, indicating good precision in the label-free PRM.

To compare the quantitative differences due to the various labels, the correlation coefficients of redundant proteins in the same treatment and at the same time point (24 hr) between the discovery and targeted analyses were measured with the R-squared statistic, which was 0.7959 for the WCP and SEC experiments (Figure 2-9 B). This result indicates that both approaches had high correlation and reproducibility.

To compensate for the drawbacks of the label-free targeted analysis, a single high-purity heavy isotope-labeled reference peptide (LRP) and multiple heavy-labeled iRT peptides were used to normalize endogenous target peptides and retention times, allowing me to assess and improve the system by LRP normalization and correct for the variations in retention time shifts between LC runs by RT regression. I examined how normalization by LRP affected the results of the PRM analysis in the WCP and SEC groups by comparing the distribution of technical CVs of the iRT peptides before and after normalization (Figure 2-9 C, D). The CVs of

normalized endogenous target peptides by LRP demonstrated better performance than before the normalization, as shown in Figure 2-10.

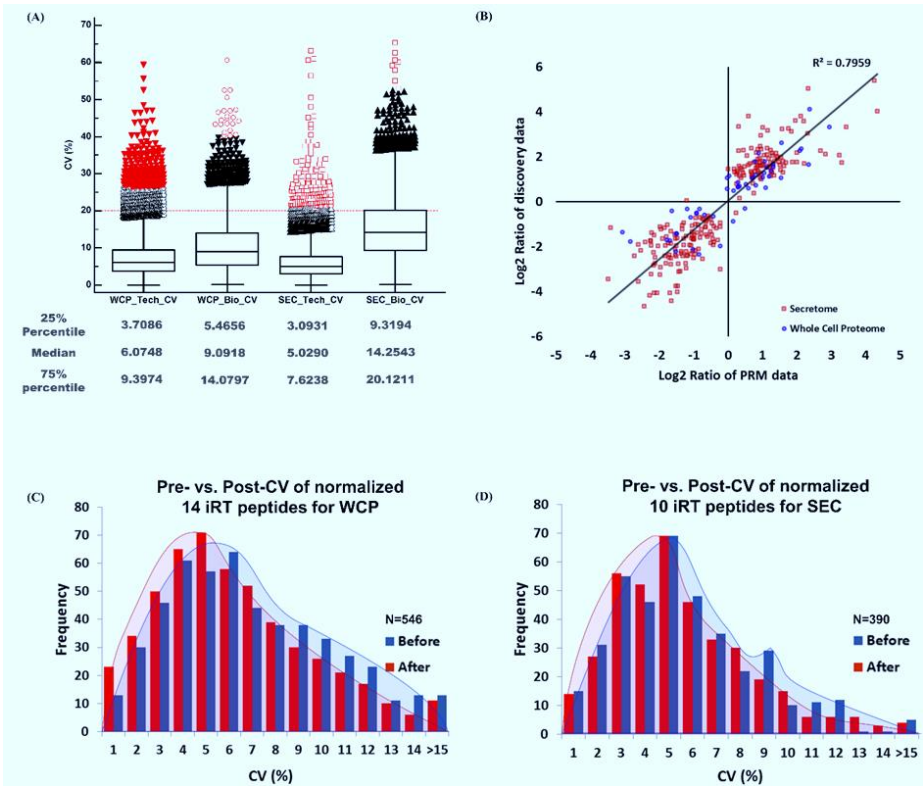

Figure 2-9. Characterization of label-free PRM analysis

(A) CVs between technical replicates and biological replicates in the WCP and SEC groups were plotted to determine the precision of the label-free PRM analysis. Box and whisker plots with statistical summaries were calculated in MedCalc (Ver. 12.3.0.0). (B) Redundant proteins between the discovery and targeted analyses were compared using the ratio of the treated versus control group at 24 hours. (C, D) CVs before and after normalization using LRP were compared in iRT heavy-labeled peptides. The CVs of the technical triplicates were calculated using Excel and drawn as a histogram.

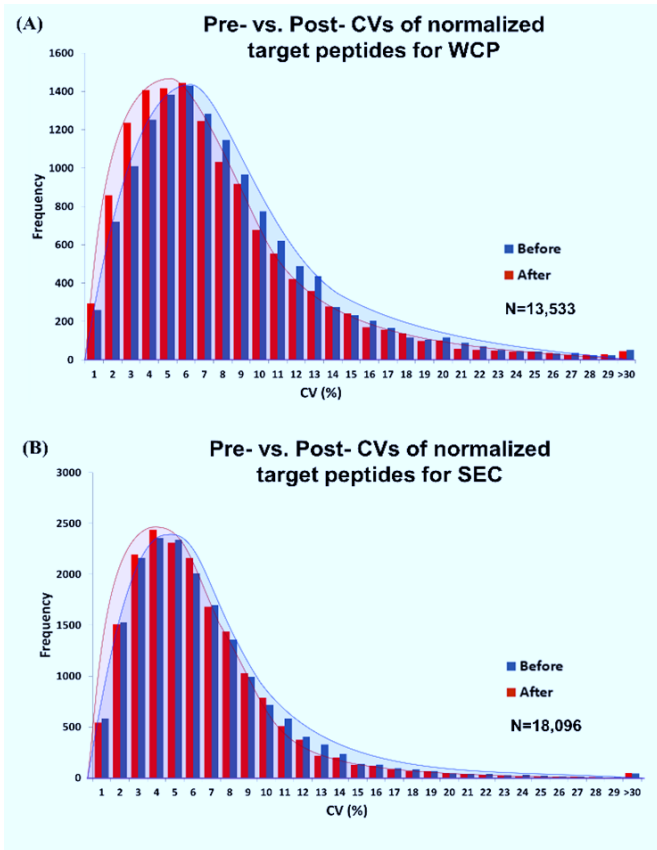

Figure 2-10. Distribution of XIC peak areas before and after normalization.

CVs before and after normalization using LRP were compared in all targeted peptides for the (A) WCP and (B) SEC groups. The CVs of technical triplicates were calculated using Excel and expressed as histograms.

Intracellular protein expression alteration by microglia activation

The normalized XIC of peak areas of target peptides were analyzed statistically in MSstats, based on linear mixed models. By longitudinal PRM analysis of target proteins, I observed several inconsistently expressed proteins between the 3 treatment groups. Of 217 target proteins in the WCP group, 176 were significantly changed, based on an adjusted *p-value* < 0.05, whereas 41 were unchanged between groups during activation (Figure 2-12A). In the Toll-like receptor pathway, 25 proteins were upregulated over time in each treatment group, whereas 6 were downregulated (Figure 2-11 A). With regard to the NK cell-mediated cytotoxicity pathway, 29 proteins rose and 5 proteins decreased over time under each condition (Figure 2-11 B). For antigen processing and presentation, LPS, IFN-γ, and their combination induced MHC I (Figure 2-11 C). These findings are consistent with studies that have concluded that microglia express MHC I and present antigens to T and B lymphocytes when stimulated [56-57].

Most proteins that are associated with metabolism were downregulated on stimulation. Several enzymes that mediate glutamate metabolism, such as Gfpt1, Gfpt2, Cad, and Cps1, were exceptions that increased after treatment with LPS or IFN-γ (Figure 2-11 D, E). This result confirms earlier conclusions that microglia release substantial levels of glutamate once they are activated by pro-inflammatory stimuli and thus contribute to neuronal damage during neuro-inflammation [58-59].

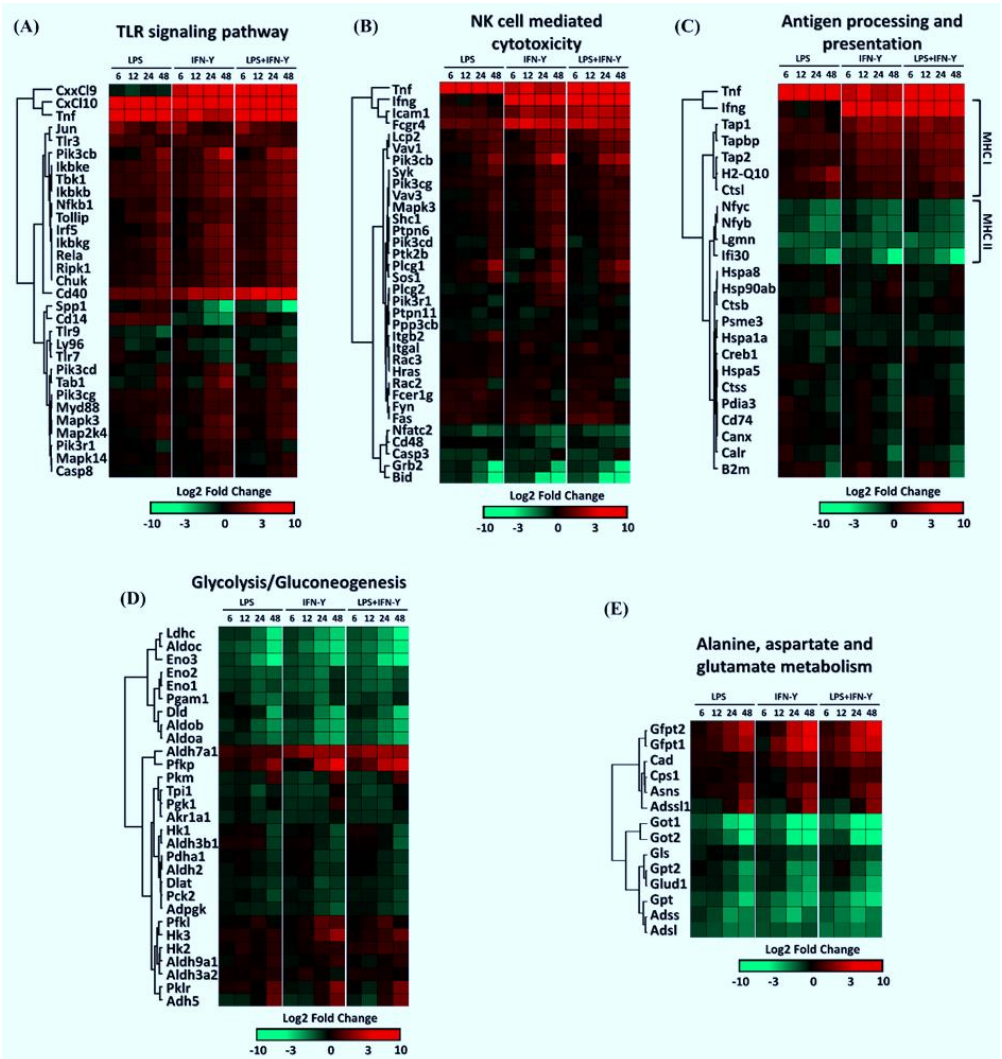

Figure 2-11. Proteomic changes in the WCP group

Five distinct pathways related to microglial activation were selected from the KEGG pathway enrichment list: (A) Toll-like receptor signaling, (B) natural killer cell-mediated cytotoxicity, (C) antigen processing and presentation, (D) glycolysis and gluconeogenesis, and (E) alanine, aspartate, and glutamate metabolism. Heatmap of fold-change in expression compared with control group was visualized using Perseus. Red indicates upregulation, whereas green indicates downregulation.

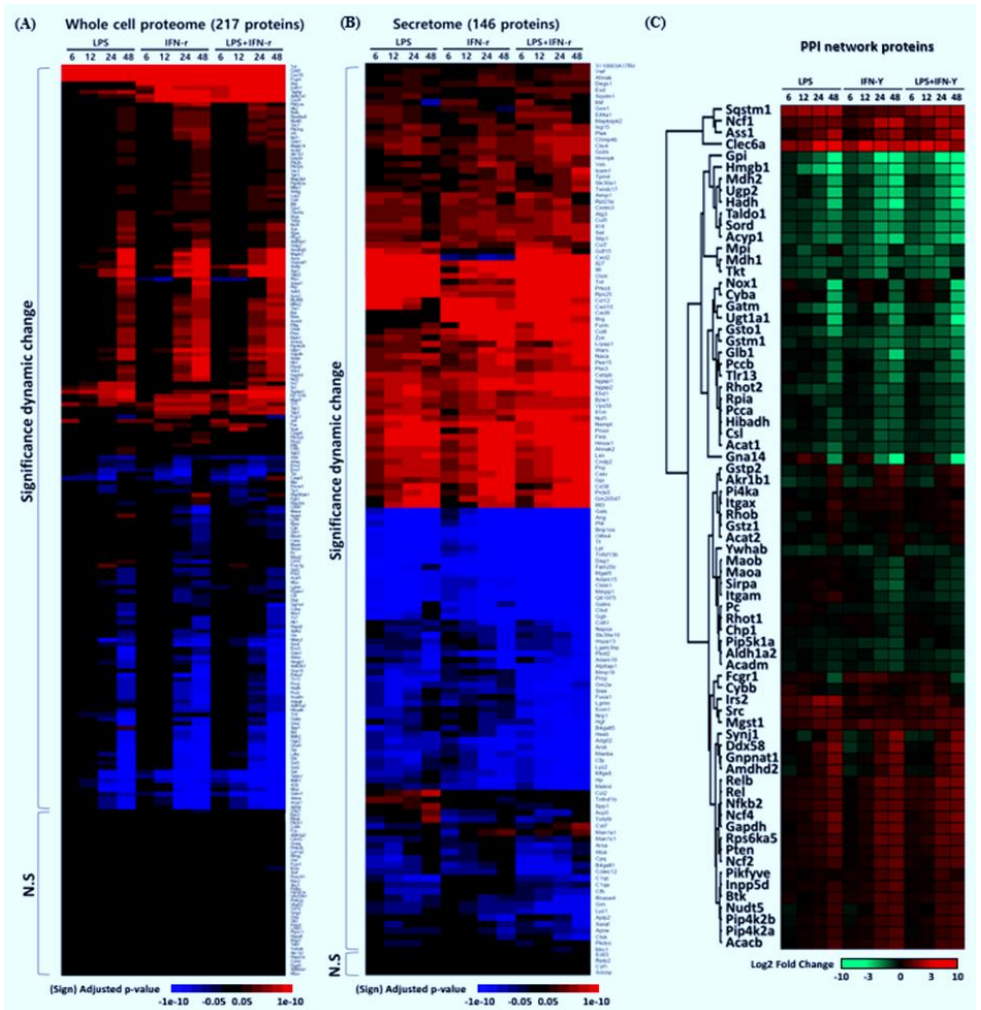

Figure 2-12. Significant proteomic changes and PPI network proteins in the WCP group

Significant proteomic changes in each treatment group against the control in the (A) WCP and (B) SEC groups were analyzed using MSstats, based on the linear mixed model package in R. NS indicates a non-significant change, with an adjusted *p-value* less than 0.05. (C) Temporal changes in the proteome that interact or bind with proteins associated with a KEGG pathway.

Quantitative network map of dynamic proteome during microglial activation

Despite the knowledge of what roles protein play in microglia activation, the alteration network of proteome during activated microglia remains unclear. PPI network model was constructed to track the proteomic changes in the 5 pathways during microglial stimulation (Figure 2-13). In inflammatory responses, Tnf, Cxc110, and Jun were upregulated during the early stages of LPS treatment. In contrast, Cd40, Pik3cb, Chuk, Ikbke, Plcg1, H2-Q10, and Ctsb rose during the later stages of LPS stimulation. Several proteins were downregulated, such as Ifi30, Bid, Grb1, Nfyb, and Nfyc.

Of the proteins that were associated with metabolism, Gfpt2, Pfkp, Adh5, and Adssl1 increased gradually during activation, whereas Aldoa, Aldoc, Eno3, Ldhc, Pgam1, Got1, Got2, and Gpt fell over time (Figure 2-13 A). Unlike the LPS group, IFN-γ treated microglial cells produced Ifng, Fcgr4, and Cxcl9 early during stimulation, and Spp1 and Cd14 declined compared with the control group during the later stages of activation. Hk3 and Pklr levels rose toward the end of the stimulation, whereas Aldh7a1 increased early on (Figure 2-13 B). Although the levels of proteins in the LPS/IFN-γ treated group generally remained unchanged versus the individual treatments, Grb, Cd14, and H2-Q1 content was more similar to that in the LPS treated group, and Spp1, Pfkp, Cxc19, Icam1, Ifng, and Tab1 approximated such levels in IFN-γ treated cells (Figure 2-13 C). The results of the PPI network model support that stimulation of microglia activates immune and inflammatory responses while restraining metabolic processes.

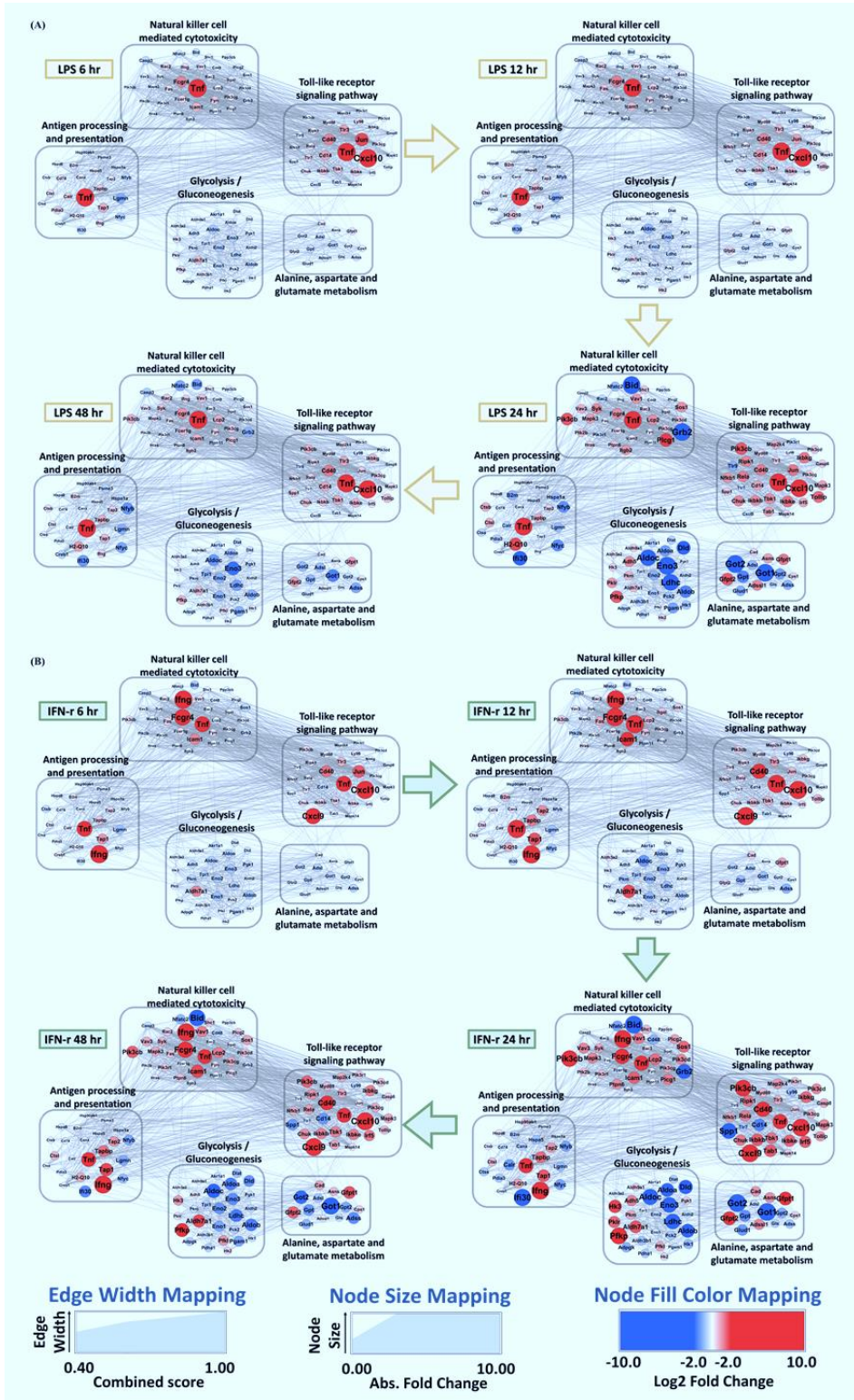
(A)
LPS 6 hr
LPS 12 hr
LPS 24 hr
LPS 48 hr
(B)
IFN-r 6 hr
IFN-r 12 hr
IFN-r 24 hr
IFN-r 48 hr
Natural killer cell mediated cytotoxicity
Toll-like receptor signaling pathway
Antigen processing and presentation
Glycolysis / Gluconeogenesis
Alanine, aspartate and glutamate metabolism
Edge Width Mapping
Edge Width
0.40
1.00
Combined score
Node Size Mapping
Node Size
0.00
10.00
Abs. Fold Change
Node Fill Color Mapping
-10.0
-2.0
-2.0
10.0
Log2 Fold Change

Continue..

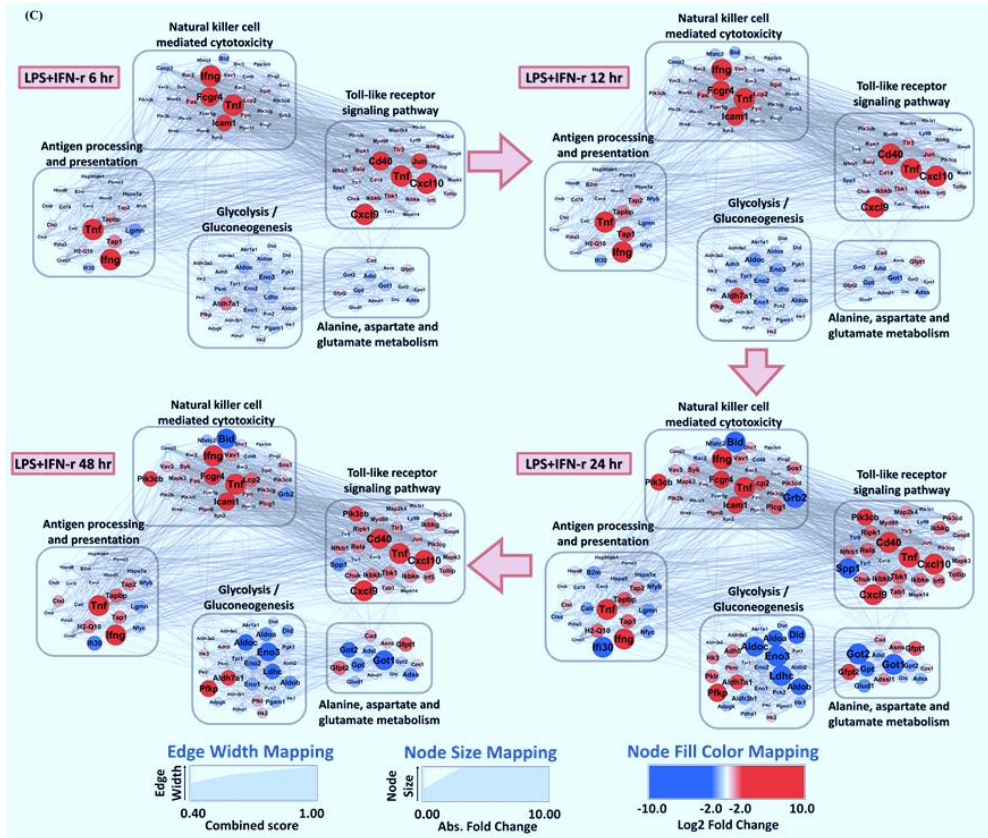

Figure 2-13. Proteomic changes in pathway networks.

Significantly changed proteins between control and (A) LPS, (B) IFN-γ, and (C) LPS plus IFN-γ treatment were visualized in Cytoscape (ver 3.4.0) with the PPI network from STRING. Enriched proteins in the 5 pathways were clustered into gray boxes. Blue and red represent down- and upregulation, respectively, of proteins with $\log_2$ fold-change obtained from the PRM analysis; the size of the nodes was mapped with the absolute fold-change value. The depth of the edges indicates the PPI score using a combination of scores from the experiments and databases

Secreted protein expression alteration in activated microglia

I determined which proteins were secreted by activated microglia versus astrocytes, neurons, and other cells in the surrounding environment. Total 141 secreted proteins changed their expression level during microglial activation, based on an adjusted *p-value* < 0.05 (Figure 2-12 B). By GO analysis of the target proteins, 3 terms were enriched: immune response, lysosomal acid hydrolase activity, and cytokine activity (Figure 2-7 B). Of the 141 proteins, 29 were related to the immune response (Figure 2-14 A). Whereas most of the secreted cytokines were released at high levels on LPS, IFN-γ, and LPS/IFN-γ stimulation, the secretion of 3 (C1qa, Cfh, and C1qc) was higher only with IFN-γ treatment. Notably, LPS alone had a stronger effect on Cxcl2, also known as macrophage inflammatory protein 2, a chemokine that is induced by IL-17. These results are consistent with earlier transcriptome data [60-61].

Further, 37 of the 141 target proteins are involved in lysosomal acid hydrolase activity (Figure 2-14 B), 5 of which (Cd38, Hmox1, Furin, Cndp2, and Ehd1) increased gradually over time; the secretion of 2 (Esd, Eif4a1) rose only at the outset of activation. Acp5 was upregulated only during LPS treatment and decreased when with IFN-γ. Twenty-three target proteins had molecular functions in cytokine activity (Figure 2-14 C). The secretion of Grn, Pf4, and Tnfsf13b declined over time with LPS and IFN-γ treatment, whereas Ccl2 and Tnfsf9 increased exclusively with LPS. Thus, our analysis of proteins that are secreted by endotoxin-activated BV2 microglia demonstrates that the secretion of inflammatory cytokines is enhanced, whereas that of lysosomal proteins decreases.

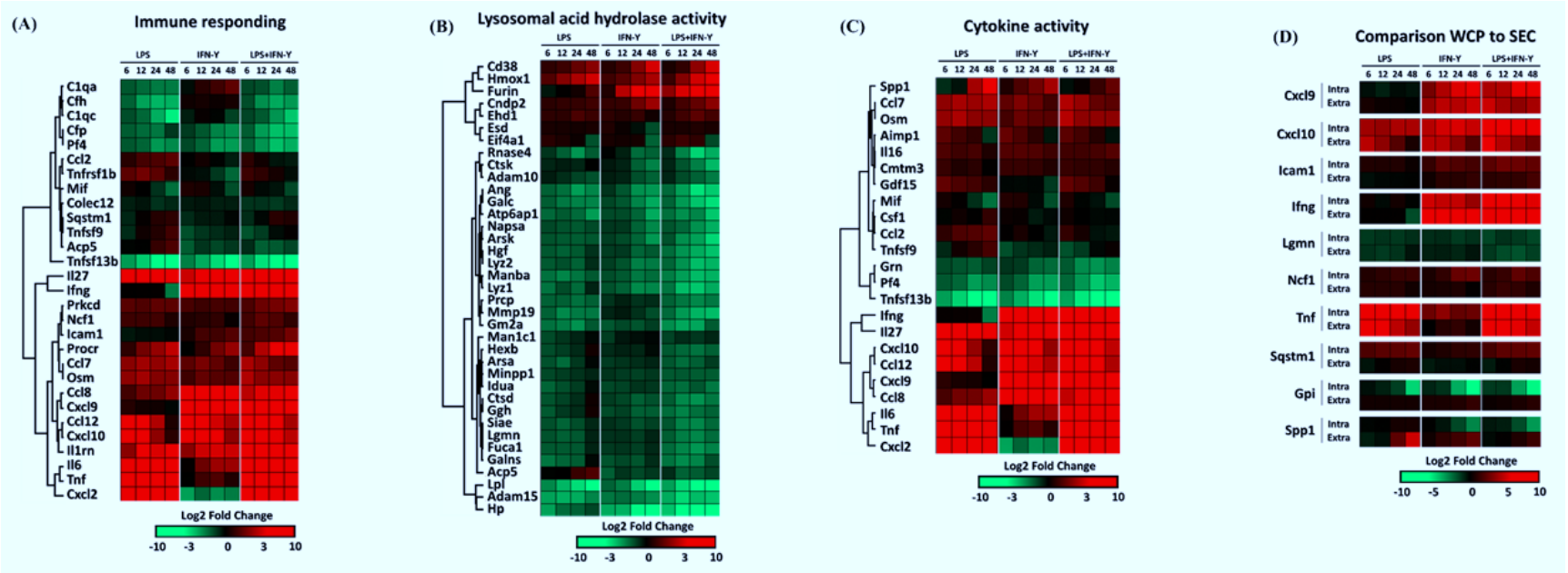

Figure 2-14. Proteomic changes in the SEC group

Three representative molecular functions of DESPs (A) immune response, (B) lysosomal acid hydrolase activity, and (C) cytokine activity were revealed by GO analysis on the DAVID website. (D) Ten redundant proteins in the WCP and SEC groups were compared with regard to expression and secretion levels. Heatmap of fold-change in expression versus control group was visualized using Perseus. Red indicates upregulation, and green indicates downregulation

Differential proteins between intracellular and extracellular

Of the target list in the PRM analysis, 10 proteins were simultaneously quantitated in the WCP and SEC groups (Figure 2-14 D). Six (Cxcl9, Cxcl10, Icam1, Ifng, Lgmn, and Ncf1) of the proteins were altered with same pattern at intra- and extracellular locations, but expression level of Tnf was higher at the WCP group than SEC group in IFN-γ treated microglia. Moreover, Sqstm1, a late endosome protein and an extracellular exosome marker, underwent few changes in secretion compared with the WCP group, rising gradually in secretion during microglial activation.

Notably, Gpi and Spp1 developed contradictory expression patterns in the 2 groups they were downregulated overall in cells but their secretion increased. Gpi is a cytosolic glycolytic enzyme, and in mammals, it functions as a neurotrophic factor for spinal and sensory neurons when secreted [62]. While function of Spp1 in extracellular space were well known as neurotrophic factor or cytokine of immune-inflammatory responding [63], the expression and function of Spp1 in immune cells are not sufficiently defined. Recently, intracellular Spp1 was found to inhibit TLR signaling and effect on liver carcinogenesis [64]. These results indicate that the intracellular and extracellular functions of these proteins differ and that the activation of microglia effects neurotrophic activity.

Microglia specific expression proteins

I conducted a meta-analysis with transcriptome data to further identify markers for proteins that specifically expressed in microglia. I compared the target

proteins used in PRM analysis with 1016 genes known to express microglia specifically by RNA-sequencing [65] (Figure 2-15 A). Among the transcriptome data, proteins overlapping with proteomics data were 42%, of which 53 proteins were DEPs at discovery level (Figure 2-15 B). The proteins are specific for expression in microglia, different from those expressed in astrocyte, neuron, and oligodendrite cell lines. As a result, I were able to get a list of the proteins for WCP group and SEC group in Table 2-3 and 2-4, respectively. Using the linear mixed model in the Msstats analysis, I selected only those proteins with a statistically significant (adjusted p-value <0.05). Among these proteins, only those molecules known as microglia specific proteins based on a transcriptome database were selected and sorted. When microglia activation was performed by treatment with small molecules, it was found that most of the changes in the amount of protein in the cells lysate occurred after 24 hours, while the secreted proteins were responded quickly within 6 hours after the treatments. I have presented 34, 41, and 41 proteins within the cell as microglia specific activation markers that vary dynamically in the LPS, IFN-r, and LPS + IFN-r combined treatment groups. In addition, 47, 37, and 49 extracellular secreted proteins were presented as activated microglia specific secretome markers. Proteins on this list could be used as an important marker of intracellular and extracellular of activated microglia in the further study, and are expected to be very useful as a major marker of neurodegenerative disease including amyotrophic lateral sclerosis, Parkinson's, Alzheimer's, and Huntington's diseases.

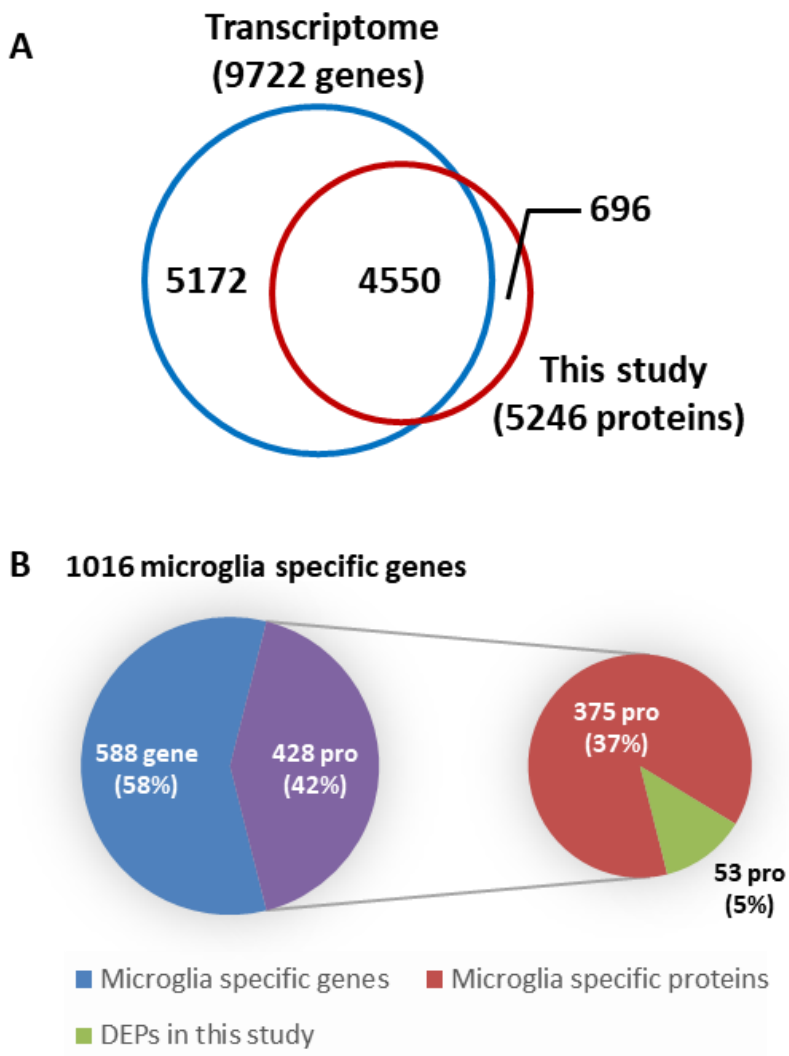

Figure 2-15. Comparison proteomics data with transcriptome data to reveal microglia specific proteins.

(A) The Venn diagram shows the degree of crossing between the transcriptome data of mRNA known to be expressed in microglia and the WCP group protein of activated microglia found in this study (B) The pie chart shows the distribution of microglia specific mRNA and proteins found in this study. The sub-chart shows the distribution of proteins selected as DEPs among microglia specific proteins.

Table 2-3. List of cell specific differentially expressed proteins on WCP group

Protein	LPS treatment in WCP							
	6hr		12hr		24hr		48hr	
	log2FC	adj.pvalue	log2FC	adj.pvalue	log2FC	adj.pvalue	log2FC	adj.pvalue
Cxcl10	3.46477	0	3.25224	4.82E-14	3.68389	0	3.63506	0
Tnf	5.46743	0	5.59178	0	5.34025	0	6.09681	0
H2-Q10	0.26859	0.662065	0.68506	0.017148	1.01429	2.61E-05	1.80346	1.28E-12
Ifi30	-0.5439	0.244524	-0.8199	0.022981	-1.3361	1.03E-05	-2.1797	3.45E-12
Tlr9	-0.1588	0.694165	-0.3868	0.040621	-0.3459	0.035522	-1.0213	1.06E-10
Fcgr4	1.22076	2.36E-09	1.29016	3.33E-10	1.10044	4.07E-08	1.15687	3.03E-09
Eno3	-0.5822	0.890512	-0.8426	0.679106	-1.8717	0.0932	-4.973	4.98E-07
Bid	-0.4043	0.898889	-0.2583	0.939655	-1.2092	0.166258	-3.3886	5.75E-06
Tapbp	0.56922	0.064584	0.73801	0.00563	0.81164	0.000479	0.86233	7.00E-05
Tlr13	0.10989	0.953298	-0.2446	0.754354	-0.2283	0.604241	-1.1512	0.000515
Rela	0.265	0.887492	0.23385	0.83565	0.43138	0.395116	1.28952	0.000914
Itgax	0.15276	0.887492	0.06079	0.939655	0.01757	0.949969	0.74766	0.001335
Cyba	0.09775	0.991868	0.21069	0.939655	0.07801	0.934868	-1.9413	0.001554
Fcgr1	0.25414	0.804111	0.40343	0.466135	0.28799	0.433928	-0.8752	0.001607
Ncf4	0.17463	0.940081	0.25528	0.857937	0.80969	0.141433	1.40172	0.00199
Ptpn6	-0.0391	0.991868	0.06473	0.939655	0.16991	0.535928	0.59607	0.003007
Sord	-0.509	0.636827	-0.3667	0.665249	-1.0808	0.016092	-1.1661	0.003152
Ncf2	0.29333	0.700864	0.25085	0.665249	0.38548	0.269202	0.78644	0.003482
Nfkb2	0.33259	0.794404	0.48487	0.505513	0.71699	0.082543	0.99125	0.004478
Inpp5d	0.08504	0.940081	0.23717	0.622407	0.23948	0.433928	0.62986	0.006316
Itgam	0.04745	0.991868	0.05628	0.939655	0.28934	0.358426	0.62947	0.008291
Itgb2	-0.012	0.999653	-0.1186	0.939655	0.37463	0.492659	1.03929	0.011488
Ctsb	0.00089	0.999653	-0.1159	0.939655	0.34712	0.426774	0.81239	0.013094
Relb	0.24151	0.92634	0.35911	0.754354	0.67242	0.279117	1.18846	0.013094
Pik3cg	0.30176	0.623991	0.36487	0.38388	0.50104	0.061604	0.54918	0.015132
Vav1	0.32284	0.887492	0.36813	0.7004	0.62383	0.279117	1.05214	0.018083
Nfkb1	0.07789	0.991868	0.46643	0.631304	0.34309	0.589716	1.08055	0.02078
Myd88	0.19015	0.831693	0.34141	0.438015	0.27237	0.355974	0.47033	0.035293
Tlr7	0.43696	0.127934	0.13898	0.754354	-0.0273	0.923587	-0.3889	0.037959
Cd14	0.88848	0.222043	1.06681	0.077904	0.89255	0.079631	0.88861	0.039152
Hk2	0.03354	0.991868	0.39429	0.180947	0.08243	0.774845	0.39105	0.044981
Ptk2b	0.04545	0.991868	-0.0575	0.946388	0.02621	0.949969	0.65883	0.047086
Spp1	-0.1047	0.940081	-0.0181	0.964297	0.52602	0.124529	0.55317	0.049928
Fcer1g	0.48426	0.096262	0.3514	0.252707	0.66961	0.001527	0.34426	0.06961

Continue…

Protein	IFN-γ treatment in WCP							
	6hr		12hr		24hr		48hr	
	log2FC	adj.pvalue	log2FC	adj.pvalue	log2FC	adj.pvalue	log2FC	adj.pvalue
Cxcl10	3.92696	0	4.52446	0	4.61119	0	4.24949	0
Fcgr4	2.65939	0	3.14734	0	2.6146	0	2.42782	0
Ifi30	-0.3476	0.632536	-0.4185	0.280505	-1.4965	3.48E-07	-2.8953	0
Spp1	-0.0198	0.989224	-0.3887	0.33797	-1.3474	5.22E-06	-2.5072	2.75E-14
Hk3	-0.0153	0.989224	0.21759	0.592033	1.00531	0.000124	1.84322	4.14E-11
Tapbp	0.56729	0.039186	1.28651	3.31E-08	1.43051	8.79E-10	1.46439	1.76E-10
Bid	-0.6575	0.793819	-0.6152	0.592033	-2.7041	0.000251	-4.4826	5.05E-09
Tnf	2.42024	3.95E-08	3.10032	8.19E-12	2.22711	1.38E-07	2.36012	1.45E-08
Ptpn6	-0.0205	0.989224	0.15575	0.624565	0.63848	0.001603	1.13347	6.45E-08
Inpp5d	0.19691	0.818112	0.31752	0.33797	0.86598	0.000243	1.1752	7.11E-07
Tlr13	-0.0597	0.989224	-0.1836	0.733692	-0.8036	0.013847	-1.6114	1.35E-06
Ncf2	0.09478	0.989224	0.25713	0.550073	1.04192	0.00017	1.2886	2.56E-06
Cd48	-0.1395	0.944813	-0.0645	0.876227	-0.5489	0.015545	-1.0089	1.04E-05
H2-Q10	0.24296	0.725592	0.8295	0.000595	0.8591	0.000158	0.93875	2.26E-05
Icam1	1.21734	0.008613	2.06096	3.60E-07	1.8135	3.13E-06	1.56503	2.43E-05
Sord	-0.5773	0.507119	-0.738	0.156345	-1.7966	1.30E-05	-1.5536	7.64E-05
Tlr7	0.28449	0.473821	0.21741	0.438145	-0.2951	0.118794	-0.704	0.000142
Cd14	-0.4666	0.725592	-0.3439	0.607353	-1.357	0.001722	-1.6145	0.000153
Irf5	0.15457	0.989224	0.39708	0.564206	1.3183	0.00272	1.57693	0.000266
Pik3cg	0.09811	0.989224	0.29878	0.368646	0.83801	0.00028	0.8135	0.000268
Nfkb2	0.08407	0.989224	0.40539	0.438145	1.08629	0.001968	1.18587	0.000536
Rela	0.19211	0.989224	0.44442	0.438145	0.98818	0.010286	1.27911	0.000726
Ncf1	0.65432	0.818112	1.13261	0.280505	2.28767	0.002304	2.43238	0.000912
Myd88	0.15938	0.894157	0.29808	0.361183	0.71411	0.001521	0.71967	0.000956
Itgam	0.10491	0.989224	0.04355	0.926359	-0.3747	0.122607	-0.725	0.001997
Ncf4	0.06683	0.989224	0.36636	0.60452	1.2245	0.006858	1.36481	0.002027
Vav1	0.32587	0.888602	0.36746	0.600963	1.26638	0.004579	1.33002	0.002308
Relb	0.02373	0.989224	0.50859	0.489583	1.29968	0.006884	1.37248	0.003445
Plcg2	-0.0522	0.989224	-0.048	0.946012	0.58286	0.115083	0.96203	0.006661
Eno3	-0.7622	0.831692	-0.945	0.522	-1.4925	0.118595	-2.4453	0.007749
Lcp2	0.10122	0.989224	0.71303	0.444032	1.29682	0.041147	1.43556	0.018677
Btk	0.30878	0.879696	0.3558	0.585269	0.96617	0.017446	0.91852	0.019108
Sirpa	0.09467	0.989224	-0.0208	0.978406	-0.7338	0.118486	-1.0362	0.020309
Hk2	-0.0487	0.989224	0.13845	0.653836	0.38611	0.04948	0.41939	0.02644
Itgax	0.219	0.777605	0.28728	0.404229	0.36004	0.124355	0.489	0.029119
Pik3cd	-0.0185	0.989224	0.04937	0.965761	0.65764	0.264753	1.18754	0.030189
Nfkb1	0.10374	0.989224	0.3608	0.626608	0.80765	0.089303	0.95044	0.035824
Ptk2b	-0.2477	0.882017	-0.5848	0.20218	0.11193	0.765729	0.66869	0.036513
Lgmn	-0.8422	0.355987	-0.7974	0.255878	-1.126	0.021295	-0.9246	0.048416
Fcgr1	0.67562	0.070416	0.95261	0.001712	0.82773	0.002802	0.37269	0.161158
Itgal	0.11416	0.902981	0.58643	0.001129	0.12858	0.45727	-0.099	0.535409

Continue…

Protein	LPS+IFN-γ treatment in WCP							
	6hr		12hr		24hr		48hr	
	log2FC	adj.pvalue	log2FC	adj.pvalue	log2FC	adj.pvalue	log2FC	adj.pvalue
Cxcl10	5.57955	0	5.91902	0	6.66394	0	5.85293	0
Fcgr4	2.5726	0	2.71025	0	2.34087	0	2.30419	0
Ifi30	-0.6883	0.045998	-0.9238	0.002299	-1.6834	1.85E-08	-3.2453	0
Spp1	-0.4327	0.330491	-0.544	0.110024	-1.4096	1.95E-06	-2.8778	0
Tnf	5.13562	0	5.80484	0	5.34843	0	6.11683	0
Tapbp	0.93162	7.72E-05	1.34383	7.46E-09	1.54346	5.57E-11	1.68259	1.25E-12
H2-Q10	0.53465	0.055194	0.84642	0.000412	1.28754	6.23E-08	1.4908	3.67E-10
Bid	-0.7641	0.560082	-0.9411	0.34696	-2.8957	0.000106	-4.8001	5.35E-10
Icam1	1.97903	1.35E-06	2.47576	1.78E-09	2.37173	4.27E-09	2.18192	1.93E-08
Tlr9	-0.1566	0.539045	-0.128	0.522859	-0.1917	0.199148	-0.8104	4.85E-08
Eno3	-1.0605	0.527519	-1.1849	0.365262	-2.5667	0.007149	-4.9495	3.69E-07
Hk3	0.05746	0.930551	0.30115	0.387977	0.52707	0.041016	1.19559	3.82E-06
Tlr13	-0.1469	0.826783	-0.5525	0.179542	-0.8455	0.010725	-1.419	1.67E-05
Sord	-0.723	0.195996	-1.1117	0.011032	-1.7723	1.66E-05	-1.7015	1.81E-05
Ptpn6	0.0579	0.921681	0.10534	0.692468	0.55791	0.005994	0.83189	3.16E-05
Ncf2	0.2994	0.536917	0.15632	0.669123	0.95706	0.000541	1.07988	5.57E-05
Myd88	0.33109	0.341554	0.25378	0.409639	0.73448	0.001179	0.8902	5.57E-05
Rela	0.71222	0.192966	0.58304	0.235546	1.20759	0.002096	1.52753	6.59E-05
Tlr7	0.28372	0.334576	0.22726	0.376822	-0.351	0.066064	-0.7074	0.000124
Nfkb2	0.45774	0.422424	0.63613	0.136513	1.26113	0.000431	1.29238	0.000169
Cyba	0.12275	0.930551	0.43329	0.614843	-0.138	0.832446	-2.0927	0.000488
Inpp5d	0.10577	0.826783	0.17433	0.59093	0.58847	0.011653	0.77434	0.00061
Ncf4	0.20155	0.826783	0.46499	0.464412	1.12127	0.014439	1.47854	0.000842
Relb	0.58399	0.463569	0.59197	0.376822	1.47823	0.002442	1.51112	0.001334
Fcgr1	0.39612	0.375125	0.51263	0.129311	0.29266	0.320924	-0.8283	0.002209
Irf5	0.3389	0.694288	0.48635	0.428334	1.07944	0.01505	1.30355	0.002386
Hk2	0.30633	0.316458	0.38982	0.097985	0.66237	0.00089	0.5758	0.002511
Lgmn	-1.312	0.024751	-0.9383	0.110024	-1.1041	0.024665	-1.3544	0.00434
Itgax	0.01702	0.96762	0.13685	0.669123	0.29633	0.222074	0.63557	0.004914
Cd48	-0.0652	0.921681	-0.0735	0.827482	-0.4157	0.073355	-0.6195	0.005068
Nfkb1	0.56141	0.475829	0.35972	0.589627	1.07147	0.023943	1.23451	0.006919
Lcp2	0.5719	0.645995	0.97383	0.228454	1.55721	0.014913	1.65649	0.006954
Vav1	0.4407	0.604459	0.54809	0.376822	1.18636	0.008807	1.13339	0.008951
Pik3cg	0.23998	0.560082	0.26797	0.387977	0.74143	0.001296	0.54971	0.012205
Itgam	-0.1704	0.730797	-0.2184	0.521926	-0.476	0.050618	-0.5617	0.015289
B2m	0.10209	0.930551	0.55839	0.455999	0.28595	0.622719	-1.2271	0.016726
Ncf1	0.96363	0.422424	1.24749	0.188373	2.15824	0.004485	1.68011	0.019964
Ptk2b	0.06695	0.930551	-0.1336	0.776437	0.35716	0.316254	0.7041	0.027501
Btk	0.18516	0.826783	0.35134	0.542544	0.84154	0.041016	0.81138	0.038087
Fcer1g	0.31584	0.272217	0.51758	0.015109	0.15048	0.476757	-0.2733	0.146979
Itgal	0.37083	0.083755	0.71208	6.05E-05	0.29785	0.077094	-0.02	0.902953

Table 2-4 List of cell specific differentially secreted proteins on SEC group

Protein	LPS treatment in SEC							
	6hr		12hr		24hr		48hr	
	log2FC	adj.pvalue	log2FC	adj.pvalue	log2FC	adj.pvalue	log2FC	adj.pvalue
Acp5	4.77849	0	4.86113	0	4.49361	0	4.91289	0
Adam15	1.0862	2.50E-06	1.73085	1.82E-11	2.22287	0	2.69162	0
Ang	-0.53	0.134784	-0.2387	0.5012	2.09927	1.38E-07	4.30057	0
B4galt1	6.26834	1.62E-14	7.12559	0	6.14529	2.43E-14	5.51018	8.86E-13
C1qa	1.22407	2.10E-09	1.10927	2.69E-08	1.32017	3.63E-10	1.2882	4.62E-10
C1qc	-1.938	0.000759	-2.6114	1.00E-05	-3.1812	1.89E-07	-3.5422	1.28E-08
Ccl12	1.84757	4.81E-06	2.13454	2.16E-07	1.96757	8.34E-07	2.21506	8.06E-08
Ccl2	5.59272	8.17E-12	5.07426	1.68E-10	4.03037	7.75E-08	3.24608	5.53E-06
Ccl7	-1.013	0.003322	-1.1597	0.00075	-1.7672	7.77E-07	-1.5873	7.10E-06
Ccl8	0.93046	0.037345	1.49663	0.00099	1.46795	0.001067	1.98654	1.87E-05
Cebpb	-0.7506	0.076524	-0.5088	0.23926	-0.6367	0.128525	-1.9146	1.87E-05
Cfh	-1.1216	0.0234	-1.8807	0.00024	-2.1169	3.08E-05	-2.0665	4.82E-05
Cfp	-0.8923	0.173994	-1.1777	0.07535	-2.0292	0.002397	-2.7876	5.23E-05
Cndp2	1.90583	3.23E-05	2.16882	3.38E-06	1.78093	6.69E-05	1.80006	5.67E-05
Csf1	-1.097	0.001358	-1.5485	1.26E-05	-1.3929	5.36E-05	-1.3741	6.34E-05
Cst7	0.58509	0.065441	0.99666	0.00216	1.06668	0.000877	1.25352	0.000111
Ctsd	1.85834	0.042253	3.19035	0.00065	2.83778	0.00186	3.38352	0.000258
Cxcl10	-1.0867	0.017431	-1.2775	0.00502	-1.7967	9.39E-05	-1.5205	0.000823
Cxcl2	0.59454	0.03018	0.73266	0.00782	0.80846	0.003006	0.89938	0.001109
Furin	-0.2349	0.497836	0.03063	0.93652	0.24177	0.494936	1.08407	0.003805
Galns	-1.8502	0.000973	-2.019	0.00035	-1.9706	0.000353	-1.5092	0.006365
Gdf15	0.57827	0.07863	0.66139	0.04833	0.69966	0.034035	0.84545	0.012959
Grn	-0.8077	0.019217	-0.9225	0.00733	-1.0021	0.003128	-0.8336	0.015915
Hexb	-0.5327	0.0234	-0.3819	0.09733	-0.739	0.001645	-0.5546	0.019558
Hmox1	-0.0807	0.774844	0.18244	0.52274	-0.0044	0.992764	0.66506	0.02409
Hp	0.55028	0.019612	0.25362	0.28172	0.26784	0.243031	-0.5284	0.025472
Icam1	-1.104	0.00072	-0.9022	0.00477	-0.9408	0.00283	-0.6183	0.057102
Il27	0.87824	0.000453	0.88043	0.00042	0.92836	0.000161	0.46593	0.059286
Isg15	0.51343	0.43539	1.29126	0.06002	1.96641	0.004331	1.27229	0.072811
Lgmn	3.95719	0	3.11249	2.46E-12	1.92294	6.11E-07	0.60075	0.105106
Lyz1	-0.5926	0.325592	-1.0716	0.07563	-1.693	0.005378	-1.0191	0.105106
Mapkapk2	1.28903	0.000222	0.99884	0.00318	0.87127	0.008665	0.53418	0.121277
Metrnl	-1.0737	0.042694	-1.2212	0.02212	-1.3619	0.009144	-0.637	0.256934
Mmp19	-1.8325	0.008679	-1.2157	0.07535	-1.098	0.105023	-0.7835	0.286325
Mrc1	3.34568	2.01E-12	3.70631	8.10E-14	2.36092	4.93E-08	0.42503	0.301653
Napsa	-0.9184	0.018212	-1.0839	0.00513	-0.9959	0.008665	-0.3912	0.330805
Ncf1	-0.9973	0.067985	-0.8856	0.10114	-1.1192	0.038368	-0.5096	0.374317
Olfm4	1.00649	0.016722	0.79441	0.05471	0.9186	0.024723	0.38002	0.377433
Pf4	1.25786	0.080031	1.56396	0.03411	1.24445	0.083863	0.63058	0.405928
Plek	-0.9463	0.00117	-0.7534	0.00828	-0.516	0.067419	0.19946	0.516418
Pnp	-0.8598	0.019612	-0.6993	0.05475	-0.4671	0.193408	0.25262	0.520614
Prkcd	0.73873	0.00033	0.63023	0.00188	0.6774	0.000709	0.13231	0.531258
Spp1	-1.3507	1.26E-09	-1.1505	7.18E-08	-1.0428	5.33E-07	-0.0769	0.736103

Continue…

Protein	IFN-γ treatment in SEC							
	6hr		12hr		24hr		48hr	
	log2FC	adj.pvalue	log2FC	adj.pvalue	log2FC	adj.pvalue	log2FC	adj.pvalue
Acp5	2.64511	7.17E-05	6.29223	1.30E-14	7.13251	0	6.87385	0
Adam15	0.83521	0.00024	1.17547	5.78E-07	1.69056	2.63E-11	2.18796	4.05E-15
Ang	3.04209	4.35E-09	3.95185	8.00E-13	3.99091	6.74E-13	4.45629	6.48E-15
B4galt1	0.44918	0.23485	2.35855	1.78E-08	3.06409	7.89E-12	3.7085	6.48E-15
C1qa	0.69401	0.01528	0.80563	0.00369	1.31667	3.69E-06	1.68798	1.75E-08
C1qc	0.70156	0.04145	0.73657	0.03002	1.44533	2.26E-05	2.00755	3.13E-08
Ccl12	0.37126	0.31279	1.00529	0.00597	1.46523	6.32E-05	2.12362	5.37E-08
Ccl2	4.54746	0	4.388	0	2.75819	4.48E-10	2.24557	6.39E-08
Ccl7	-0.8259	0.00073	-0.7625	0.0014	-1.1067	4.95E-06	-1.3557	6.39E-08
Ccl8	-0.8344	0.01731	-1.1451	0.0009	-1.8154	4.41E-07	-1.8161	3.21E-07
Cebpb	4.01795	0	3.96205	0	3.12591	1.77E-12	1.90239	5.11E-07
Cfh	1.01692	3.66E-07	0.84753	1.01E-05	0.99566	2.43E-07	0.94118	5.23E-07
Cfp	-0.5563	0.21056	-0.2901	0.50438	-0.7684	0.06304	-2.1069	2.04E-06
Cndp2	-1.943	0.00652	-2.0302	0.00369	-2.8546	4.58E-05	-3.2758	3.83E-06
Csf1	-1.5271	0.00817	-1.8623	0.00107	-2.4798	1.44E-05	-2.6172	4.56E-06
Cst7	0.39541	0.14384	0.95155	0.00039	0.91081	0.00037	1.17852	7.25E-06
Ctsd	-0.6273	0.07489	-0.6335	0.07033	-1.1254	0.00085	-1.5377	9.26E-06
Cxcl10	-1.8449	3.66E-07	-1.1362	0.00072	-1.6345	1.62E-06	-1.4316	1.30E-05
Cxcl2	-0.5881	0.21018	-0.9681	0.03409	-1.6505	0.00024	-1.72	0.00013
Furin	0.84128	7.17E-05	0.69951	0.00068	0.76568	0.00012	0.74275	0.00017
Galns	-0.6856	0.01995	-0.7916	0.0059	-1.0827	0.00014	-0.9056	0.0012
Gdf15	-0.6497	0.23223	-1.0106	0.06299	-1.5156	0.00341	-1.6686	0.00133
Grn	-1.363	0.01701	-1.2299	0.02689	-1.4261	0.00718	-1.6276	0.0024
Hexb	1.83364	0.05023	2.69483	0.00366	2.82376	0.00165	2.67828	0.00276
Hmox1	0.89542	0.04613	1.38449	0.00179	1.2114	0.0044	1.15611	0.00628
Hp	-0.9388	8.04E-06	-0.8115	7.43E-05	-0.9539	2.33E-06	-0.4971	0.00797
Icam1	-0.4042	0.23576	-0.2677	0.43779	-0.5538	0.08489	-0.8602	0.00802
Il16	-0.7149	0.21018	-0.933	0.09559	-1.4539	0.0066	-1.3895	0.00871
Il1rn	1.24334	0.00139	1.6206	5.54E-05	1.3447	0.00032	0.88092	0.01524
Il27	1.08124	0.01212	1.08916	0.00927	1.02857	0.01045	0.80987	0.04239
Isg15	-0.1038	0.77245	-0.1307	0.69138	-0.1129	0.71076	-0.6519	0.0431
Lgals3bp	0.50465	0.03871	0.43888	0.06769	0.31719	0.15575	-0.45	0.0446
Lgmn	-0.9155	0.25902	-1.0994	0.1872	-1.5679	0.04428	-1.5148	0.04878
Lyz1	-0.7565	0.02051	-0.7483	0.01895	-0.7646	0.01262	-0.5891	0.05103
Lyz2	-0.0175	0.98625	-0.3502	0.56996	-1.229	0.03826	-1.1211	0.05514
Napsa	0.44249	0.53761	0.7355	0.31444	1.51207	0.0247	0.8683	0.19779
Spp1	0.51344	0.03983	0.57835	0.01821	0.69333	0.00341	0.14976	0.50547

Continue…

Protein	LPS+IFN-γ treatment in SEC							
	6hr		12hr		24hr		48hr	
	log2FC	adj.pvalue	log2FC	adj.pvalue	log2FC	adj.pvalue	log2FC	adj.pvalue
Acp5	1.85522	2.09E-06	2.78728	8.01E-11	3.24348	6.54E-13	3.96231	0
Adam15	0.76994	0.00039	1.7267	9.83E-12	2.68535	0	3.30143	0
Ang	7.71479	0	8.65536	0	8.39975	0	7.97518	0
B4galt1	1.06784	5.11E-08	1.46389	7.86E-12	1.5968	3.60E-13	1.761	1.18E-14
C1qa	4.01098	0	3.2629	8.10E-15	3.28789	4.05E-15	3.09114	2.49E-14
C1qc	2.46521	2.61E-07	2.93635	2.98E-09	3.00176	1.39E-09	3.67857	3.14E-12
Ccl12	-0.9727	0.02209	-0.8719	0.03164	-1.204	0.00307	-3.0567	2.51E-10
Ccl2	0.5306	0.05077	1.00719	0.0002	1.39663	7.67E-07	1.9301	3.29E-10
Ccl7	5.50125	0	3.93457	0	3.04745	1.96E-12	2.44437	9.53E-10
Ccl8	-0.6327	0.00696	-1.1888	1.04E-06	-1.4561	9.50E-09	-1.5828	9.76E-10
Cebpb	-1.2038	0.00039	-1.7362	7.87E-07	-2.0617	1.25E-08	-2.1586	3.64E-09
Cfh	6.03791	4.54E-13	5.32477	2.23E-11	4.90234	1.95E-10	4.20706	8.46E-09
Cfp	0.97837	0.00021	1.0587	4.18E-05	1.1563	8.13E-06	1.59276	9.46E-09
Cndp2	-1.9651	0.00046	-2.6923	2.73E-06	-3.4165	1.32E-08	-3.4279	1.05E-08
Csf1	0.71145	0.00039	1.00189	1.11E-06	1.01458	7.30E-07	1.21439	1.12E-08
Cst7	-1.1902	0.00045	-1.7132	1.01E-06	-2.244	1.75E-09	-2.0283	1.62E-08
Ctsd	-0.9514	0.00572	-1.1775	0.00045	-1.6406	2.48E-06	-2.0033	3.18E-08
Cxcl10	5.42031	0	4.45134	0	3.1674	5.55E-12	2.20841	6.33E-08
Cxcl2	0.42362	0.19529	0.92432	0.00387	1.31573	6.36E-05	1.80583	2.09E-07
Furin	-1.2114	0.00696	-1.8126	5.54E-05	-2.602	4.69E-08	-2.3214	5.36E-07
Galns	-1.053	0.00029	-1.5538	2.44E-07	-1.653	4.13E-08	-1.3618	2.41E-06
Gdf15	4.61371	1.75E-06	4.63021	1.05E-06	4.3411	2.95E-06	4.34914	2.63E-06
Grn	-1.3284	1.54E-09	-1.5771	7.88E-12	-1.5085	2.33E-11	-0.8695	7.33E-06
Hexb	-2.2416	0.00118	-2.9402	2.43E-05	-3.1312	6.81E-06	-3.1043	7.33E-06
Hmox1	2.33847	5.01E-07	1.85004	2.44E-05	1.86635	1.78E-05	1.82608	2.34E-05
Hp	-1.0611	0.04293	-1.8075	0.00051	-2.2408	2.19E-05	-2.2017	2.68E-05
Icam1	-1.9531	0.0004	-2.5028	6.80E-06	-2.1556	6.23E-05	-2.2464	3.16E-05
Il16	-1.166	0.03198	-1.6623	0.00175	-2.1666	6.23E-05	-2.0573	0.00013
Il1rn	-0.1912	0.56848	0.11114	0.74776	0.72751	0.0299	1.31781	0.00018
Il27	-0.8755	0.07043	-1.6381	0.00067	-1.9692	5.33E-05	-1.7652	0.00022
Isg15	-0.7744	0.23692	-1.0226	0.10085	-1.7142	0.00656	-2.3202	0.00033
Lgals3bp	-1.1511	0.00034	-1.2012	0.00013	-1.2897	3.85E-05	-1.0471	0.00055
Lgmn	-0.4845	0.41085	-1.4888	0.01017	-2.4331	5.62E-05	-1.9812	0.00071
Lyz1	-1.0645	0.00586	-1.423	0.00018	-1.5338	5.33E-05	-1.2313	0.00078
Lyz2	2.2529	5.11E-08	1.92095	9.95E-07	1.31816	0.0003	1.17904	0.00101
Mapkapk2	-0.9973	0.00669	-1.1828	0.0009	-1.314	0.00022	-1.078	0.0019
Metrnl	-0.486	0.33052	0.14076	0.76739	0.93284	0.04804	1.48236	0.00237
Mmp19	0.93809	0.00016	1.3007	3.52E-07	1.12181	4.64E-06	0.6899	0.00256
Mrc1	0.86434	0.03446	0.83342	0.03261	0.91907	0.01728	1.11566	0.00426
Napsa	-1.3369	0.08979	-2.1438	0.00514	-2.2786	0.00279	-1.9437	0.00989
Ncf1	0.01263	0.96569	-0.195	0.53548	-0.4285	0.163	-0.7704	0.01517
Olfm4	0.3847	0.09361	0.69063	0.00222	0.3796	0.07511	-0.5017	0.02067
Osm	1.17637	0.14946	1.65457	0.0363	1.86849	0.01728	1.76291	0.02364
Pf4	-1.0268	0.19936	-1.5505	0.04424	-1.6567	0.02959	-1.483	0.04994
Plek	0.53037	0.41983	1.56413	0.01724	2.11443	0.00142	1.17168	0.0654
Pnp	-0.8343	0.2526	-0.9187	0.18724	-1.4752	0.03225	-1.0878	0.10995
Prkcd	-0.4931	0.3471	-1.1002	0.03261	-1.035	0.03867	-0.7696	0.1203
Rnase4	0.66088	0.03509	0.2662	0.36656	-0.2198	0.43939	-0.2844	0.32452
Tnf	1.31833	0.00014	1.07909	0.00091	0.81799	0.00928	0.0939	0.75572

DISCUSSION

One of the goals of this study was to develop a systematic proteomic analysis method that eliminates the inconveniences that are caused by using 2 platforms for the global and targeted analyses. This aim was achieved using a dimethyl stable-isotope labeling strategy and label-free PRM, based on orbitrap mass spectrometry, during the activation of microglia as our model. By obviating the need to preselect ions in the assay development stage, the conversion of DDA results to PRM data was accelerated. Moreover, with label-free PRM, over 450 peptides can be analyzed precisely in a single run.

Another goal was to analyze the intracellular proteomic changes in immuno-inflammatory responses and metabolic pathways and examine the intercellular proteins that accompany activation by endotoxin and pro-inflammatory molecules in a microglia cell line. In the pathway network model that resulted from the systematic analysis of the intracellular proteome, immuno-inflammatory responses tended to activate, whereas metabolic pathways were suppressed during microglial activation by endotoxin and pro-inflammatory molecules. These results are consistent with previous studies that have suggested a link between pro-inflammatory cytokine generation and mitochondrial function [66]. Activation of local microglia induces them to function as antigen-presenting cells [67] and initiates TLR signaling, resulting in immune responses against microbial infections [68-70]. Moreover, LPS inhibits metabolism in microglia through excessive synthesis of NO, which is harmful to adjacent neurons and the microglial cells that produce it [71-72]. Our results support earlier findings on the function of metabolic reprogramming in the regulation of

innate inflammatory responses to LPS activated microglia. They also suggest that activating microglia with IFN-γ affects such metabolic pathways. Moreover, I quantified an additional 73 proteins that were not involved in any of the 5 pathways above but were associated with the pathways that were predicted by PPI (Figure 2-12 C). For instance, Nox1, which mediates the release of ROS to eliminate invading microorganisms in macrophages and neutrophils, has been suggested to interact directly with Rac2 and transfer electrons from the cytosol to the membrane via a multidomain complex [73]. The extra information of quantitative proteome for activated microglia could be useful for further study of the relationships between associated proteins.

In addition to intracellular proteome, the secretome data shows that the microglial inflammatory response contributes to neuronal degeneration through excessive production of NO and other pro-inflammatory cytokines. For example, the secretion of macrophage migration inhibitory factor (Mif) decreased gradually after the initial exposure to bacterial toxins and cytokines. Mif mediates the innate immune response to endotoxin and gram-negative bacteria by modulating the expression of Toll-like receptor 4 (TLR4), a signal-transducing component of the LPS receptor complex [74]. The expression levels of platelet factor 4 (Pf4) and granulins (Grns) also declined in the 3 treatment groups. Pf4, known as chemokine C-X-C motif ligand 4 (Cxcl4), is expressed specifically in microglia and is a ligand of Cxcr3, which is associated with various neurodegenerative diseases [75]. According to Eiko et al., Cxcl4 attenuates LPS induced microglial activation, as evidenced by the reduction in NO production and phagocytosis [76].

Grn is a secreted form of progranulin (PGRN), which is cleaved by neutrophil elastase or proteinase. Despite our knowledge of the functions of Grn [77], the regulation of Grn in microglia has not been studied extensively. According to Suh et al, LPS suppresses PGRN secretion in human microglia, consistent with our data [78]. Stimulation with LPS alone had a stronger effect on Tnf release than IFN-γ alone, supporting findings from the previous study [79], which showed that LPS induced Tnf production is independent of IFN-γ, whereas the induction of other pro-inflammatory mediators, such as iNOS, is highly dependent on IFN-γ. Thus, the conversion of cytotoxic, classically activated microglia into anti-inflammatory cells over time can potentially prevent serious damage [80].

Our systematic proteomic analysis has demonstrated that activation of BV2 microglia with LPS or IFN-γ promotes pro-inflammatory activities, such as increased expression of MHC and lower secretion of lysosomal proteins. Additional studies will be needed to fully characterize the dynamics of protein expression patterns that are associated with the development of the pro-inflammatory and anti-inflammatory states of activated BV2 and primary microglial cells.

Conclusion

In this study, I examined the secretory proteins at the protein molecular level of the neuro-immune system in three cell lines including neuron and glia using high-resolution orbitrap based mass spectrometry. Not only did I look at the differences in the expression of the secreted proteins by each cell line through this dataset, but I could also see what pathways the proteins that differ in expression affect. I have also developed proteomics techniques for secretome analysis and have been able to utilize it in researching the proteomics of activated microglia.

Moreover, our systematic quantitative approach using a high-resolution orbitrap allows me to evaluate the dynamic alternation of the whole-cell proteome and secretome during BV2 microglial activation. In particular, it was found that several proteins related to the immune-inflammation response and metabolism dynamically changed as cells responded to inflammation-associated molecules. These data will be integral in discovering biomarkers for neurodegenerative diseases that are associated with microglial activation. The development of a single platform that combines dimethyl-labeled shotgun proteomics and label-free PRM provides an alternative method of assessing peptides of interest that are unique to a specific protein in a large-scale targeted analysis. This platform will be beneficial for and applicable to a wide variety of fields in biology and neurodegenerative diseases from a system- omics perspective.

REFERENCES

1. Allen, N. J.; Barres, B. A., Neuroscience: Glia - more than just brain glue. *Nature* **2009,** *457* (7230), 675-7.

2. Aloisi, F., The role of microglia and astrocytes in CNS immune surveillance and immunopathology. *Advances in experimental medicine and biology* **1999,** *468*, 123-33.

3. Barres, B. A., The mystery and magic of glia: a perspective on their roles in health and disease. *Neuron* **2008,** *60* (3), 430-40.

4. Ullian, E. M.; Sapperstein, S. K.; Christopherson, K. S.; Barres, B. A., Control of synapse number by glia. *Science* **2001,** *291* (5504), 657-61.

5. Jha, M. K.; Kim, J. H.; Suk, K., Proteome of brain glia: the molecular basis of diverse glial phenotypes. *Proteomics* **2014,** *14* (4-5), 378-98.

6. Han, D.; Jin, J.; Woo, J.; Min, H.; Kim, Y., Proteomic analysis of mouse astrocytes and their secretome by a combination of FASP and StageTip-based, high pH, reversed-phase fractionation. *Proteomics* **2014,** *14* (13-14), 1604-9.

7. Skorupa, A.; Urbach, S.; Vigy, O.; King, M. A.; Chaumont-Dubel, S.; Prehn, J. H.; Marin, P., Angiogenin induces modifications in the astrocyte secretome: relevance to amyotrophic lateral sclerosis. *Journal of proteomics* **2013,** *91*, 274-85.

8. Jeon, H.; Lee, S.; Lee, W. H.; Suk, K., Analysis of glial secretome: the long pentraxin PTX3 modulates phagocytic activity of microglia. *Journal of neuroimmunology* **2010,** *229* (1-2), 63-72.

9. Thouvenot, E.; Urbach, S.; Dantec, C.; Poncet, J.; Seveno, M.; Demettre, E.; Jouin, P.; Touchon, J.; Bockaert, J.; Marin, P., Enhanced detection of CNS cell secretome in plasma protein-depleted cerebrospinal fluid. *Journal of proteome research* **2008,** *7* (10), 4409-21.

10. Nimmerjahn, A.; Kirchhoff, F.; Helmchen, F., Resting microglial cells are highly dynamic surveillants of brain parenchyma in vivo. *Science* **2005,** *308* (5726), 1314-8.

11. Chastain, E. M.; Duncan, D. S.; Rodgers, J. M.; Miller, S. D., The role of antigen presenting cells in multiple sclerosis. *Biochim Biophys Acta* **2011,** *1812* (2), 265-74.

12. Brown, J. N.; Ortiz, G. M.; Angel, T. E.; Jacobs, J. M.; Gritsenko, M.; Chan, E. Y.; Purdy, D. E.; Murnane, R. D.; Larsen, K.; Palermo, R. E.; Shukla, A. K.; Clauss, T.

R.; Katze, M. G.; McCune, J. M.; Smith, R. D., Morphine produces immunosuppressive effects in nonhuman primates at the proteomic and cellular levels. *Mol Cell Proteomics* **2012,** *11* (9), 605-18.

13. Raivich, G.; Bohatschek, M.; Kloss, C. U.; Werner, A.; Jones, L. L.; Kreutzberg, G. W., Neuroglial activation repertoire in the injured brain: graded response, molecular mechanisms and cues to physiological function. *Brain Res Brain Res Rev* **1999,** *30* (1), 77-105.

14. Lull, M. E.; Block, M. L., Microglial Activation and Chronic Neurodegeneration. *Neurotherapeutics* **2010,** *7* (4), 354-365.

15. Fu, R. Y.; Shen, Q. Y.; Xu, P. F.; Luo, J. J.; Tang, Y. M., Phagocytosis of Microglia in the Central Nervous System Diseases. *Molecular Neurobiology* **2014,** *49* (3), 1422-1434.

16. Perry, V. H.; Holmes, C., Microglial priming in neurodegenerative disease. *Nat Rev Neurol* **2014,** *10* (4), 217-224.

17. Palsson-McDermott, E. M.; O'Neill, L. A. J., Signal transduction by the lipopolysaccharide receptor, Toll-like receptor-4. *Immunology* **2004,** *113* (2), 153-162.

18. Chen, Z. H.; Jalabi, W.; Shpargel, K. B.; Farabaugh, K. T.; Dutta, R.; Yin, X. H.; Kidd, G. J.; Bergmann, C. C.; Stohlman, S. A.; Trapp, B. D., Lipopolysaccharide-Induced Microglial Activation and Neuroprotection against Experimental Brain Injury Is Independent of Hematogenous TLR4. *Journal of Neuroscience* **2012,** *32* (34), 11706-11715.

19. Hu, X.; Herrero, C.; Li, W. P.; Antoniv, T. T.; Falck-Pedersen, E.; Koch, A. E.; Woods, J. M.; Haines, G. K.; Ivashkiv, L. B., Sensitization of IFN-gamma Jak-STAT signaling during macrophage activation. *Nat Immunol* **2002,** *3* (9), 859-66.

20. Koide, N.; Mu, M. M.; Hassan, F.; Islam, S.; Tumurkhuu, G.; Dagvadorj, J.; Naiki, Y.; Mori, I.; Yoshida, T.; Yokochi, T., Lipopolysaccharide enhances interferon-gamma-induced nitric oxide (NO) production in murine vascular endothelial cells via augmentation of interferon regulatory factor-1 activation. *J Endotoxin Res* **2007,** *13* (3), 167-75.

21. Papageorgiou, I. E.; Lewen, A.; Galow, L. V.; Cesetti, T.; Scheffel, J.; Regen, T.; Hanisch, U. K.; Kann, O., TLR4-activated microglia require IFN-gamma to induce severe neuronal dysfunction and death in situ. *Proc Natl Acad Sci U S A* **2016,** *113* (1), 212-7.

22. Liu, N.; Zhuang, Y.; Zhou, Z.; Zhao, J.; Chen, Q.; Zheng, J., NF-kappaB dependent up-regulation of TRPC6 by Abeta in BV-2 microglia cells increases COX-2 expression and contributes to hippocampus neuron damage. *Neurosci Lett* **2017,** *651*, 1-8.

23. Luo, Q.; Yan, X.; Bobrovskaya, L.; Ji, M.; Yuan, H.; Lou, H.; Fan, P., Anti-neuroinflammatory effects of grossamide from hemp seed via suppression of TLR-4-mediated NF-kappaB signaling pathways in lipopolysaccharide-stimulated BV2 microglia cells. *Mol Cell Biochem* **2017,** *428* (1-2), 129-137.

24. Han, Q.; Yuan, Q.; Meng, X.; Huo, J.; Bao, Y.; Xie, G., 6-Shogaol attenuates LPS-induced inflammation in BV2 microglia cells by activating PPAR-gamma. *Oncotarget* **2017,** *8* (26), 42001-42006.

25. Wang, B.; Zhang, Y. J.; Cao, W.; Wei, X. B.; Chen, J.; Ying, W. H., SIRT2 Plays Significant Roles in Lipopolysaccharides-Induced Neuroinflammation and Brain Injury in Mice. *Neurochem Res* **2016,** *41* (9), 2490-2500.

26. Ge, Y.; Bruno, M.; Wallace, K.; Leavitt, S.; Andrews, D.; Spassova, M. A.; Xi, M. Y.; Roy, A.; Haykal-Coates, N.; Lefew, W.; Swank, A.; Winnik, W. M.; Chen, C.; Woodard, J.; Farraj, A.; Teichman, K. Y.; Ross, J. A., Systematic Proteomic Approach to Characterize the Impacts of Chemical Interactions on Protein and Cytotoxicity Responses to Metal Mixture Exposures. *Journal of Proteome Research* **2015,** *14* (1), 183-192.

27. Kim, W.; Bennett, E. J.; Huttlin, E. L.; Guo, A.; Li, J.; Possemato, A.; Sowa, M. E.; Rad, R.; Rush, J.; Comb, M. J.; Harper, J. W.; Gygi, S. P., Systematic and Quantitative Assessment of the Ubiquitin-Modified Proteome. *Mol Cell* **2011,** *44* (2), 325-340.

28. Stutzer, I.; Selevsek, N.; Esterhazy, D.; Schmidt, A.; Aebersold, R.; Stoffel, M., Systematic Proteomic Analysis Identifies beta-Site Amyloid Precursor Protein Cleaving Enzyme 2 and 1 (BACE2 and BACE1) Substrates in Pancreatic beta-Cells. *J Biol Chem* **2013,** *288* (15), 10536-10547.

29. Wu, C.; Shi, T.; Brown, J. N.; He, J.; Gao, Y.; Fillmore, T. L.; Shukla, A. K.; Moore, R. J.; Camp, D. G., 2nd; Rodland, K. D.; Qian, W. J.; Liu, T.; Smith, R. D., Expediting SRM assay development for large-scale targeted proteomics experiments. *J Proteome Res* **2014,** *13* (10), 4479-87.

30. Gallien, S.; Duriez, E.; Crone, C.; Kellmann, M.; Moehring, T.; Domon, B., Targeted proteomic quantification on quadrupole-orbitrap mass spectrometer.

Mol Cell Proteomics **2012,** *11* (12), 1709-23.

31. Gallien, S.; Kim, S. Y.; Domon, B., Large-Scale Targeted Proteomics Using Internal Standard Triggered-Parallel Reaction Monitoring (IS-PRM). *Mol Cell Proteomics* **2015,** *14* (6), 1630-44.

32. Rauniyar, N., Parallel Reaction Monitoring: A Targeted Experiment Performed Using High Resolution and High Mass Accuracy Mass Spectrometry. *Int J Mol Sci* **2015,** *16* (12), 28566-81.

33. Sherrod, S. D.; Myers, M. V.; Li, M.; Myers, J. S.; Carpenter, K. L.; Maclean, B.; Maccoss, M. J.; Liebler, D. C.; Ham, A. J., Label-free quantitation of protein modifications by pseudo selected reaction monitoring with internal reference peptides. *J Proteome Res* **2012,** *11* (6), 3467-79.

34. Khristenko, N. A.; Larina, I. M.; Domon, B., Longitudinal Urinary Protein Variability in Participants of the Space Flight Simulation Program. *J Proteome Res* **2016,** *15* (1), 114-24.

35. Han, D.; Moon, S.; Kim, Y.; Kim, J.; Jin, J.; Kim, Y., In-depth proteomic analysis of mouse microglia using a combination of FASP and StageTip-based, high pH, reversed-phase fractionation. *Proteomics* **2013,** *13* (20), 2984-8.

36. Cox, J.; Mann, M., MaxQuant enables high peptide identification rates, individualized p.p.b.-range mass accuracies and proteome-wide protein quantification. *Nat Biotechnol* **2008,** *26* (12), 1367-72.

37. Cox, J.; Neuhauser, N.; Michalski, A.; Scheltema, R. A.; Olsen, J. V.; Mann, M., Andromeda: a peptide search engine integrated into the MaxQuant environment. *Journal of proteome research* **2011,** *10* (4), 1794-805.

38. Wisniewski, J. R.; Ostasiewicz, P.; Dus, K.; Zielinska, D. F.; Gnad, F.; Mann, M., Extensive quantitative remodeling of the proteome between normal colon tissue and adenocarcinoma. *Molecular systems biology* **2012,** *8*, 611.

39. Zhang, J.; Xin, L.; Shan, B.; Chen, W.; Xie, M.; Yuen, D.; Zhang, W.; Zhang, Z.; Lajoie, G. A.; Ma, B., PEAKS DB: de novo sequencing assisted database search for sensitive and accurate peptide identification. *Molecular & cellular proteomics : MCP* **2012,** *11* (4), M111 010587.

40. Low, T. Y.; van Heesch, S.; van den Toorn, H.; Giansanti, P.; Cristobal, A.; Toonen, P.; Schafer, S.; Hubner, N.; van Breukelen, B.; Mohammed, S.; Cuppen, E.; Heck, A. J.; Guryev, V., Quantitative and qualitative proteome characteristics extracted from in-depth integrated genomics and proteomics analysis. *Cell*

reports **2013,** *5* (5), 1469-78.

41. Thomas, P. D.; Kejariwal, A.; Campbell, M. J.; Mi, H.; Diemer, K.; Guo, N.; Ladunga, I.; Ulitsky-Lazareva, B.; Muruganujan, A.; Rabkin, S.; Vandergriff, J. A.; Doremieux, O., PANTHER: a browsable database of gene products organized by biological function, using curated protein family and subfamily classification. *Nucleic acids research* **2003,** *31* (1), 334-41.

42. Dowell, J. A.; Johnson, J. A.; Li, L., Identification of astrocyte secreted proteins with a combination of shotgun proteomics and bioinformatics. *Journal of proteome research* **2009,** *8* (8), 4135-43.

43. Dityatev, A.; Schachner, M.; Sonderegger, P., The dual role of the extracellular matrix in synaptic plasticity and homeostasis. *Nature reviews. Neuroscience* **2010,** *11* (11), 735-46.

44. Greco, T. M.; Seeholzer, S. H.; Mak, A.; Spruce, L.; Ischiropoulos, H., Quantitative mass spectrometry-based proteomics reveals the dynamic range of primary mouse astrocyte protein secretion. *Journal of proteome research* **2010,** *9* (5), 2764-74.

45. Kim, S.; Ock, J.; Kim, A. K.; Lee, H. W.; Cho, J. Y.; Kim, D. R.; Park, J. Y.; Suk, K., Neurotoxicity of microglial cathepsin D revealed by secretome analysis. *Journal of neurochemistry* **2007,** *103* (6), 2640-50.

46. Kuhn, P. H.; Koroniak, K.; Hogl, S.; Colombo, A.; Zeitschel, U.; Willem, M.; Volbracht, C.; Schepers, U.; Imhof, A.; Hoffmeister, A.; Haass, C.; Rossner, S.; Brase, S.; Lichtenthaler, S. F., Secretome protein enrichment identifies physiological BACE1 protease substrates in neurons. *The EMBO journal* **2012,** *31* (14), 3157-68.

47. Thouvenot, E.; Urbach, S.; Vigy, O.; Seveno, M.; Galeotti, N.; Nguyen, G.; Bockaert, J.; Marin, P., Quantitative proteomic analysis reveals protein expression changes in the murine neuronal secretome during apoptosis. *Journal of proteomics* **2012,** *77*, 394-405.

48. Woo, J.; Han, D.; Park, J.; Kim, S. J.; Kim, Y., In-depth characterization of the secretome of mouse CNS cell lines by LC-MS/MS without prefractionation. *Proteomics* **2015,** *15* (21), 3617-22.

49. Wisniewski, J. R.; Zougman, A.; Nagaraj, N.; Mann, M., Universal sample preparation method for proteome analysis. *Nature methods* **2009,** *6* (5), 359-U60.

50. Boersema, P. J.; Raijmakers, R.; Lemeer, S.; Mohammed, S.; Heck, A. J., Multiplex peptide stable isotope dimethyl labeling for quantitative proteomics.

Nat Protoc **2009,** *4* (4), 484-94.

51. Escher, C.; Reiter, L.; MacLean, B.; Ossola, R.; Herzog, F.; Chilton, J.; MacCoss, M. J.; Rinner, O., Using iRT, a normalized retention time for more targeted measurement of peptides. *Proteomics* **2012,** *12* (8), 1111-21.

52. Shannon, P.; Markiel, A.; Ozier, O.; Baliga, N. S.; Wang, J. T.; Ramage, D.; Amin, N.; Schwikowski, B.; Ideker, T., Cytoscape: A software environment for integrated models of biomolecular interaction networks. *Genome Res* **2003,** *13* (11), 2498-2504.

53. Szklarczyk, D.; Franceschini, A.; Wyder, S.; Forslund, K.; Heller, D.; Huerta-Cepas, J.; Simonovic, M.; Roth, A.; Santos, A.; Tsafou, K. P.; Kuhn, M.; Bork, P.; Jensen, L. J.; von Mering, C., STRING v10: protein-protein interaction networks, integrated over the tree of life. *Nucleic Acids Res* **2015,** *43* (Database issue), D447-52.

54. MacLean, B.; Tomazela, D. M.; Shulman, N.; Chambers, M.; Finney, G. L.; Frewen, B.; Kern, R.; Tabb, D. L.; Liebler, D. C.; MacCoss, M. J., Skyline: an open source document editor for creating and analyzing targeted proteomics experiments. *Bioinformatics* **2010,** *26* (7), 966-968.

55. Hoing, S.; Rudhard, Y.; Reinhardt, P.; Glatza, M.; Stehling, M.; Wu, G. M.; Peiker, C.; Bocker, A.; Parga, J. A.; Bunk, E.; Schwamborn, J. C.; Slack, M.; Sterneckert, J.; Scholer, H. R., Discovery of Inhibitors of Microglial Neurotoxicity Acting Through Multiple Mechanisms Using a Stem-Cell-Based Phenotypic Assay. *Cell Stem Cell* **2012,** *11* (5), 620-632.

56. Melchior, B.; Puntambekar, S. S.; Carson, M. J., Microglia and the control of autoreactive T cell responses. *Neurochem Int* **2006,** *49* (2), 145-53.

57. Pla, A.; Pascual, M.; Renau-Piqueras, J.; Guerri, C., TLR4 mediates the impairment of ubiquitin-proteasome and autophagy-lysosome pathways induced by ethanol treatment in brain. *Cell Death Dis* **2014,** *5*, e1066.

58. Barger, S. W.; Goodwin, M. E.; Porter, M. M.; Beggs, M. L., Glutamate release from activated microglia requires the oxidative burst and lipid peroxidation. *J Neurochem* **2007,** *101* (5), 1205-13.

59. Yelamanchi, S. D.; Jayaram, S.; Thomas, J. K.; Gundimeda, S.; Khan, A. A.; Singhal, A.; Keshava Prasad, T. S.; Pandey, A.; Somani, B. L.; Gowda, H., A pathway map of glutamate metabolism. *J Cell Commun Signal* **2016,** *10* (1), 69-75.

60. Kim, H. Y.; Kim, H. S., Upregulation of MIP-2 (CXCL2) expression by 15-deoxy-Delta(12,14)-prostaglandin J(2) in mouse peritoneal macrophages.

Immunol Cell Biol **2007,** *85* (1), 60-7.

61. Hoeksema, M. A.; Scicluna, B. P.; Boshuizen, M. C.; van der Velden, S.; Neele, A. E.; Van den Bossche, J.; Matlung, H. L.; van den Berg, T. K.; Goossens, P.; de Winther, M. P., IFN-gamma priming of macrophages represses a part of the inflammatory program and attenuates neutrophil recruitment. *J Immunol* **2015,** *194* (8), 3909-16.

62. Repiso, A.; Andres, R.; Climent, F.; Urena, J. M., Expression patterns in mouse embryos of neuroleukin/glucose-6-phosphate isomerase and autocrine motility factor receptor. *Anat Histol Embryol* **2008,** *37* (5), 380-2.

63. Li, X.; O'Regan, A. W.; Berman, J. S., IFN-gamma induction of osteopontin expression in human monocytoid cells. *J Interferon Cytokine Res* **2003,** *23* (5), 259-65.

64. Fan, X.; He, C.; Jing, W.; Zhou, X.; Chen, R.; Cao, L.; Zhu, M.; Jia, R.; Wang, H.; Guo, Y.; Zhao, J., Intracellular Osteopontin inhibits toll-like receptor signaling and impedes liver carcinogenesis. *Cancer Res* **2015,** *75* (1), 86-97.

65. Zhang, Y.; Chen, K.; Sloan, S. A.; Bennett, M. L.; Scholze, A. R.; O'Keeffe, S.; Phatnani, H. P.; Guarnieri, P.; Caneda, C.; Ruderisch, N.; Deng, S.; Liddelow, S. A.; Zhang, C.; Daneman, R.; Maniatis, T.; Barres, B. A.; Wu, J. Q., An RNA-sequencing transcriptome and splicing database of glia, neurons, and vascular cells of the cerebral cortex. *J Neurosci* **2014,** *34* (36), 11929-47.

66. Wang, W. Y.; Tan, M. S.; Yu, J. T.; Tan, L., Role of pro-inflammatory cytokines released from microglia in Alzheimer's disease. *Ann Transl Med* **2015,** *3* (10), 136.

67. Shaked, I.; Porat, Z.; Gersner, R.; Kipnis, J.; Schwartz, M., Early activation of microglia as antigen-presenting cells correlates with T cell-mediated protection and repair of the injured central nervous system. *J Neuroimmunol* **2004,** *146* (1-2), 84-93.

68. Barton, G. M.; Medzhitov, R., Toll-like receptor signaling pathways. *Science* **2003,** *300* (5625), 1524-5.

69. Hemmati, F.; Ghasemi, R.; Mohamed Ibrahim, N.; Dargahi, L.; Mohamed, Z.; Raymond, A. A.; Ahmadiani, A., Crosstalk between insulin and Toll-like receptor signaling pathways in the central nervous system. *Mol Neurobiol* **2014,** *50* (3), 797-810.

70. Wang, Y.; Abarbanell, A. M.; Herrmann, J. L.; Weil, B. R.; Poynter, J.; Manukyan, M. C.; Crisostomo, P. R.; Meldrum, D. R., Toll-like receptor signaling

pathways and the evidence linking toll-like receptor signaling to cardiac ischemia/reperfusion injury. *Shock* **2010,** *34* (6), 548-57.

71. Moss, D. W.; Bates, T. E., Activation of murine microglial cell lines by lipopolysaccharide and interferon-gamma causes NO-mediated decreases in mitochondrial and cellular function. *Eur J Neurosci* **2001,** *13* (3), 529-38.

72. Chenais, B.; Morjani, H.; Drapier, J. C., Impact of endogenous nitric oxide on microglial cell energy metabolism and labile iron pool. *J Neurochem* **2002,** *81* (3), 615-23.

73. Ueyama, T.; Geiszt, M.; Leto, T. L., Involvement of Rac1 in activation of multicomponent Nox1- and Nox3-based NADPH oxidases. *Mol Cell Biol* **2006,** *26* (6), 2160-74.

74. Calandra, T.; Froidevaux, C.; Martin, C.; Roger, T., Macrophage migration inhibitory factor and host innate immune defenses against bacterial sepsis. *J Infect Dis* **2003,** *187 Suppl 2*, S385-90.

75. Lasagni, L.; Francalanci, M.; Annunziato, F.; Lazzeri, E.; Giannini, S.; Cosmi, L.; Sagrinati, C.; Mazzinghi, B.; Orlando, C.; Maggi, E.; Marra, F.; Romagnani, S.; Serio, M.; Romagnani, P., An alternatively spliced variant of CXCR3 mediates the inhibition of endothelial cell growth induced by IP-10, Mig, and I-TAC, and acts as functional receptor for platelet factor 4. *J Exp Med* **2003,** *197* (11), 1537-49.

76. de Jong, E. K.; de Haas, A. H.; Brouwer, N.; van Weering, H. R.; Hensens, M.; Bechmann, I.; Pratley, P.; Wesseling, E.; Boddeke, H. W.; Biber, K., Expression of CXCL4 in microglia in vitro and in vivo and its possible signaling through CXCR3. *J Neurochem* **2008,** *105* (5), 1726-36.

77. Lui, H.; Zhang, J.; Makinson, S. R.; Cahill, M. K.; Kelley, K. W.; Huang, H. Y.; Shang, Y.; Oldham, M. C.; Martens, L. H.; Gao, F.; Coppola, G.; Sloan, S. A.; Hsieh, C. L.; Kim, C. C.; Bigio, E. H.; Weintraub, S.; Mesulam, M. M.; Rademakers, R.; Mackenzie, I. R.; Seeley, W. W.; Karydas, A.; Miller, B. L.; Borroni, B.; Ghidoni, R.; Farese, R. V., Jr.; Paz, J. T.; Barres, B. A.; Huang, E. J., Progranulin Deficiency Promotes Circuit-Specific Synaptic Pruning by Microglia via Complement Activation. *Cell* **2016,** *165* (4), 921-35.

78. Suh, H. S.; Choi, N.; Tarassishin, L.; Lee, S. C., Regulation of progranulin expression in human microglia and proteolysis of progranulin by matrix metalloproteinase-12 (MMP-12). *PLoS One* **2012,** *7* (4), e35115.

79. Negishi, M.; Izumi, Y.; Aleemuzzaman, S.; Inaba, N.; Hayakawa, S.,

Lipopolysaccharide (LPS)-induced Interferon (IFN)-gamma production by decidual mononuclear cells (DMNC) is interleukin (IL)-2 and IL-12 dependent. *Am J Reprod Immunol* **2011,** *65* (1), 20-7.

80. Beins, E.; Ulas, T.; Ternes, S.; Neumann, H.; Schultze, J. L.; Zimmer, A., Characterization of inflammatory markers and transcriptome profiles of differentially activated embryonic stem cell-derived microglia. *Glia* **2016,** *64* (6), 1007-20.

ABSTRACT IN KOREAN

국 문 초 록

고분해능 단백체 프로파일링 및 표적단백체 기술을 이용한 신경-면역 시스템에 대한 기능 단백체 연구

서론: 의학의 발전으로 이제는 100 세 시대라고 할 정도로 인간의 평균수명은 점차 증가하고 있지만, 노후화로 인해 발생하는 많은 질병 중 Alzheimer disease (AD), Parkinson disease (PD), 또는 Amyotrophic lateral sclerosis (ALS)와 같은 퇴행성 뇌신경 질환은 삶의 질을 감소시키고 있다. 이러한 퇴행성 뇌신경 질환의 원인과 기작에 대한 연구를 진행하기 위해 분자수준에서의 접근이 필수적이며, 고해상도 질량분석기를 이용한 프로테오믹스 기술은 이러한 표지자 단백질 발굴에 매우 유용한 기술로 대두 되고 있다. 또한 표적 단백질 간의 체계적인 네트워크 분석은 향후 퇴행성 뇌신경 질환의 메커니즘 연구에 사용될 수 있을 것이다.

방법: 1 장에서 중추신경계 세포들의 분비단백질 분석 최적화와 세포주들간의 단백체 차이를 보기 위해 뇌신경세포주 (HT-22), 성상교세포주 (C8-D1A), 미세아교세포주 (BV-2)를 사용하였다. 1x10e6 개의 cell 을 100mm dish 에 24 시간 배양 후, 농축 시켜 얻은 단백질들을 FASP (Filter Aided Sample Preparation) 기법을 사용하여 펩타이드로 시료처리를 하여 고해상도 질량분석기기인 Q-Exactive 로 4 시간 분석을 진행하였다. 분석결과 data 는 Andromeda 알고리즘 기반의 MaxQuant 프로그램으로 데이터 처리를 하였고 annotation 되지 않은 MS/MS 데이터는 de-novo 기반의 PEAKS-7 프로그램으로 분석하여 추가적인 단백질 동정을 하였다. 각 세포주들의 분비단백질들은 label-free quantitation 기법으로 비교분석 하였으며 bioinformatics tool 을 사용하여 분비단백질들의 중요한 기능을 확인하였다. 2 장에서는 미세아교세포주에 24 시간동안 lipopolysaccharide (LPS)와 interferon gamma (IFN-γ)를 처리하여 활성화 시킨 후 intracellular 와 extracellular 에서의 단백체 차이를 dimethyl labeling 기법을 사용하여 동시정량분석을 진행하였다. 6, 12, 24, 48 시간동안 LPS, IFN-γ, LPS/IFN-γ 로 활성화 시킨 미세아교세포의 intra-, extracellular 에서의 표지자 후보 단백질군에 대해서 변화를 보기 위해 표적 단백체학 기법인 label-free PRM (Parallel Reaction Monitoring) 으로 상대정량을 하여 시간에 따라 변화하는 단백체들의 체계적인 네트워크 분석을 진행하였다.

결과: 1 장에서는 고해상도 질량분석기를 사용하여 3 가지 세포주에서 2795 개의 분비 단백질들을 동정하였으며 각 세포주 당 156 개 (BV-2), 44 개 (C8-D1A), 93 개 (HT-22)의 특이적인 단백질을 발굴하였다. 또한 de-novo sequencing 분석 기법을 사용하여 302 개의 추가적인 단백질들을 ID 하였다. 발굴한 분비단백질들의 신뢰도를 높이기 위하여 SignalP, SecretomeP, Exocarta, TMHMM database tool 을 이용하여 2351 개의 잠재적 분비단백질들을 분류하였고, 정량비교분석 기법을 통해 각 세포주 분비단백질들간에 2 fold change 의 차이를 보이며 student t-test 에서 p-value 0.05 이하의 유의수준을 보이는 단백질 573 개 (BV-2 vs. C8-D1A), 694 개 (BV-2 vs. HT-22), 475 개 (C8-D1A vs. HT-22) 를 확인하였다. 또한 정량된 단백질들의 pathway 분석을 통해 lysosome, phagocytosis 등과 같은 분비 단백질들의 중요한 기능을 확인하였고, Parkinson disease, Huntington disease 와 같은 퇴행성 뇌신경 질환과도 연관이 있는 단백질들을 발굴하였다. 2 장에서는 LPS 와 LPS/ IFN-γ 로 활성화 시킨 모델의 세포내 단백체 (WCP) 분석을 통해 5492 개 단백질을 동정하였고 4748 개의 단백질을 정량 할 수 있었으며 동일 모델의 세포외 분비단백체 (SEC) 분석을 통해 4938 개 단백질 동정 및 3558 개 단백질을 정량 할 수 있었다. 디스커버리 수준의 분석을 통해 유의한 차이를 보이는 단백질들과 KEGG pathway 등 bioinformatics 분석을 통해 319 개의 세포내단백질, 170 개의 분비단백질을 최종 타겟 후보군으로 선정하였다. 450 개 이상의 peptide 를 동시정량분석이 가능하도록 최적화 시킨 label-free PRM 기법을

사용하여 미세아교세포 활성화 시간대별로 모은 시료에서 표적단백체학 분석을 진행한 결과, 시간대 별로 변화하는 pathway 네트워크 지도를 그릴 수 있었으며 활성화 미세아교세포 모델에서 세포내와 세포외에서 차이를 보이는 표지자 단백질 후보군을 제시 할 수 있었다.

결론: 1 장에서는 분비단백체 기법의 최적화 및 개발을 통해 3 가지 세포주들의 분비단백질 차이를 label-free quantification 기법으로 확인하였다. 이러한 분비단백체학 기법은 적은 양으로 존재하고 있는 세포외 단백질들을 심도 있고 정확하게 연구를 할 수 있는 기반을 마련하였다. 2 장에서는 단일플랫폼에서 체계적인 정량 프로테오믹스 접근법을 통해 중추신경계 안에서 면역을 담당하고 있는 미세아교세포의 활성화 시 발현하는 표지자 단백질을 발굴하여 퇴행성 뇌신경 질환 메커니즘 연구에 도움을 주고자 하였다. 보다 정밀하고 정확한 정량 분석을 위하여 dimethyl labeling 동시 정량 기법과 label-free PRM 표적단백체학 기법을 확립하였고, 미세아교세포의 활성화 시에 면역-염증 반응과 신진대사에 관련한 단백질들의 변화를 하나의 플랫폼으로 정량 분석하여 LPS 와 IFN-γ 특이적으로 발현의 차이를 보이는 표지자 단백질들을 발굴 할 수 있었다.

주요어 : 중추신경계, 성상교세포, 미세아교세포, 뇌신경세포, 미세아교세포 활성화, 분비단백체, Dimethyl labeling, Label-free PRM, 표적단백체학

학 번 : 2013-21781

*본 내용은 Proteomics 학술지 (*Proteomics* 2015, 15 (21), 3617-22.) 와 Journal of proteome research (*J Proteome Res* 2017, 16 (9), 3419-3432.) 학술지에 출판 완료된 내용임